P.4 Thermal Evaluation

P.4.1 Discussion

This chapter presents the thermal evaluations which demonstrate that the NUHOMS®-24PTH system meets the thermal requirements of 10CFR72 for the dry storage of spent fuel. The NUHOMS®-24PTH system is designed to passively reject decay heat during storage and transfer for normal, off-normal and accident conditions while maintaining temperatures and pressures within specified regulatory limits.

Several thermal design criteria are established for the thermal analysis of the 24PTH DSC basket as discussed below.

- Maximum temperatures of the confinement structural components must not adversely affect the confinement function,
- Maximum fuel cladding temperature limit of 400°C (752°F) is applicable to normal conditions of storage and all short term operations including vacuum drying and helium backfilling of the 24PTH DSC per Interim Staff Guidance (ISG) No. 11, Revision 2 [4.19]. In addition, ISG-11 does not permit thermal cycling of the fuel cladding with temperature differences greater than 65°C (117°F) during drying and backfilling operations,
- Maximum fuel cladding temperature limit of 570°C (1058°F) is applicable to accidents or off-normal thermal transients [4.19],
- The maximum DSC cavity internal pressures during normal, off-normal and accident conditions must be below the design pressures of 15 psig, 20 psig and 120 psig, respectively, and
- A total of five (5) Heat Load Zoning Configurations (HLZCs) are allowed for the 24PTH DSCs as shown in Figures P.2-1 through P.2-5. The maximum total heat load per DSC is 40.8 kW, 31.2 kW or 24 kW depending upon the specific DSC types and HLZCs. The thermal analysis is carried out for HLZC 1 shown in Figure P.4-36 with 40.8 kW heat load because it bounds the HLZCs 2 and 3. In HLZC 1, the fuel assemblies at the center 4 locations in the DSC basket have a maximum heat load of 1.7 kW per assembly as compared to zero (empty locations) for HLZC 2 and 1.5 kW for HLZC 3. Therefore, HLZC 1 results in higher fuel cladding and basket temperatures compared to HLZCs 2 or 3. To bound all possible combinations of heat loads from fuel assemblies allowed in HLZC 5 of Figure P.2-5, the thermal analysis is carried out for the HLZC shown in Figure P.4-38. In this thermal analysis configuration, the highest possible allowed decay heat assemblies are assumed to be at the center and upper half of the basket locations resulting in bounding fuel cladding and basket temperatures.

The thermal analysis is carried out for the three NUHOMS®-24PTH DSC configurations (24PTH-S, 24PTH-L, and 24PTH-S-LC DSC types in combination with six basket types of the NUHOMS®-24PTH system described in Section P.2.1). A summary of the three system configurations analyzed in this chapter are summarized below:

System Configuration	DSC Type	Aluminum Inserts in Basket	Fuel Type	Total Heat Load per DSC, kW	Transfer Cask	Storage Module
1	24PTH-S OR 24PTH-L	With inserts	All Fuels	40.8	OS197FC	HSM-H
				31.2	OS197/ OS197H	HSM-H
2	24PTH-S or 24PTH-L	No inserts	All Fuels	31.2	OS197FC	HSM-H
3	24PTH-S-LC(1)	No inserts	B&W 15x15	24	Standardized TC	HSM-H or HSM Model 102

(1) The maximum heat load allowed in the 24PTH-S-LC DSC is 24 kW. The HSM Model 102 is designed for a maximum heat load of 24 kW from a NUHOMS® 24P DSC as described in Section 8.1.3. Therefore no additional analysis of HSM Model 102 is required with 24PTH-S-LC DSC.

The thermal evaluations presented herein include steady state and transient analyses of the thermal response of the NUHOMS®-24PTH system components to a defined set of thermal loading conditions. These loading conditions envelope the thermal conditions expected during all normal, off-normal, and postulated accident loading, transfer and dry storage operations for the design basis thermal conditions as defined in Section P.2. The applicable allowable temperatures are presented and comparisons are made with calculated temperatures as the basis for acceptance.

The analyses conservatively apply a uniform maximum peaking factor of 1.11 [4.1] along the active fuel length to bound the effect of the decay heat flux varying axially along the active fuel length.

A description of the detailed analyses performed for the storage of NUHOMS®-24PTH DSC under normal, off-normal, and accident conditions is provided in Sections P.4.4 and for transfer is provided in Section P.4.5. Section P.4.6 describes the 24PTH DSC basket and fuel cladding analysis for storage and transfer conditions. The DSC cavity internal pressures are also calculated in Section P.4.6 for all conditions of storage and transfer. Section P.4.7 describes the evaluation performed for loading/unloading conditions. The thermal evaluation concludes that each of the three NUHOMS®-24PTH systems configurations listed above meets all the design criteria.

The effective thermal conductivity of the fuel assemblies used in the 24PTH DSC thermal analysis is based on the conservative assumption of radiation and conduction heat transfer only, where any convection heat transfer is neglected. In addition, the lowest effective thermal conductivity among the fuel assemblies to be stored using 24PTH-S DSC, -L DSC, and -S-LC DSC is selected as the basis for the thermal analysis. Section P.4.8 presents the calculations that determined the fuel assembly effective thermal conductivity in a helium or vacuum environment. The thermal analysis model conservatively neglects convection heat transfer in the basket regions.

The DSC basket and fuel cladding temperature calculation methodology has been benchmarked [4.20] against experimental data [4.21] obtained for the TN-24 cask.

Although the NUHOMS® HSM is a proven design with extensive operational experience, the HSM-H incorporates several design variations to the basic HSM design to increase the module's thermal rating. The effectiveness of these design modifications was evaluated using a combination of computer (i.e., ANSYS finite element) modeling, and hand calculations. In addition, an independent confirmation of the thermal performance of the HSM-H using an alternative methodology was performed and is presented in Section P.4.10. This confirmatory analysis evaluates the thermal

performance of the HSM-H under off-normal conditions of storage. This evaluation uses a computational fluid dynamics (CFD) methodology to directly calculate the HSM-H concrete and DSC shell temperatures.

P.4.2 Summary of Thermal Properties of Materials

The analyses performed herein use interpolated values where appropriate for intermediate temperatures. The interpolation assumes a linear relationship between the reported values. The use of linear interpolation between temperature values in the tables for determining intermediate value of property is justified by the near-linear behavior as a function of temperature for the range of interest.

The emissivity of stainless steel is 0.587 [4.5]. For additional conservatism an emissivity of 0.46 for stainless steel is used for the basket steel plates in the analysis. The emissivity assumed for oxidized Zircaloy cladding surfaces, including Babcock & Wilcox (B&W) M5 cladding material, is 0.8 [4.11]. The emissivity assumed for anodized and non-anodized aluminum portion of side heat shields are 0.8 and 0.1, respectively [4.26] [4.30] [4.47].

The tables below provide the thermal properties of materials used in the analysis of the NUHOMS®-24PTH DSC.

The effective thermal properties are the lowest calculated values among the various PWR fuel assembly types that may be stored in 24PTH DSC. Since 24PTH-S-LC DSC is designed for storage of B&W 15x15 fuel, an additional subset of bounding effective thermal properties are reported.

1. PWR Fuel with Helium Backfill

Temperature, °F	k, Btu/min-in-°F	ρ, lb_m/in^3	T, °F	C_p,Btu/lb_m-°F
Bounding Fuel in Helium, Transverse (Used in 24PTH-S and 24PTH-L DSC Analysis) **[See Section P.4.8]**				
178	2.798E-04	0.1114	80	0.05924
267	3.257E-04		260	0.06538
357	3.829E-04		692	0.07255
448	4.547E-04		1502	0.07779
541	5.389E-04			
635	6.326E-04			
730	7.398E-04			
826	8.558E-04			

Bounding B&W 15x15 Fuel in Helium, Transverse (Used in 24PTH-S-LC DSC Analysis) **[See Section P.4.8]**				
162	3.560E-04	0.1265	80	0.05931
254	4.064E-04		260	0.06544
346	4.780E-04		692	0.07261
439	5.639E-04		1502	0.07790
533	6.620E-04			
629	7.733E-04			
725	8.957E-04			
822	1.031E-03			

Bounding Fuel in Helium, Axial (Used in 24PTH-S and 24PTH-L DSC Analysis) **[See Section P.4.8]**			
200	7.596E-04	0.1114	See values above (for all fuels)
300	8.014E-04		
400	8.432E-04		
500	8.781E-04		
600	9.129E-04		
800	9.896E-04		

Bounding B&W 15x15 Fuel in Helium, Axial (Used in 24PTH-S-LC DSC Analysis) **[See Section P.4.8]**			
200	9.081E-04	0.1265	See values above (for BW 15x15 fuels)
300	9.581E-04		
400	1.008E-03		
500	1.050E-03		
600	1.091E-03		
800	1.183E-03		

2. PWR Fuel in Vacuum

Bounding Fuel in a Vacuum, Transverse (Used in 24PTH-S and 24PTH-L DSC Analysis) **[See Section P.4.8]**				
250	1.455E-04	0.1114	80	0.05924
321	1.803E-04		260	0.06538
397	2.249E-04		692	0.07255
478	2.797E-04		1502	0.07779
563	3.463E-04			
651	4.278E-04			
742	5.195E-04			
835	6.234E-04			

Bounding B&W 15x15 Fuel in a Vacuum, Transverse (Used in 24PTH-S-LC DSC Analysis) **[See Section P.4.8]**				
233	1.658E-04	0.1265	80	0.05931
307	2.056E-04		260	0.06544
386	2.556E-04		692	0.07261
470	3.176E-04		1502	0.07790
556	3.931E-04			
646	4.830E-04			
738	5.887E-04			
831	7.087E-04			

Bounding Fuel in a Vacuum, Axial (Used in 24PTH-S and 24PTH-L DSC Analysis)			
200	7.596E-04	0.1114	See values above (for all fuels)
300	8.014E-04		
400	8.432E-04		
500	8.781E-04		
600	9.129E-04		
800	9.896E-04		

Bounding B&W 15x15 Fuel, Axial (Used in 24PTH-S-LC DSC Analysis)			
200	9.081E-04	0.1265	See values above (for BW 15x15 fuels)
300	9.581E-04		
400	1.008E-03		
500	1.050E-03		
600	1.091E-03		
800	1.183E-03		

3. Zircaloy

Temperature (°F)	K (Btu/min-in-°F) [4.11]	ρ (lbm/in^3) [4.11]	C_p (Btu/lb$_m$-°F) [4.11]	
200	0.0109	0.237	80	0.067
300	0.0115		260	0.072
400	0.0121		692	0.079
500	0.0126		1502	0.090
600	0.0131			
800	0.0142			

4. B&W 15x15 Mark B11 M5 Cladding Material

Temperature (°F)	K (Btu/min-in-°F) [4.25]	ρ (lbm/in^3)(1)	C_p (Btu/lb$_m$-°F) [4.25]	
-40	0.0142	0.237		
0	0.0141		31.73	0.0671
100	0.0140		100	0.0685
200	0.0140		200	0.0707
300	0.0140		300	0.0728
400	0.0140		400	0.0749
500	0.0142		500	0.0770
600	0.0144		600	0.0791
700	0.0146		700	0.0812
800	0.0149		800	0.0833
900	0.0153		900	0.0854
1000	0.0157		1000	0.0875
1100	0.0162		1100	0.0897

(1) Assumed to be the same as Zircaloy

5. UO2 Fuel Pellet

Temperature (°F)	K (Btu/min-in-°F [4.11]	ρ (lbm/in^3) [4.11]	C_p (Btu/lb$_m$-°F) [4.11]	
200	5.537E-3	0.396	32	0.056
300	5.038E-3		212	0.063
400	4.622E-3		392	0.068
500	4.270E-3		752	0.072
600	3.968E-3		2192	0.079
700	3.707E-3			
800	3.478E-3			

6. SA-240, Type 304 Stainless Steel [4.2]

Temperature (°F)	K (Btu/min-in-°F)	ρ (lbm/in^3)	C_p (Btu/lb$_m$-°F)
70	0.0119	0.284	0.116
100	0.0121		0.117
150	0.0125		0.119
200	0.0129		0.121
250	0.0133		0.124
300	0.0136		0.125
350	0.0140		0.127
400	0.0144		0.128
500	0.0151		0.130
600	0.0157		0.132
700	0.0164		0.134
800	0.0169		0.135

7. A-36, Carbon Steel (C-Mu-Si) [4.2]

Temperature (°F)	K (Btu/min-in-°F)	ρ (lbm/in^3)	C_p (Btu/lb$_m$-°F)
100	0.0383	0.284	0.1098
200	0.0383		0.1157
300	0.0378		0.1224
400	0.0371		0.1271
500	0.0360		0.1326
600	0.0347		0.1362
700	0.0333		0.1413
800	0.0319		0.1474

8. Aluminum, Type 1100 [4.2]

Temperature (°F)	K (Btu/min-in-°F)	ρ (lb_m/in^3)	C_p (Btu/lb_m-°F)
70	0.185	0.098	0.214
100	0.183		0.216
150	0.181		0.219
200	0.178		0.222
250	0.177		0.224
300	0.175		0.227
350	0.174		0.229
400	0.173		0.232
860	0.173(*)		0.232*

(*) For aluminum Type 1100 the calculated maximum temperatures do not exceed 860°F during transfer accident conditions. The assumption of constant conductivity value at 400°F for temperatures up to 860°F is justified since, for pure aluminum, the conductivity change is approximately 2.5% for range of 400°F – 860°F [4.15]. Therefore, this small change would have a negligible impact on thermal results.

9. Aluminum, Type 6061 [4.2]

Temperature (°F)	K (Btu/min-in-°F)	ρ (lb_m/in^3)	C_p (Btu/lb_m-°F)
70	0.134	0.098	0.213
100	0.135		0.215
150	0.136		0.218
200	0.138		0.221
250	0.139		0.223
300	0.140		0.226
350	0.141		0.228
400	0.142		0.230
860	0.142(*)		0.230(*)

(*) For aluminum Type 6061 the calculated maximum temperatures do not exceed 860°F during transfer accident conditions. The assumption of constant conductivity value at 400°F for temperatures up to 860°F is justified since, for pure aluminum, the conductivity change is approximately 2.5% for range of 400°F–860°F [4.15]. Therefore, this small change would have a negligible impact on thermal results.

10. ASTM B29 Lead [4.3, 4.26]

Temperature (°F)	K (Btu/min-in-°F)
32	0.0279
212	0.0264
572	0.0250

Temperature (°F)	ρ (lb_m/in^3)	C_p (Btu/lb_m-°F)
80	0.4093	0.0308
260	0.4057	0.0315
440	0.4021	0.0327
620	0.3978	0.0339

11. Air [4.4]

Temperature (°F)	K (Btu/min-in-°F)[1]	ρ (lb_m/in^3)	C_p (Btu/lb_m-°F)
71	2.075E-5	4.323e-5	0.240
107	2.199E-5	4.051e-5	0.241
206	2.528E-5	3.443e-5	0.242
314	2.869E-5	2.963e-5	0.243
404	3.139E-5	2.656e-5	0.245
512	3.447E-5	2.361e-5	0.248
602	3.693E-5	2.159e-5	0.251
692	3.929E-5	1.991e-5	0.253
764	4.114E-5	1.875e-5	0.256
800	4.203E-5	1.823e-5	0.257

12. Helium [4.4]

Temperature (°F)	K (Btu/min-in-°F)(1)	ρ (lb_m/in^3)	C_p (Btu/lb_m-°F)
200	1.361E-4	4.81E-6	1.240
300	1.493E-4	4.18E-6	
400	1.635E-4	3.69E-6	
500	1.793E-4	3.31E-6	
600	1.949E-4	2.99E-6	
700	2.094E-4	2.74E-6	
800	2.232E-4	2.52E-6	
900	2.364e-4	2.33E-6	

(1) Thermal properties as listed are for atmospheric pressure, however, thermal conductivities for air and helium are assumed to be constant between atmospheric pressure and 3 Torr, absolute [4.18].

13. 24PTH DSC basket effective thermal properties (See Section P.4.8.3)

24PTH DSC Basket Effective Transverse Thermal Conductivity

24PTH S/L DSC with inserts,		24PTH-S and 24PTH-L DSC without inserts		24PTH-S-LC DSC without inserts	
Temperature (°F)	K (Btu/min-in-°F)	Temperature (°F)	K (Btu/min-in-°F)	Temperature (°F)	K (Btu/min-in-°F)
248	3.676E-03	251	2.759E-03	249	2.103E-03
338	3.949E-03	341	2.952E-03	340	2.249E-03
427	4.275E-03	430	3.195E-03	429	2.432E-03
518	4.615E-03	521	3.442E-03	520	2.619E-03
610	4.958E-03	613	3.697E-03	612	2.811E-03
703	5.292E-03	706	3.945E-03	705	3.000E-03
799	5.522E-03	801	4.119E-03	800	3.134E-03
897	5.618E-03	899	4.217E-03	898	3.208E-03

24PTH DSC Basket Effective Axial Thermal Conductivity

Temperature (°F)	24PTH-S and 24PTH-L DSC with or without inserts K (Btu/min-in-°F)	24PTH-S-LC DSC without inserts K (Btu/min-in-°F)
200	4.197E-04	3.763E-04
300	4.428E-04	3.970E-04
400	4.659E-04	4.177E-04
500	4.851E-04	4.351E-04
600	5.044E-04	4.521E-04
800	5.467E-04	4.902E-04

24PTH DSC Basket Effective Specific Heat and Density

Temperature (°F)	$c_{p\text{-}eff}$ (Btu/lb$_m$-°F)	ρ_{eff} (lbm/in^3)
100	0.0970	0.0928
200	0.1010	
300	0.1043	
400	0.1067	
1000	0.1125	

14. Water properties [4.27]

Temp. (°F)	Thermal Conductivity (BTU/min-in-°F)	Specific Heat (BTU/ lb$_m$ -°F)	Coef. Of Exp., 1/°R	Density (lbm/ft^3)	Dynamic Viscosity (lb$_m$/hr-ft)
44	4.671E-04	1.003	2.56E-05	62.428	3.440
62	4.799E-04	0.999	9.67E-05	62.366	2.613
80	4.919E-04	0.998	1.534E-04	62.241	2.068
98	5.040E-04	0.998	2.01E-04	61.994	1.681
116	5.136E-04	0.998	2.43E-04	61.749	1.396
134	5.216E-04	0.999	2.80E-04	61.445	1.183
152	5.296E-04	1.000	3.14E-04	61.144	1.016
170	5.361E-04	1.002	3.468E-04	60.787	0.883
188	5.409E-04	1.004	3.88E-04	60.375	0.784
206	5.449E-04	1.006	4.05E-04	59.969	0.699
224	5.481E-04	1.009	4.38E-04	59.512	0.629
242	5.505E-04	1.012	4.67E-04	59.006	0.573
260	5.521E-04	1.017	4.978E-04	58.508	0.525
296	5.521E-04	1.028	5.61E-04	57.379	0.448

15. Soil thermal conductivity [4.28]

K (Btu/min-in-°F)	ρ (lb$_m$/in^3)	C_p (Btu/lb$_m$-°F)
0.00024	0.0578	0.191

16. Concrete[1]

Temperature (°F)	K (Btu/min-in-°F) [4.29]	ρ (lb_m/in^3)[1]	C_p (Btu/lb_m-°F) [4.42]	Emissivity [4.30]
70	1.597E-3	0.084	0.22	0.9
1382	7.983E-4			

(1) Conservatively, the properties used herein for the HSM-H walls, roof and/or floor do not include the effects of rebar. Additionally, the ISFSI pad is conservatively modeled as concrete and does not include the effects of rebar. Including the effects of rebar would otherwise increase the effective conductivity of the HSM-H concrete walls, roofs, floor slabs and ISFSI pad.

17. Effective Neutron Shield Thermal Conductivity vs. Circumferential Cask Position

Angle On Cask Body	k_{eff}, Btu/min-in-°F [4.38]	
	Water-Filled	Air-Filled
0°	0.011520	0.000385
30°	0.010848	0.000393
60°	0.010933	0.000408
90°	0.010708	0.000417
120°	0.008868	0.00391
150°	0.008695	0.000322
180°	0.007403	0.000227

18. Borated Aluminum and Boral Thermal Conductivity [See Section P.4.3]

P.4.3 Specifications for Components

The 24PTH DSC design allows for the use of various poison materials. The tables below show the required minimum thermal conductivity for poison materials in the 24PTH DSCs. Boral® has the lowest thermal conductivity compared to the other poison materials. The neutron poison plates must have the following minimum thermal conductivity. The thermal analysis is carried out with the lowest thermal conductivity values for the poison material to bound the various poison materials used.

Boral

Temperature (°F)	K (Btu/min-in-°F)
100	0.0761
500	0.0699
774	0.0699(*)

Enriched Borated Aluminum

Temperature (°F)	K (Btu/min-in-°F)
68	0.136
212	0.141
392	0.149
774	0.149*

Natural Borated Aluminum

Temperature (°F)	K (Btu/min-in-°F)
68	0.120
212	0.144
482	0.148
571	0.148
774	0.148*

Notes:

* Assumed values.

P.4.4 Thermal Analysis of HSM Model 102 and HSM-H with 24PTH DSC

The maximum decay heat loads that are considered for the NUHOMS®-24PTH-S and 24PTH-L DSCs as described in Section P.4.1 are 40.8 kW and 31.2 kW.

The maximum heat load allowed in the 24PTH-S-LC DSC is 24 kW. The HSM Model 102 is designed for a maximum heat load of 24 kW from a NUHOMS®-24P DSC as described in Section 8.1.3. There is no change in this thermal analysis due to the storage of 24PTH-S-LC inside HSM Model 102. The 24PTH-S-LC and 24P DSCs have same heat loads and analytically equivalent outer shell geometry (outside diameter and length), therefore the shell temperatures calculated in Section 8.1.3.1 for 24P DSC in HSM Model 102 are also applicable to 24PTH-S-LC DSC. The DSC shell temperatures are summarized in Table P.4-34. These shell temperatures are used in the 24PTH-S-LC DSC model in Section P.4.8 to calculate the basket and fuel temperatures.

P.4.4.1 Ambient Temperature Specification

Ambient temperatures in the range of 0-100°F are considered as normal storage conditions. A maximum day temperature of 117°F is considered as off-normal, hot storage condition. A 24-hour average ambient temperature of 105°F is conservatively used for the off-normal steady state analysis, based on the 102°F calculated in Section M.4.5 [4.38]. The lowest off-normal ambient temperature is considered to be -40°F.

P.4.4.2 Thermal Analysis of HSM-H with 24PTH DSC

The HSM-H is an improved version of the HSM Model 102, described in the FSAR, with the following unique design features to enhance its heat rejection and shielding capabilities:

- Module internals optimized for heat transfer by enhanced DSC support structure design,
- Use of slotted plates and holes in the DSC support rails to increase airflow at the bottom portion of canister,
- Increased height of the module to increase module cavity height resulting in an increased stack height and minimum flow resistance in the module cavity,
- Use of finned side heat shields option at high heat loads to improve convection heat transfer by increasing surface area of heat shield, and
- Use of louvered top heat shield to minimize flow resistance.

The design of 24PTH DSC shell, top and bottom cover plates and shield plugs is similar to the other NUHOMS® canisters like 24P. The design of the basket is similar to the licensed TN-68 [4.43] with additional design features to greatly improve the heat rejection capability of the canister as follows:

- Use of thick aluminum plates results in uninterrupted radial conduction path,

- Use of slotted aluminum and poison plates with interlocking feature to form "eggcrate" type basket that minimizes gaps between components,

- Offsets in the structural steel insert plates (straps) to eliminate hot spots, and

- Use of aluminum and steel transition rails with aluminum inserts (depending upon the DSC type and heat loads) to transfer heat from the basket interior regions to the DSC shell.

The HSM-H is designed to provide an independent, passive system with substantial structural capacity to ensure safe storage of spent fuel assemblies in NUHOMS®-24PTH DSCs.

Ambient air enters the HSM-H through ventilation inlet openings in the lower part of the HSM-H side walls and circulates around the DSC and the side heat shields. Warm air passes through the top heat shield and exits the HSM-H through the outlet openings in the upper part of the HSM side walls. Decay heat is rejected from the DSC to the HSM-H air space by convection and then is removed from the module by natural air circulation. Heat is also radiated from the DSC surface to the heat shields and module walls, where again natural air circulation and conduction through the walls remove the heat. Typical flow paths are shown in Figure P.4-1.

A metal heat shield is placed axially around the top and sides of the 24PTH DSC to shield the HSM-H concrete surfaces above and to the side of 24PTH DSC from direct thermal radiation effects and to significantly increase the surface area for convection cooling inside the HSM-H cavity. The concrete surfaces above and to the side of the 24PTH DSC are subjected to thermal radiation from the backside of the heat shield. However, the radiation is emanated at substantially lower temperature than the direct thermal radiation from the 24PTH DSC surfaces.

This analysis determines the temperature distribution on the DSC shell, which is used to calculate the basket and fuel peak cladding temperature in a detailed model of the DSC basket (see Section P.4.6). The HSM-H wall temperatures are also determined in this analysis.

The HSM-H roof and front wall are the primary concrete surfaces conducting heat to the outside environment. For the analytical purpose of calculating maximum temperatures, an HSM-H centered in a group of HSM-Hs, each loaded with a 24PTH DSC, is assumed. Rows of modules are assumed to exist back-to-back for this model.

For the purpose of calculating maximum concrete temperature gradients, a stand-alone single HSM-H, with no adjacent modules is conservatively assumed. To maximize the temperature gradients in the HSM-H concrete structure, an ambient temperature of -40°F is considered for the off-normal cold storage condition. To consider the maximum thermal stresses in the structural evaluation, the temperature distribution in the HSM-H is calculated at 0°F and 100°F ambient temperatures for normal conditions with a maximum decay heat load of 40.8 kW.

Since the HSM-H is located outdoor, there is a remote probability that the air inlet or outlet openings become blocked by debris from events such as flooding, high wind, and tornados. The perimeter security fence around ISFSI and the location of the air inlet and outlet openings reduces the probability of such an accident. A complete blockage of all air inlets and outlets simultaneously is not a credible event. However, to bound this scenario, analysis is carried out assuming complete blockage of the inlet and outlet vents as an accident case.

The temperature distributions for the normal and off-normal conditions are determined using steady-state models. For the accident case, a transient model is utilized that has a necessarily coarser mesh than the steady state model to preclude possible computational resource problems.

P.4.4.3 HSM-H Air flow Analysis (Stack Effect Calculations)

The HSM-H airflow analysis (stack effect calculations) uses the same methodology as is presented in Section 8.1.3.1. The temperature difference (ΔT), and the height difference (Δh) between the HSM-H vent inlet and outlet creates a "stack effect" to drive air through the HSM-H. The ventilation air has sufficient velocity to provide adequate cooling for the 24PTH DSC so that the spent fuel cladding temperature remains below acceptable limits. The ventilation flow paths inside the HSM-H are designed such that for the required cooling airflow rate, the stack effect pressure difference (ΔP_s) is in equilibrium with the total dynamic pressure difference (ΔP_f). The total dynamic pressure difference within the HSM-H is calculated to include the effects of plenum losses, expansion / contraction losses due to vent area changes, losses due to flow direction changes, orifice effect losses, inlet / outlet vent dynamic losses, etc. Equations are derived from [4.40] to describe the stack effect.

The pressure loss due to friction is calculated by summing the individual friction losses through the air inlet opening, the air outlet openings and the flow path through the HSM-H cavity.

$$\sum_i \frac{k_i}{n_i^2 \cdot A_i^2}$$

where:

k_i = loss coefficient,
A_i = flow area,
n_i = number of divergent paths.

Standard loss coefficients for entrances, exits, screens, elbows, slots, friction, flow over curved enclosures, flow between parallel plates, flow path expansions and contractions are taken from [4.33, 4.39]. The total pressure drop due to the flow losses is determined by:

$$\Delta P_f = \frac{\dot{m}^2}{2 \cdot \overline{\rho}} \cdot \sum_i \frac{k_i}{n_i^2 \cdot A_i^2},$$

where:

$\dot{m}$ = mass flow rate (lbm/s),
$\overline{\rho}$ = average density (lbm/ft^3).

The entering air mass flow rate is calculated using the following equation based on the assumption that all the decay heat energy is dissipated only by convection to the circulating air within the HSM-H.

$$\dot{m} = \frac{\dot{Q}}{C_p * (T_{exit} - T_c)},$$

where:

$\dot{Q}$ = The amount of energy dissipated (Btu/s),
C_p = Average specific heat (Btu/lbm-°F),
T_c = Ambient temperature (°F), and
T_{exit} = Exit air temperature (°F).

The total pressure drop from stack effect is calculated as follows:

$$\Delta P_S = g \cdot h \cdot \rho_0 \cdot \left(1 - \frac{T_{amb}}{T_S}\right),$$

where:

ΔP_S = pressure difference due to stack effect (lbf/ft^2),
h = stack height (ft),
g = acceleration due to gravity (ft/min),
ρ_0 = air density at ambient conditions (lbm/ft^3),
T_{amb} = ambient temperature (°R), and
T_S = stack average temperature (°R).

The above equations are solved iteratively to determine values of T_S and $\dot{m}$ at specific values of $\sum_i \frac{k_i}{n_i^2 \cdot A_i^2}$ for $\Delta P_f \leq \Delta P_S$. The flow rate calculation accounts for flow separation around the circumference of the 24PTH DSC which then consolidates and flows through the outlet vent. Using the calculated values of $\dot{m}$, the HSM-H bulk air temperatures surrounding the 24PTH DSC are determined assuming isotropic heat flow from 24PTH DSC canister surface so that temperature of the air increases linearly across the circumference of the canister shell surface. It is conservatively assumed that 100% of the decay heat is removed by convection to the bulk air surrounding the 24PTH DSC.

The temperature rise (ΔT_{HSM-H}) from the HSM-H air inlet (ambient temperature) to the HSM-H outlet (exit air temperature) is given by the following equation (Section 8.1.3.1).

$$\Delta T_{HSM-H} = \left[\frac{\dot{Q}^2}{2gh} * \frac{T_s}{C_p^{\,2} * \overline{\rho} * \rho_s * \Delta T_{avg}} * \Sigma \frac{K_{Ei}}{(A_{Ei})^2}\right]^{1/2}$$

Where:

T_s = Stack average air temperature (°R),
ΔT_{avg} = Change in temperature across the stack height (°R), = T_s-T_c,
T_{avg} = (T_c + T_{exit}) / 2 (°R),
$\overline{\rho}$ = Average density of air at T_{avg} (lbm/in^3),
ρ_s = Stack average density of air at T_s (lbm/in^3),
h = vertical distance between the entrance and exhaust (in), and

The above equation is solved by an iterative method, because the average temperature is initially unknown.

The exit air temperature is calculated as follows:

$T_{exit} = T_c + \Delta T_{HSM\text{-}H.}$

The DSC outer surface is divided into eight equal regions along the DSC circumference in this analysis. These regions are shown in Figure P.4-2.

It is assumed that the temperature rise in each region is equal, so that:

$$T_i = T_{i-1} + (\Delta T_{HSM-H}/8),$$

where:

T_i = Temperature of air leaving region *i*.

It is assumed that the air temperature entering the first region is equal to the average of the ambient temperature and the temperature of the first region. In this case, the temperature of the air leaving region 8 is equal to the exit air temperature.

The temperature used to determine the properties inside the HSM-H cavity is called the stack average temperature. The following equation determines the stack average temperature.

$$T_s = \frac{\sum_0^i (T_i * V_i)}{\sum_0^i (V_i)},$$

where:

V_i = Volume of air region = $A_i * L_{DSC}$,

A_i = HSM-H cavity cross sectional area – DSC cross sectional area.

A summary of the steady state and transient cases considered for the HSM-H analysis are listed below:

Summary of the Steady State Cases considered for HSM-H Thermal Analysis

Decay Heat Load (kW)	Case Numbers	Operating Condition	Ambient Temperature (°F)
40.8	1	Off-Normal	117
	2	Normal	100
	3	Normal	0
	4	Off-Normal	-40
31.2[1]	5	Off-Normal	117
	6	Off-Normal	-40
24	7	Off-Normal	117
	8	Off-Normal	-40

(1) The analysis for 31.2 kW case was performed with and without side heat shield fins to demonstrate that fins are not required for heat loads of 31.2 kW or less.

Summary of the Transient Cases considered for HSM-H Thermal Analysis

Decay Heat Load (kW)	Case Numbers	Operating Condition	Ambient Temperature (°F)
40.8	9	Accident	117
	10	Accident	-40

The total equivalent loss coefficients calculated for the steady state cases for the HSM-H regions are:

Decay Heat Load (kW)	Ambient Temperature (°F)	Total equivalent loss coefficient K (ft^{-4})
40.8	-40	0.0710
	0	0.0714
	100	0.0724
	117	0.0724
31.2	-40	0.0711
	117	0.0726
24	-40	0.0713
	117	0.0728

Using these loss coefficients in equation for ΔT_{HSM-H}, the exit and stack air temperature for the normal and off-normal cases are calculated.

The bulk air temperatures at each of the eight specified regions on the DSC are shown in Table P.4-1 for the range of ambient conditions. These bulk air temperatures are used in the subsequent HSM-H analyses to calculate the temperatures throughout HSM-H and 24PTH DSC shell.

P.4.4.4 Description of the Thermal Model of HSM-H with 24PTH DSC

A half symmetric, three dimensional, ANSYS [4.31] finite element model of the HSM-H loaded with 24PTH DSC is shown in Figure P.4-3.

The thermal model consists of SOLID70 conduction elements that simulate concrete and steel support structures of the HSM-H, and SHELL57 elements superimposed on SOLID70 elements, as required, to model radiating surfaces using MATRIX50 super elements. As such, radiation between the DSC shell, heat shields, and HSM-H walls is modeled using the ANSYS /AUX12 methodology. For elements wherein radiation is not applicable, the SHELL57 elements are unselected prior to solving the model. Additionally, to reduce the number of the nodes associated with the model's super-elements, the web of the supporting beam is modeled using only SHELL57 elements. As such, conservatively, radiation is not applied on the web of the supporting beam. This methodology is valid since the supporting beam's web greatly shields the support steel from the DSC radiation via its own flanges. The properties and dimensions of the support beam, such as the thickness of the web are given as real constants to the appropriate SHELL57 elements.

The base plate of the side heat shields are modeled as flat plates. Convection from the fins attached to the side shields is modeled using an equivalent convection coefficient. The purpose of adding fins on the side heat shield is to provide more surface area for the convection.

This analysis assumes that the side heat shield is fabricated completely out of Al-1100. Since the main purpose of the side heat shield is to protect the concrete walls against direct thermal radiation from the DSC, reducing the side heat shield conductivity from Al-1100 to stainless steel does not have any significant effect on the temperature distribution within the HSM-H, provided that the emissivity values of the front and back side of the heat shield remain unchanged. As such, the emissivity values used for the side heat shield are the same as those used for stainless steel.

The top shield is a louvered design that is supported from the ceiling of the HSM-H. The louver top shield design is modeled as a flat plate with an effective convection coefficient.

The lower part of the HSM-H sidewall is offset by 6" toward the HSM-H cavity. The thickness of the offset wall is 18". To simplify the analysis, the HSM-H sidewall is modeled as a straight, 12" thick wall without the 6-inch offset. The modeling simplification has an insignificant effect on resultant temperature distribution output. This modeling simplification is justified since majority of the heat removal is via convection, and only a small portion of the heat removal is via conduction through the walls. Modeling of this short segment of the HSM-H wall thinner than it is in actuality does not impact the overall results.

Boundary Conditions

The maximum off-normal ambient temperature of 117°F is considered. In the thermal analysis, a 24-hour average ambient temperature of 105°F, calculated in Section M.4.5 [4.38] is used as the ambient air temperature for the off-normal steady- state analyses.

Convection Coefficients

The correlation for heat transfer convection coefficients over the HSM-H surfaces, including the HSM-H vertical flat surfaces, horizontal surfaces, the side finned heat shield, the top heat shield and the horizontal DSC cylinder surface are determined in Section P.4.9.

The circumference of the DSC model is divided into eight regions. The first of these regions covers the area between the supporting rails from -90 to -64.4 degree angle. The second region begins at the center line of the supporting beam at -60 degree angle and extends to the -45 degree angle. For conservatism, the surface area of the DSC shell from -64.4 to -60 degrees (all located above the upper edge of the slots in the slotted bar) are modeled as a dead zone with no free convection. The other DSC circumferential regions are equivalent 22.5 degree arcs. Figure P.4-2 shows the regions of the DSC lower half. The bulk temperatures for the DSC circumferential regions around the DSC are calculated in Section 4.4 and listed in Table P.4-1.

For the space between the HSM-H sidewall and the HSM-H side shield, free convection correlation for a narrow channel is also presented in Section P.4.9.

Convection and radiation from the HSM-H roof and the front wall to the ambient are combined as a total effective coefficient as discussed in Section P.4.9.3.

Solar Heat Load

Insolation is modeled on the surfaces of the HSM-H roof and front wall that are exposed to the ambient. The value of the solar heat flux is taken from [4.32] averaged over a 24-hour period. The insolation is applied as a constant heat flux over the SURF152 elements and are superimposed on the SOLID70 elements of the HSM-H roof and front wall. The absorptivity of the concrete surface is 0.73 - 0.91 at 300K [4.30]. For conservatism, a solar absorptivity of 1 is considered for the exposed HSM-H concrete surfaces. The values of the applied heat fluxes are listed below :

HSM-H Surface	Insolation [4.32] (gcal/cm^2)	Averaged over 24 hr (Btu/hr-in^2)
HSM-H roof	800	0.8537
HSM-H front wall	200	0.2134

Insolation is conservatively neglected for the minimum ambient temperatures of 0° and -40°F.

Since the HSM-H's are located side by side, the worst case for the maximum temperatures occurs when DSC's with the maximum decay heat load are stored in adjacent HSM-H's. To evaluate this worst case, adiabatic boundary conditions are applied over the outer surfaces of the HSM-H side and back walls (to bound for a back-to-back and single row HSM arrays).

The soil temperature of 70°F is assumed for depths of 10' and below the HSM-H basemat for hot conditions. The soil temperature for the cold condition (0°F or -40°F) is assumed to be 45°F. These assumptions are consistent with the assumptions used in the standardized HSM design in Section 8.1.3. The HSM-H basemat is assumed to be a 4' thick concrete slab. Due to the low conductivity of concrete and soil, the model is insensitive to the thickness of the basemat / soil and the soil temperature. The HSM-H concrete surfaces are reinforced with steel rebars. Conservatively, the thermal conductivity used herein for the HSM-H concrete walls, roof and base slab does not include the effect of rebar.

Heat load

The heat flux used in the HSM-H thermal model is determined for a DSC heat load of 24, 31.2 or 40.8 kW. The decay heat is distributed over the entire internal cavity of the 24PTH DSC. Use of the entire 24PTH DSC cavity volume and exclusion of an axial peaking factor for the HSM-H thermal analysis is consistent with the methodology given in Section 8.1.3 which is based on the test data contained in [4.21]. The reference test data for cylindrical casks show that the measured surface temperature profiles are relatively flat over the entire length, indicating that the heat flux is nearly uniform over the surface and axial peaking is not affecting the surface temperature distribution. One reason for the relatively flat temperature profiles is the high thermal conductivity of the 24PTH DSC basket, rails and shell materials. The resulting heat generation is therefore more representative of the manner in which heat is actually rejected to the HSM-H air space by the 24PTH DSC. The active fuel length of 144 inches and the peaking factor of 1.11 are conservatively used in the thermal analysis of the 24PTH DSC basket presented in Section P.4.6 for the evaluation of the peak fuel clad temperature. The decay heat flux is calculated as follows:

$$\text{Decay heat flux} = \frac{Q}{\pi D_i L} \quad \text{Btu/hr-in}^2$$

where,

Q = decay heat load (24, 31.2, or 40.8 kW)
Di = inner DSC diameter = 66.19"
L = DSC cavity length = 169.6"

To maximize the applied heat flux, the minimum cavity length of 169.6 inches which bounds the 24PTH-S and 24PTH-L or –S-LC DSCs, is used in the above equation. The calculated decay heat flux values are as follows:

Heat Load (kW/DSC)	Decay Heat flux (Btu/hr/in^2)
24	2.322
31.2	3.019
40.8	3.948

The thermal analysis of a typical HSM-H is performed for a loaded 24PTH DSC located in the interior of a multiple module array with a 24PTH DSC present in the two adjacent HSM-Hs. The HSM-H top and front surfaces are modeled as exposed to the prevailing ambient conditions in this model. The side and back surfaces are modeled as being adiabatic in order to simulate the adjacent modules.

Single/End HSM-H model

An additional model was constructed for the specific purpose of calculating the maximum concrete gradients. For this model, the thermal analysis is performed for a free standing HSM-H with the top and front, as well as the back and side surfaces exposed to the prevailing ambient conditions.

The maximum temperature gradient occurs in a single (stand-alone) or an end HSM-H wherein one or two of the HSM-H sidewalls are exposed to the cold ambient temperature. To bound the maximum temperature gradient across the HSM-H concrete walls, the associated finite element model is modified such that the three feet thick shield walls are added to the side and back walls of the HSM-H. An average gap of 0.125" is considered between the shield walls and the HSM-H module. The single/end HSM-H model simulates a single HSM-H module exposed to –40°F ambient temperature without solar heat flux. The finite element model of the single HSM-H module is depicted in Figure P.4-4.

P.4.4.5 Description of the HSM-H Blocked Vent Model

To determine the maximum temperatures of the HSM-H and the DSC shell for the blocked vent accident case, the finite element model of the HSM-H is modified to a transient model.

The effective thermal conductivity of air is determined using the methodology described in Section P.4.8.4. This effective thermal conductivity is applied to the transient model to simulate the

convection within the closed HSM-H cavity during blockage of the air inlet and outlet vents. The mesh size of the model is increased slightly to preclude possible computer resource problems for the transient run.

The DSC basket and associated fuel assemblies for the transient case are modeled as a homogenized material with suitable effective properties as determined in Section P.4.8.3. Heat generating boundary conditions are applied uniformly on all of the elements representing the DSC contents. The amount of generated heat per unit volume of the DSC contents is calculated as follows:

$$\text{Heat generation rate} = \frac{Q}{(\pi/4\ D_i^2\ L)} \quad \text{Btu/hr-in}^3$$

where:

Q = decay heat load (24, 31.2, or 40.8 kW)
Di = inner DSC diameter = 66.19"
L = DSC cavity length = 169.6"

The heat generating rates for 40.8, 31.2, and 24 kW decay heat are shown in the table below:

Heat Load, kW/DSC	Heat Generation Rate $\left(\frac{\text{Btu}}{\text{hr}-\text{in}^3}\right)$
40.8	0.239
31.2	0.182
24	0.140

The nodes of the DSC contents are disconnected in the axial direction from the DSC shield plugs to simulate the uniform heat generation over the radial surface of the DSC.

The initial conditions for the blocked vent accident case are identical to the boundary conditions applied for the off-normal case with a 105°F daily average temperature (117°F max. daylight temperature) and maximum solar heat flux. The emissivity of the support structure is assumed to be 0.3. The finite element model utilized for the transient runs is depicted in Figure P.4-5. This model assumes the maximum decay heat load of 40.8 kW to bound the maximum temperatures within the HSM-H for the accident conditions.

P.4.4.6 Description of Cases Evaluated for the HSM-H

The HSM-H thermal analyses are performed for the design basis normal ambient air temperatures defined in Section P.4.4.1.

A summary of the cases considered for HSM-H thermal analysis is presented in Section P.4.4.3.

P.4.4.7 HSM-H Thermal Model Results

P.4.4.7.1 Normal and Off-normal Operating Condition Results

Temperature distributions for the normal and off-normal cases are show in Figure P.4-6 through Figure P.4-13. The maximum component temperatures for the normal and off-normal cases are listed in Table P.4-2, Table P.4-3, and Table P.4-4. Temperature distributions for the single HSM-H which provides maximum temperature gradients in concrete walls, are shown in Figure P.4-16.

As seen from Table P.4-2 and Table P.4-3, the HSM-H concrete and DSC shell temperatures without the fins on the side heat shield for 31.2 kW are bounded by the case with the fins for 40.8 kW decay heat load. Therefore, fins are not required on the side heat shields in the HSM-H, if the total heat load is 31.2 kW or less. This is summarized in Table P.4-43.

P.4.4.7.2 Accident Condition Results

Temperature distributions for the blocked vent accident case with 40.8 kW decay heat load at 38.5 hours after blockage of the vents are shown in Figure P.4-14. The maximum component temperatures for the blocked vent accident case are listed in Table P.4-5.

Figure P.4-15 shows the time-temperature history of HSM-H components for this transient.

The maximum component temperatures for these cases are listed in Table P.4-6. Figure P.4-17 provides maximum temperature gradients in concrete walls during accident conditions.

P.4.4.8 Evaluation of HSM-H Performance

The thermal performance of the HSM-H is evaluated under normal, off-normal, and accident conditions of operation as described above and is shown to satisfy all the temperature limits and criteria. The DSC shell temperatures calculated here, are used in the DSC basket and fuel cladding models as a boundary condition in Section P.4.6. The results show that all the basket and fuel cladding material temperature limits are satisfied. The results of the HSM-H temperatures are used in Section P.3 to show that thermal stresses in the HSM-H are also within these allowables.

The results of the 117°F ambient blocked vent condition show that the maximum concrete temperature at the end of 38.5 hours in the blocked vent accident is 405°F. This is above the 350°F limit given in NUREG 1536 [4.42] for accident conditions. To account for the effect of higher concrete temperature on the concrete compressive strengths, the structural analysis of HSM-H concrete components in Section P.3 is based on 10% reduction in concrete material properties. Testing will be performed to document that concrete compressive strength will be greater than that used in the structural analysis documented in Section P.3.

P.4.5 Thermal Analysis of Transfer Casks with 24PTH DSC

The NUHOMS® OS197FC Transfer Cask (TC), OS197/OS197H TC or Standardized TC are used to transfer loaded 24PTH DSCs between the fuel building and the ISFSI. The design of the OS197FC TC is identical to the design of the OS197 or OS197 TCs with the modification to the cask top lid as described in Section P.1. Therefore, the TC thermal models described in Section P.4.5.2 and P.4.5.3 are applicable to OS197, OS197H, and OS197FC TCs. The analyses results for OS197FC TC in Section P.4.5.5, (excluding P.4.5.5.2), and the first accident case described in Section P.4.5.5.3 are also applicable to OS197 and OS197H TCs. Note that the OS197 and OS197H TCs are only allowed with a 24PTH-S or –L DSC with 31.2 kW or less heat load and aluminum inserts in R45 transition rails in the basket.

The following cask/DSC decay heat loads are analyzed herein:

- The NUHOMS® OS197FC TC is designed and analyzed for transferring 24PTH-S and 24PTH–L DSCs with total heat loads of 40.8 kW (basket with aluminum insert) and 31.2 kW (basket without inserts),
- The NUHOMS® OS197/OS197H TC is designed and analyzed for transferring 24PTH-S and 24PTH–L DSCs with total heat load of 31.2 kW (basket with aluminum inserts), and
- The NUHOMS® Standardized TC is designed and analyzed for transferring 24PTH-S-LC DSC with a total heat load of 24 kW (basket without aluminum inserts).

P.4.5.1 Thermal Analysis of the NUHOMS® Standardized Cask with 24PTH DSC

The thermal analysis of the NUHOMS® Standardized TC for a 24 kW total heat load was performed in Section 8.1.3 and the DSC shell temperatures reported in Section 8.1.3 are summarized in Table P.4-39. These DSC shell temperatures are also applicable to the 24PTH-S-LC DSC transfer in the Standardized TC because the maximum heat load is the same and the DSC diameters and the total lengths are also the same.

P.4.5.2 Thermal Model of 24PTH DSC in the OS197FC TC

The NUHOMS® OS197FC TC is used to transfer the 24PTH-S and –L DSCs between the fuel building and the HSM-H at the ISFSI site. The thermal performance of these TCs with 24PTH-S and-L DSCs is evaluated under normal, off-normal, and accident conditions of operation. The longer 24PTH–L DSC has larger inner cavity and surface area to distribute and dissipate heat as compared to the shorter 24PTH-S DSC. Therefore, the 24PTH-S DSC is used to bound the 24PTH-L DSC. The thermal evaluation is conducted for a range of decay heat load, ambient conditions, and cask configurations.

The SINDA/FLUINT™ [4.36] and Thermal Desktop® [4.37] computer codes are used to model the OS197FC TC (or OS197/OS197H TC) and the 24PTH-S and –L DSCs to determine the temperature distribution in the TC and the DSC shell. These DSC shell temperatures are then used in the model of the 24PTH-S and –L DSCs to determine the basket and fuel cladding temperatures. A brief description of the computer code is provided below.

P.4.5.2.1 SINDA/FLUINT™ Thermal Desktop® General Code Description

The Thermal Desktop® and SINDA/FLUINT™ computer programs are designed to work together to provide the functions needed to build, exercise, and post-process a thermal model. The Thermal Desktop® computer program is used to provide graphical input and output display functions, as well as computing the radiation exchange conductors for the defined geometry and optical properties. Thermal Desktop® is designed as a module to the AutoCAD™ application. As such, all of the CAD tools available for generating geometry within AutoCAD™ can be used for generating a thermal model. In addition, the use of the AutoCAD™ layers tool presents a convenient means of segregating the thermal model into its various elements.

The SINDA/FLUINT™ computer program is a general-purpose code suitable for either finite difference or finite-element models. SINDA/FLUINT™ has been validated for simulating the thermal response of spent fuel packages.

The Thermal Desktop® and SINDA/FLUINT™ codes provide the capability to simulate steady state and transient temperatures using temperature dependent material properties and heat transfer via conduction, convection, and radiation. Complex algorithms may be programmed into the solution process for the purposes of computing heat transfer coefficients as a function of the local geometry, gas thermal properties as a function of species content, temperature, and pressure, or, for example, to estimate the effects of buoyancy driven heat transfer as a function of density differences and flow geometry.

P.4.5.2.2 OS197FC TC SINDA/FLUINT™ Thermal Model

The thermal model used to simulate the thermal response of the OS197FC TC represents a 180° segment of the cask. The use of a 180° model permits the accurate simulation of the temperature distribution within the cask when the cask is in the horizontal orientation and the axis of the DSC is eccentric to that of the cask. Figure P.4-20 presents a perspective view of the thermal model of the cask and the DSC assembly (i.e., the cask body, closure lid, DSC, and spacer). The model uses approximately 5,100 nodes, 3,300 solids, and 2,700 planar elements to define the cask body geometry and to provide thermal resolution. The modeling divides the cask circumference into 15° segments with axial lengths of 8 inches or less. As seen in Figure P.4-20 the thermal model captures the fact that the structural shell increases from 1.5-inches thick to 2-inches thick at the upper portion of the cask.

Heat transfer across the water filled neutron shield is computed using the effective thermal properties from Section M.4.9 [4.38]. Under accident conditions where the neutron shield is assumed to be filled with air, radiation exchange is added to the appropriate effective thermal conductivity values from Section M.4.9 [4.38]. Heat transfer from the outer skin of the neutron shield is computed using the free convection correlation and thermal radiation exchange.

Figure P.4-21 illustrates the thermal modeling used for the cask closure lid and the spacer. The cask closure lid model utilizes approximately 600 thermal nodes, 325 solids, and 474 planar surfaces. For the spacer, the model uses 24 planar surfaces and 52 nodes to represent the stainless steel plates that make up the spacer. The analysis is performed to verify that the model is mesh independent.

P.4.5.2.3 DSC Steady State and Transient Conditions Thermal Models

Two thermal models (steady state and transient conditions) for the 24PTH DSC are used in this analysis. The first thermal model (see Figure P.4-22) includes only the DSC shell and ends. Approximately 970 nodes and 940 solids are used. The decay heat loading from the DSC is applied as a heat flux only to the cylindrical surface of the DSC. This thermal model is used for steady-state analyses where the thermal mass of the fuel basket is unimportant. Given the uniform application of the decay heat flux to the cylindrical surfaces, the thermal model will yield conservative temperatures for the DSC shell for normal conditions. A separate, detailed model of the DSC and its basket uses the computed shell temperatures as boundary conditions for the determination of the peak temperatures for the fuel cladding and other basket components. The analyses are performed to verify that these models are mesh independent.

Given the significant thermal mass of the DSC basket, the determination of the transient performance of the OS197FC TC requires that the thermal mass of the fuel basket be simulated. Figure P.4-23 illustrates the thermal model of the DSC and its basket. The modeling for the DSC shell and ends used for transient analysis are the same as those presented in Figure P.4-22. However, in addition to these components, the fuel basket is simulated using a solid cylinder with anisotropic thermal conductivity from Section P.4.2 and evenly distributed volumetric heat generation.

P.4.5.2.4 Natural Convection Heat Transfer Coefficients

Natural convection from vertical surfaces are computed using Equations 6-39 to 6-42 of [4.34], where the characteristic length is the height of the surface. These equations are applicable over the range $1 < Ra < 10^{12}$ as follows:

$$Nu^T = \overline{C}_L Ra^{1/4}$$

$$\overline{C}_l = \frac{4}{3}\left[\frac{0.503}{\left(1+(0.492/Pr)^{9/16}\right)^{4/9}}\right]$$

$$Nu_L = \frac{2.8}{\ln\left(1+2.8/Nu^T\right)}$$

$$Nu_t = C_t^V Ra^{1/3}$$

$$C_t^V = \frac{0.13\,Pr^{0.22}}{\left(1+0.61\,Pr^{0.81}\right)^{0.42}}$$

$$Nu = \frac{h_c L}{k} = \left[(Nu_L)^6 + (Nu_t)^6\right]^{1/6}$$

$$Ra = \frac{\rho^2 g_c \beta L^3 \Delta T}{\mu^2} \times Pr$$

where:

h_c = convection coefficient	Nu = Nusselt number
g_c = gravitational acceleration	β = coefficient of thermal expansion
ΔT = temperature difference	ρ = density of air at the film temperature
μ = dynamic viscosity	Pr = Prandtl number
L = characteristic length	k = thermal conductivity of air at film temperature
Ra = Rayleigh number	h_c = convection coefficient

Calculation of the convection coefficient between the cask's cylindrical surfaces and the ambient environment is computed using Equation 3-43, of [4.27]. The characteristic length, D, is the outer diameter of the cask (i.e., 85.5"). This equation, applicable for $10^{-5} < Ra < 10^{12}$, is as follows:

$$Nu = \frac{h_c D}{k} = \left\{ 0.60 + \frac{0.387 Ra_D^{1/6}}{\left[1 + (0.559/Pr)^{9/16}\right]^{8/27}} \right\}^2$$

Natural convection from horizontal surfaces is computed from Equations 3.34, 3.35, and 3.36 of [4.27], where the characteristic dimension (L) is equal to the plate surface area divided by the plate perimeter. For a heated surface facing upwards or a cooled surface facing downwards and Ra > 1:

$$Nu = \frac{h_c L}{k} = \left[(Nu_L)^{10} + (Nu_t)^{10} \right]^{1/10}$$

$$Nu_L = \frac{1.4}{\ln\left(1 + 1.677/\left(\overline{C}_L Ra^{1/4}\right)\right)}$$

$$Nu_t = 0.14 Ra^{1/3}$$

For a heated surface facing downwards or a cooled surface facing upwards and $10^5 < Ra < 10^{10}$ as follows:

$$Nu = Nu_L = C_h Ra^{1/5}$$

$$C_h = \frac{0.527}{\left(1 + (1.9/Pr)^{9/10}\right)^{2/9}}$$

P.4.5.2.5 Neutron Shield Effective Thermal Conductivity

Effective thermal conductivity of water within the neutron shield of the OS197/OS197H TC was evaluated for water and air filled cases, respectively. These values are also applicable to OS197FC TC. The table values from Section M.4-9 [4.38] are interpolated to yield values at the intermediate angles.

P.4.5.3 Analysis Cases for OS197FC TC with 24PTH DSC

The thermal performance of the NUHOMS® OS197FC TC was evaluated under normal, off-normal, and accident conditions of operation. The maximum heat load permitted when there is no time limit on DSC transfer operations was determined by using steady state conditions. If the results of steady state analysis were not acceptable relative to the fuel cladding or material temperature limits, then a transient analysis was performed to determine the time limit on DSC transfer operations for these heat load conditions. The time limit for transfer of the DSC is defined as the time after the annulus is completely drained of water and initiation of bolting of transfer cask top cover plate to the cask with a loaded DSC in the TC cavity until the time the bolted cask top cover is removed to expose the top of loaded DSC and the cask/DSC annulus to ambient conditions.

The geometry of OS197FC TC is identical to OS197/OS197H TCs except the NUHOMS® OS197FC TC includes provisions for the use of external fan for air circulation in the cask DSC annulus if the time to transfer the 24PTH-S or –L DSCs from the TC to the HSM exceeds the specified time limit as described further in Section P.4.5.5.1. See Section P.1 for OS197FC TC description.

The thermal performance of the OS197FC TC was evaluated for normal (i.e., 100°F and 0°F) and off-normal (i.e., 117°F) ambient temperatures, with and without insolation, and for various heat loads. Three accident scenarios are also evaluated for the OS197FC TC as described in Section P.4.5.5.3. Likewise, the available time to initiate air circulation via external fan or to restore the air circulation in case of system failure was determined. Table P.4-7 provides an overview of each load case analyzed.

The temperature profiles of the TCs and the 24PTH DSC shell and top and bottom cover plates and shield plugs obtained from the results of the OS197FC and Standardized TC analysis with 40.8 kW, 31.2 kW, and 24 kW heat loads are used in thermal stress calculations.

P.4.5.4 Standardized TC Thermal Model Results

The maximum temperature results for the 24PTH-S-LC DSC shell assembly during transfer in Standardized TC are presented in Table P.4-39. These results are for a 24 kW heat load, and are from the previous thermal analysis of the Standardized TC documented in Section 8.1.3. These temperatures are used as boundary conditions in the 24PTH DSC basket thermal analysis presented in Section P.4.6.

P.4.5.5 OS197FC TC Thermal Model Results

The maximum temperature results for the 24PTH-S or –L DSC shell assemblies and TC components during transfer are presented in Table P.4-9 through Table P.4-11. These results are for 40.8 kW and 31.2 kW heat loads. The DSC shell temperatures are used as boundary conditions in the 24PTH DSC basket analysis presented in Section P.4.6.

P.4.5.5.1 Normal and Off-Normal Conditions Results

Table P.4-11 presents the maximum steady state component temperatures achieved under two (2) evaluated operating conditions (100°F and 117°F ambient) for the configuration of the OS197FC TC

with a 24PTH-S DSC with 31.2 kW of decay heat and aluminum inserts in the R45 transition rails. All component temperatures are well below their associated maximum allowable limits.

Transient analyses are performed to determine the time limit for DSC transfer operations for higher than 31.2 kW heat load up to 40.8 kW heat load with aluminum inserts (in the R45 transition rails). The analyses assume that the transient begins with water in the TC/DSC annulus and that with the TC in a vertical orientation (i.e., no credit is taken for heat transferred through the canister rails). At time = 0, the annulus water is assumed to be drained and the bolting of the TC top cover is initiated. This causes the system to heat up. Figure P.4-28 illustrates the predicted thermal response of the DSC and TC for this transient, assuming a decay heat load of 40.8 kW and a 24PTH-S DSC with aluminum inserts. Figure P.4-28 also shows the steady state results of the same case. Based on a targeted DSC shell temperature of approximately 450°F to avoid excessive fuel cladding temperatures, the transient analysis indicates that approximately 11.5 hours is available to transfer the DSC into the HSM-H or take some other corrective actions. The anticipated corrective actions are:

- Complete the transfer of the DSC from the TC to the HSM-H, or
- Unbolt the TC top cover plate and flood the TC/DSC annulus with water if the TC is vertical, or
- Use of an external fan to circulate the air in the TC/DSC annulus if the TC is horizontal, or
- Initiate appropriate external cooling of the TC outer surface by other means, or
- Return the TC to the TC handling area, unbolt the TC top cover plate and reflood the TC/DSC annulus with clean water.

Figure P.4-29 illustrates the results for DSC transfer with 31.2 kW decay heat loading and no aluminum inserts in the R45 transition rails of the basket. Based on a targeted DSC shell temperature of approximately 475°F to avoid excessive fuel cladding temperature under this lower heat loading, approximately 27.3 hours are available to transfer the DSC from the TC into the HSM-H or take some other corrective actions described above for the 40.8 kW case.

These DSC shell temperatures are then used in DSC basket model described in Section P.4.6 to calculate the basket and fuel cladding temperatures. The results from Section P.4.6 documented in Table P.4-14 show that even with these shell temperatures, there is considerable margin in the calculated cladding temperatures (711°F and 732°F calculated for 40.8 kW and 31.2 kW total decay heat cases, respectively vs. 752°F limit).

To verify that the TC in the vertical mode is the controlling configuration, the canister loading transient with 40.8 kW heat load and with aluminum inserts in R45 transition rails was repeated, but with the exception that at time = 0, the annulus water is assumed to be drained, the TC top cover is bolted and TC is rotated to the horizontal position and moved outdoors with exposure to 100°F ambient air and insolation. Figure P.4-30 illustrates the predicted thermal response of the DSC and TC for this transient. Comparing the transient results with those presented in Figure P.4-28 for the TC in the vertical mode shows that the heat up rate for the DSC shell and basket are essentially the same. In contrast, the TC liner, lead, and outer shell exhibit the expected faster heat up due to a combination of the additional heating from insolation and the direct contact heating through the

canister support rails. Therefore, approximately 11.5 hours is available to transfer the DSC to HSM-H after draining of the TC/DSC annulus with the TC top cover bolted on regardless of whether the TC is left in its vertical orientation inside the fuel storage building or rotated to its horizontal orientation and moved outdoors.

P.4.5.5.2 Normal and Off-Normal Operations with Air Circulation Results

For a specific heat load limit and loading and/or transfer time periods exceeding the values determined in Section P.4.5.5.1, one of the corrective actions available to limit the temperature increase is to initiate air circulation in the TC/DSC annulus with the use of an external fan. The NUHOMS® OS197FC TC contains design provisions for the use of an external fan for air circulation in the TC DSC annulus if the time to transfer the 24PTH-S or –L DSCs from the TC handling area in the TC to the HSM-H exceeds the specified time limit depending upon the DSC heat load.

The NUHOMS® cask support skid is modified by the addition of redundant, industrial grade pressure blowers and power systems, ducting, etc. as described in Section P.1.2.1.3. When operating, the fan system will generate a minimum flow rate of 450 cfm which will be ducted to the ram access cover location at the bottom of the TC, flows through the TC spacers and then into the annulus between the DSC and the TC's inner liner, before exiting through 'slots' in the TC top lid. The benefit of the airflow will arise from a combination of a decrease in the boundary layer thickness, improve the convection heat transfer coefficients between the DSC/TC annulus air and the mass transport of the heat by the air from the TC cavity.

Figure P.4-18 illustrates plan and elevation views for a short and long spacer designed to function with the 24PTH-S and –L DCSs. A hole through the center of the spacers allows the ram to access the DSC. Figure P.4-19 shows the cut-outs provided in the bottom of the TC lid to allow the air to exit.

Given that the DSC will be eccentric to the TC axis for all horizontal operations and possibly for vertical operations, the gap between the DSC and the TC's inner liner will vary with circumferential position. The determination of the gap as a function of circumferential position was made assuming the DSC is resting on the support rails.

After exiting from the spacer, the air circulates through the annulus between the DSC and the TC's inner liner. Given the variable gap between the DSC and liner, plus variances in the heating of the air, the airflow will distribute itself around the circumference of the DSC/TC liner until equal pressure drops are achieved. For the purposes of this calculation, each half of the annulus is divided into 7 circumferential segments: 0 to 30°, 30 to 60°, 60 to 90°, 90 to 120°, 120 to 135°, 135 to 150°, and 150 to 180°. The 0° position is at the top of the horizontal TC and the 180° position is at the bottom. The flow enters the bottom of the TC and gets divided into seven (7) segments, flows out through the spacer and then up through the TC DSC annulus.

Implementation of the air circulation option consisted of the determination of the mass flow rates and the pressure drops through the cask as a function of angular position, the convective heat transfer coefficients, and the thermal conductance between the various gas nodes. The following sections describe the methodology used for these calculations.

(A) Pressure Drop Calculation

The pressure drop experienced by the circulating air from the fan discharge, through the DSC and TC annulus, and its subsequent exhausting back into the ambient is computed assuming 1-D flow pipe flow relationships. Table P.4-8 presents the calculations performed to determine the TC/DSC gap hydraulic characteristics as a function of circumferential position along the DSC shell. These gap hydraulic characteristics and loss coefficients along the flow path for the fittings and hoses from the blower to the TC top lid outlets are used to calculate the resultant total pressure drop. The loss coefficients for the fittings, hoses, entrance, exit, sudden expansion, contraction turns, bends and plenums along the flow path are taken from [4.33] and [4.34]. A pressure drop of slightly more than 6 inches water gauge is calculated.

(B) Convection Heat Transfer Coefficient for Circulating Air within the DSC Cask Annulus

The convection heat transfer within the DSC cask annulus is computed using the relationships for flow within ducts and pipes. The convection heat transfer coefficients are computed as a function of the local hydraulic diameter, the Reynolds number, and the thermophysical properties of air or water. For zero flow, the heat transfer between the DSC and the inner liner of the cask is assumed to be via conduction and radiation across the gap (i.e., Nusselt = 1.0). As the flow velocity increases, the convection heat transfer rate between the air stream and the DSC shell and the TC liner are computed using equations 7, 43, 44, 45, 57, and 57a from Chapter 7 of [4.34] as follows:

For $0.5 < Pr < 2000$ and $10^4 < Re < 5x10^6$:

$$Nu = \frac{h_c D_h}{k} = \frac{Re \times Pr \times f/2}{1.07 + 12.7(Pr^{2/3} - 1)(f/2)^{0.5}}$$

$$Re = \frac{V \times \rho \times D_h}{\mu}$$

$$f = (1.58 \times \ln Re - 3.28)^{-2}$$

For $0.5 < Pr < 2000$ and $3000 < Re \leq 10^4$:

$$Nu = \frac{h_c D_h}{k} = \frac{(Re - 1000) \times Pr \times f/2}{1.0 + 12.7(Pr^{2/3} - 1)(f/2)^{0.5}}$$

For $0.5 < Pr < 2000$ and $0 < Re \leq 3000$:

$$Nu = \frac{h_c D_h}{k} = 2.035 \times (x^*)^{-3} - 0.7, \qquad \text{for } x^* \leq 0.01$$

$$Nu = 2.035 \times (x^*)^{-3} - 0.2, \qquad \text{for } 0.01 < x^* < 0.06$$

$$Nu = 3.657 + 0.0998/x^*, \qquad \text{for } x^* \geq 0.06$$

where:

Nu = Nusselt number	h_c = convection coefficient
D_h = hydraulic diameter	k = thermal conductivity of fluid at film temperature
V = flow velocity	ρ = density of fluid at the film temperature
μ = dynamic viscosity	Pr = Prandtl number
f = friction factor	Re = Reynolds number
x* = entry length factor = $x/Re/D_h/Pr$	x = length of duct/pipe

For cases with zero flow (i.e., Re = 0.), the heat transfer coefficients are determined using conduction across the gap only, or $Nu = \frac{h_c D_h}{k} = 1.0$. The heat transfer coefficients in the region between the canister support rails (i.e., approximately 150° to 180°) always assume conduction only due to the narrowness of the gap between the DSC and the cask inner liner.

(C) Results

Table P.4-41 presents the maximum component temperatures achieved under bounding normal and off-normal ambient operating conditions for the OS197FC TC with a 24PTH-S DSC with 40.8 kW of decay heat and a flow rate of 450 cfm of air circulation. As seen, all component temperature are within their associated maximum allowable temperature limit. The fact that the peak neutron shield temperatures slightly exceeds the 287°F limit (based on the pressure rating of the neutron shield relief plugs), indicates a slight possibility for some localized boiling within the shield. However, the neutron shield will not over pressurize because the region of peak temperature is limited to a small region and any boiling will dramatically increase the heat transfer throughout the neutron shield at that region, and any local steam bubbles will quickly condense within the bulk fluid.

Examination of the model output shows that nearly 85% of the total airflow in the TC DSC annulus occurs in the upper half of the annulus. This result is expected given the combination of flow area and hydraulic diameter (see Table P.4-8) for the various angular segments. The remaining 15% of the total fan airflow occurs in the lower half of the annulus, with 2/3's of that occurring within the 60° to 90° segment of the annulus.

Table P.4-42 presents the maximum component temperatures achieved under the bounding normal and off-normal ambient operating conditions for the OS197FC TC with a 24PTH-S DSC with 31.2 kW of decay heat and a flow rate of 450 cfm of air circulation. The results are similar to that for 40.8 kW heat load, but at the expected lower temperature levels.

P.4.5.5.3 Accident Conditions

Three accident scenarios are examined for the OS197FC TC. The first case considers an evaluation of system performance for the case wherein steady-state conditions are established with the fan in operation, and, subsequently the fan airflow is lost. To minimize the occurrence of this accident condition, the OS197FC TC skid is equipped with redundant industrial grade blowers, each one of

these blowers capable of supplying the required minimum air flow rate. These blowers are also powered with a redundant power supply.

The analyses assume that the transient begins with DSC/TC at steady-state conditions with the cask horizontal, 100°F ambient, with insolation, and 40.8 kW decay heats. At time = 0, the fan airflow is lost and the system starts to heat up. Figure P.4-31 illustrates the calculated thermal response of the DSC and TC for this transient. Assuming an upper limit DSC shell temperature of 500°F, approximately 8 hours are available to complete the transfer to the HSM-H or re-establish the fan airflow. The 508°F shell temperature limit is selected because it will result in fuel cladding temperatures close to 752°F limit but will not exceed it. Figure P.4-32 illustrates the same loss of fan airflow transient, but for a decay heat load of 31.2 kW and no aluminum inserts in the 24PTH-S DSC. In this case, approximately 24 hours are required to reach a DSC shell temperature of 500°F.

The second accident case involves the loss of both the fan air circulation system and the water in the neutron shield (TC drop accident). The resulting transient behavior of the TC and DSC is illustrated in Figure P.4-33 for the case with 40.8 kW and in Figure P.4-34 for the case with 31.2 kW. The heat up rates for the DSC and fuel basket are similar to those seen in Figure P.4-31 and Figure P.4-32, but as expected, the rate of the cask's temperature response is greater due to the loss of the water in the neutron shield. Table P.4-12 presents the peak component temperatures achieved under this accident at steady-state conditions. As seen, with the exception of the NS-3, all component temperatures remain under their allowable limits. The slight over-temperature of the NS-3 for the 40.8 kW decay heat loading indicates that the shielding effectiveness of the NS-3 would still not be impaired.

The third accident scenario involves a 15-minute hypothetical fire. The maximum duration of the fire event will be controlled by limiting the available fuel sources within the vicinity of the TC. To bound the heat input into the TC, the neutron shield is assumed to be filled with water during the fire duration and then the neutron shield water is assumed to be lost at the end of the 15-minute fire. The evaluation of TC thermal performance under the hypothetical fire accident scenario is illustrated in Figure P.4-35. As expected, with the exception of the exterior surfaces of the cask, the thermal mass of the DSC and cask components is sufficient to absorb the heat flux from the fire with an approximate 60°F increase in the inner liner and structural shell temperatures. The rise in the inner liner temperature is not reflected by the lead gamma shield because the noted temperature increase only occurs for the upper portion of the liner where the liner mates with the top forging of the cask. As a result, the elevated temperature of the forging is conducted into the upper portion of the liner, raising its temperature above that seen for the remaining portions of the liner.

The cask components continue to heat up after the end of 15 minute fire because of the assumed loss of the fan air circulation system and the failure and draining of the neutron shield. As seen from the Figure P.4-35, the maximum cask temperatures achieved under the fire accident scenario, with the exception of the exterior surfaces of the cask, will occur at the post-fire steady-state condition.

Table P.4-13 presents the peak component temperatures achieved at the end of the fire (i.e., 15 minutes into the transient) and for the post-fire steady-state condition. Comparison of the post-fire steady-state temperatures from Table P.4-13 with the temperatures in Table P.4-12 shows that the loss of neutron shield accident scenario temperatures bound those for the post-fire steady-state temperatures. This occurs because the assumed sooting and oxidation of the exterior surfaces that is

assumed for the fire event raises the surface emissivity, thus improving the heat transfer between the cask and the ambient.

P.4.5.6 Evaluation of OS197FC TC Performance

The thermal performance of the OS197FC TC is evaluated under normal, off-normal, and accident conditions of operation as described above and is shown to satisfy all the temperature limits and criteria. The results of the DSC shell temperatures are used in the DSC basket and fuel cladding temperature models and the results documented in Section P.4.6 shows that all the basket and fuel cladding material temperature limits are satisfied. The results of the TC temperatures are used in Section P.3 to show that thermal stresses in the TC are also within these allowables. The TC temperatures are used in Section P.3 to show that thermal stresses in the TC are also within their allowables.

P.4.6 NUHOMS®-24PTH DSC Basket Thermal Analysis

The thermal analysis of the NUHOMS® 24PTH DSC is based on finite element models developed using the ANSYS computer code [4.6]. ANSYS is a comprehensive thermal, structural and fluid flow analysis package. It is a finite element analysis code capable of solving steady state and transient thermal analysis problems in one, two or three dimensions. Heat transfer via a combination of conduction, radiation and convection can be modeled by ANSYS. Solid entities are modeled by SOLID70 elements for 3-D.

A total of five (5) Heat Load Zoning Configurations (HLZCs) are allowed for the 24PTH DSCs as shown in Figures P.2-1 through P.2-5. The maximum total heat load per DSC is 40.8 kW, 31.2 kW or 24 kW depending upon the specific DSC types and HLZCs. The thermal analysis is carried out for HLZCs shown in Figure P.4-36 for the 40.8 kW heat load because it bounds the HLZCs 2 and 3. In HLZC 1, the fuel assemblies at the center 4 locations in the DSC basket have a maximum heat load of 1.7 kW per assembly as compared to zero (empty locations) for HLZC 2 and 1.5 kW for HLZC 3. Therefore, HLZC 1 results in higher fuel cladding and basket temperatures compared to HLZCs 2 or 3. Thermal analysis is carried out for HLZC 4 shown in Figure P.4-37 for 31.2 kW total DSC heat load. To bound all possible combinations of heat loads from fuel assemblies allowed in HLZC 5 of Figure P.2-5, the thermal analysis is carried out for the HLZC shown in Figure P.4-38. In this thermal analysis configuration, the highest possible allowed decay heat assemblies are assumed to be at the center and upper half of the basket locations resulting in bounding fuel cladding and basket temperatures.

P.4.6.1 NUHOMS® 24PTH DSC Basket and Payload Model

The three-dimensional model (Figure P.4-39) represents the NUHOMS®-24PTH DSC and includes the geometry and material properties of the basket components, the basket rails, and DSC shell. The 24PTH DSC basket components are shown in Figure P.4-40. Each component of the basket (fuel compartment tubes, poison plates, aluminum plates, R90 rails, R45 rail, and inserts) is modeled individually with SOLID70 elements. The gaps between adjacent basket components are also represented with SOLID70 elements with helium or air conductivity as appropriate. The material properties from Section P.4.2 are used for the fuel region. Within the model, heat is transferred via conduction through fuel regions, fuel compartment tubes, aluminum and poison plates, and the gas gaps between all aluminum, poison and steel members. Generally, good surface contact is expected between adjacent components within the basket structure. However, to bound the heat conductance uncertainty between adjacent components owing to imperfect contact between the neutron poison material, aluminum and steel basket components, uniform gaps along the entire surfaces are assumed. This is a conservative assumption, because although there will be imperfect contact between the adjacent plates, they will be in contact with each other at most of the locations. Therefore, thermal resistance to heat flow from the fuel assembly out to the DSC surface is lower with the actual imperfect contact as compared with the modeled uniform gaps along the entire surfaces. The gaps used in the thermal analysis of the 24PTH DSC are shown in the Figure P.4-50.

The 3D models are longitudinally full-length, one-half (180°) cross section (right half) models of the 24PTH DSC. The ANSYS models comprise the DSC shell assembly (including the shell, and top and bottom end components) and the basket assembly (including basket fuel compartment tubes, aluminum and poison plates, and the aluminum R90 and steel R45 transition rails).

The DSC shell is modeled with a 0.545" thick wall and an outer radius of 67.19". The extra shell thickness allows modeling of a 0.08" hot gap between the basket rails and the DSC shell.

As shown in Section P.4.8.1, the WE 14x14 fuel assembly is determined as the limiting assembly type based on the determination of limiting fuel effective conductivity among the fuel assemblies that are considered to be stored in 24PTH–S or –L DSC as documented in Section P.4.8. The effective thermal material properties of BW 15x15 fuel were used for all the 24PTH-S-LC DSC cases.

Due to the unsymmetrical positioning of the poison plates along the symmetry line of the basket structure, the 24PTH DSC is not entirely symmetric. Therefore, sensitivity analyses are performed using right half, left half and full 360° models of a typical axial segment of the basket to determine the half cross section of the model that produces bounding (conservative) results. Based on these sensitivity analyses, the right-half section is used for the analyses as presented herein.

Additional sensitivity analyses are performed using both full length and segment models of the full basket to optimize the finite element mesh discretization of the thermal analysis models. A fuel mesh size of 14x14 elements is used for the model based on the results of the sensitivity study, as documented in Section P.4.6.2.

The fuel in the model is shifted to the top end of the tube to the hotter airflow area when 24PTH DSC is in the OS197 TC. This adds an additional conservatism to the calculation.

P.4.6.2 Mesh Sensitivity Study

The 24PTH DSC model described above is based on a 14x14 mesh for the cross section of each fuel assembly. A sensitivity study was performed with fuel mesh sizes of 12x12 and 13x13. The results show that convergence is achieved with a 14x14 mesh and the maximum fuel cladding temperature change is 0.2°F in comparison with 13x13 mesh. Hence the 14x14 mesh size model is mesh insensitive.

P.4.6.3 Boundary Conditions for the DSC Basket Model

The boundary conditions for storage and transfer conditions are discussed in subsequent section.

P.4.6.4 Heat Generation for the DSC Basket Model

Heat generation is calculated based on the dimensions of the fuel and basket. The heat is assumed to be radially distributed evenly through the 8.9-inch square nominal fuel cell opening. Axial variations in decay heat flux are conservatively bounded in the ANSYS models by applying a uniform maximum peaking factor of 1.11 [4.1] along the active length of the PWR fuel assembly. Heat generation rates are applied along all of the active fuel length according to the decay HLZCs 1, 4, and 5, as given in Figure P.4-36, Figure P.4-37 and Figure P.4-38.

The equation below shows a typical calculation of a peak heat generation rate for 2.0 kW per fuel assembly with an active fuel length of 140.6 inches.

$$\ddot{q} = \frac{1.11 \cdot 2.0\,kW \cdot 3414 \frac{Btu/hr}{kW} \cdot \frac{1\,hr}{60\,\min}}{(8.9\,in)^2 \cdot 140.6\,in} = 1.134e-2 \frac{Btu}{\min \cdot in^3}.$$

P.4.6.5 DSC Thermal Evaluation for Normal Conditions of Storage and Transfer

The NUHOMS® System components are evaluated herein for normal conditions of storage and transfer over a range of design basis ambient temperatures. Ambient temperatures for these cases are assumed to occur for a sufficient duration such that a steady-state temperature distribution exists within the NUHOMS® System components.

P.4.6.5.1 Boundary Conditions, Storage

The NUHOMS®-24PTH-S and 24PTH-L DSC is evaluated for normal conditions of storage with maximum heat load of 40.8 kW and 31.2 kW within the HSM-H. The NUHOMS®-24PTH-S-LC DSC is evaluated for normal conditions of storage with a maximum heat load of 24 kW within the HSM Model 102. Each of these normal conditions of storage analysis cases are performed for the following ambient conditions:

- Maximum normal ambient temperature of 100°F with insolation,
- Minimum normal ambient temperature of 0°F without insolation.

The HSM-H thermal model as described in Section P.4.4 provides the surface temperatures of the 24PTH-S and 24PTH-L DSC shell. The HSM Model 102 thermal model as described in Section 8.1.3 provides the surface temperatures of the NUHOMS®-24PTH -S-LC DSC. Table P.4-34 provides the surface temperatures of the NUHOMS®-24PTH-S-LC DSC shell.

These normal conditions of storage DSC shell temperatures are then applied as boundary conditions to the DSC shell in the basket and fuel models, as presented. These models are used to calculate the temperature distributions in the basket components and fuel.

P.4.6.5.2 Boundary Conditions, Transfer

In accordance with Section P.4.5, analyses of the NUHOMS® 24PTH-S and 24PTH-L DSC with heat loads of 40.8 kW and 31.2 kW within the OS197, OS197H, or OS197FC TC and NUHOMS®-24PTH-S-LC DSC with a heat load of 24 kW within the Standardized TC are performed for the following ambient conditions:

- Maximum normal ambient temperature of 100°F with insolation, and
- Minimum normal ambient temperature of 0°F without insolation.

The 24PTH-S and 24PTH-L DSC temperature profiles calculated using the OS197FC thermal model as described in Section P.4.5 are applied to the corresponding surfaces of the DSC/basket/fuel finite

element model described in Section P.4.6.1. The DSC shell temperatures with a total heat load of 24 kW, calculated in Section 8.1.3, are provided in Table P.4-39. These temperatures are applied to the 24PTH-S-LC DSC model.

P.4.6.5.3 Maximum Temperatures

P.4.6.5.3.1 Fuel Cladding

The maximum fuel cladding temperatures during normal conditions of storage and transfer are evaluated for all decay HLZCs and compared with the corresponding fuel cladding temperature limit for normal conditions of storage and transfer as listed in Table P.4-14. Figure P.4-41 shows temperature distribution in the DSC basket for 31.2 kW heat load and 100°F ambient transfer case. The conservatisms in the basket model and in the cladding temperature limit methodology are described below:

1) No credit is taken for any convection in the DSC basket cavity and fuel regions.

2) Conservative gaps are assumed between the basket component plates even though adjacent basket components are connected to each other.

3) No credit is taken for any radiation in the gaps between the adjacent basket components.

Based on these conservatisms, there is a higher margin in the calculated maximum cladding temperatures than those shown in Table P.4-14. Thus, there is reasonable assurance that the cladding will maintain its integrity during storage conditions.

P.4.6.5.3.2 DSC Basket Material Temperatures

The maximum temperatures of the basket assembly components for normal conditions of storage and transfer for the bounding HLZCs are listed in Table P.4-15, Table P.4-16, and Table P.4-17.

P.4.6.5.4 Maximum Internal Pressures

Pressure Calculation

This section describes the internal pressure calculations for the NUHOMS®-24PTH DSC as loaded with fuel with a maximum burnup of 62 GWd/MTU for all storage and transfer operations. The limiting fuel assembly type considered in this evaluation is the B&W 15x15 assembly (refer to Section P.2). The fission gasses produced by the WE 17x17 are slightly higher than those from the B&W 15x15, but the B&W 15x15 fuel has the highest heavy metal and fuel assembly weight and therefore displaces the most free volume relative to all the other assembly types considered in Chapter P.2.

The calculations account for the DSC free volume, the quantities of DSC backfill gas, fuel rod fill gas, and fission products and the average DSC cavity gas temperature. The 24PTH-S DSC, 24PTH-L DSC, and 24PTH-S-LC DSC configurations are considered. The 24PTH-L DSC and 24PTH-S-

LC DSC internal pressure evaluations also include the contribution due to Control Components (CCs). The internal pressures are then calculated using the ideal gas law, as follows:

$$P = \frac{nRT}{V}$$

where:

n = Total number of moles of gases,

R = Universal gas constant,

T = Gas temperature (°R),

V = Gas volume, and

P = Internal pressure.

DSC Free Volume

The 24PTH DSC cavity free volume is calculated as DSC cavity volume minus DSC basket and fuel assemblies' volume. The DSC cavity volume is calculated as

$$V_{DSC\ cavity} = \frac{\pi \cdot ID^2_{DSC\ shell}}{4 \cdot L_{DSC\ cavity}},$$

where

$ID_{DSC\ shell}$ - DSC shell inside diameter,

$ID_{DSC\ shell}$ - DSC cavity length.

The calculated 24PTH DSC cavity free volumes are shown in Table P.4-35:

Quantity of Helium Fill Gas in DSC

The DSC free volume is assumed to be filled with 3.5 psig (18.2 psia) of helium. The maximum temperatures for the 70°F ambient storage case are used to estimate the number of moles of helium backfill.

The average long-term helium fill temperature for the each configuration is interpolated from analysis results of the 24PTH DSC within the HSM-H and the HSM Model 102 for an ambient temperature of 70°F. Using the ideal gas law, the quantity of helium in each type of DSC is calculated and the results are presented in Table P.4-18.

Quantity of Helium Fill Gas in Fuel Rods per DSC

The volume of the helium fill gas in a B&W 15x15 fuel pin at cold, unirradiated conditions is 1.326 in^3, and there are 208 fuel pins in an assembly. The maximum fill pressure is 415 psig (429.7 psia) and the fill temperature is assumed to be room temperature (70°F or 530°R). The mole quantity of fuel rod fill gas for 24 B&W 15x15 fuel assemblies is given by:

$$n_{he} = \frac{(429.7\,psia)(6894.8\,Pa/psi)(24 \cdot 208 \cdot 1.326\,in^3)(1.6387x10^{-5}\,m^3/in^3)}{(8.314\,J/mol \cdot K)(530°R)(5/9\,K/°R)}$$

$$n_{he} = 131.4\,g-moles$$

Based on NUREG 1536 [4.7], the maximum fraction of the fuel pins that are assumed to rupture and release their fill and fission gas for normal, off-normal and accident events is 1, 10 and 100%, respectively. For all of these events, 100% of the fill gas in each ruptured rod is assumed to be released. The amount of helium fill gas released per DSC for each of these conditions is summarized in Table P.4-36.

Quantity of Fission Gases released as a Result of Irradiation in Fuel Rods per DSC

The B&W 15x15 fuel assembly used in the pressure calculations is assumed to have a maximum burnup of up to 62,000 MWd/MTU, which is the highest burnup proposed for the NUHOMS®-24PTH system configuration. The maximum burnup creates a bounding case for the amount of fission gases produced in the fuel rod during reactor operation. The amounts of gases produced because of irradiation at STP for each assembly are summarized below.

The number of moles of gas released into the DSC cavity from one assembly because of irradiation is given by:

$$n_{ig\,1\,FA} = 47.61\ g\text{-}moles * 0.3 = 14.28\ g\text{-}moles$$

The amount of fission gas released into the DSC cavity for normal, off-normal and accident cases assuming a 30% gas release from the fuel pellets [4.7]and a 1%, 10%, and 100% rod rupture, respectively, is summarized in Table P.4-37.

Quantity of Helium Gas in CCs per DSC

The 24PTH-L DSC and 24PTH-S-LC DSC configurations may include CCs. The evaluation of gas quantities for CC is based on the B&W 15x15 BPRAs. For the controlling B&W 15x15 assembly, up to 24 BPRAs may be present. These BPRAs have an initial helium fill of 14.7 psia, and if 100% of the boron is consumed and 30% released into the DSC, a total of 53.8 g-moles of gas could be released to the DSC assuming 100% cladding rupture (the 53.8 g-moles is based on 24 BPRAs in the 24P DSC; from Appendix J, Section J.4).

The percentage of CC rods ruptured during normal, off-normal and accident conditions is assumed to be 1%, 10% and 100%, respectively, similar to the assumptions for the fuel rod rupturing. The maximum amount of gas released to the DSC cavity from the for normal, off-normal and accident conditions is given in Table P.4-38.

The maximum average helium backfill gas temperature for normal conditions of storage and transfer occurs when the 24PT-S-LC DSC is in the Standardized TC with an ambient temperature of 100°F and maximum insolation. In addition, the maximum pressure will occur with the 62,000 MWd/MTU burnup fuel so that lesser burnups will be enveloped by this calculation. The average

helium backfill gas temperature based on the results in Section P.4.6.5.3, is 523°F (983°R). The maximum normal operating condition pressures are summarized in Table P.4-19.

P.4.6.5.5 Maximum Thermal Stresses

The maximum thermal stresses for the normal conditions of storage and transfer for the NUHOMS®-24PTH DSC are calculated in Section M.3.

P.4.6.5.6 Evaluation of 24PTH DSC Performance for Normal Conditions

The NUHOMS®-24PTH DSC shell and basket are evaluated for the calculated temperatures and pressures as presented in Section P.3. The maximum fuel cladding temperatures are well below the allowable fuel temperature limit of 752°F (400°C) [4.19] as documented in Table P.4-14. The maximum DSC internal pressure remains below 15.0 psig used in Section P.3 during normal conditions of storage and transfer operations. Hence, it is concluded that the NUHOMS®-24PTH DSC design meets all applicable normal condition thermal requirements.

P.4.6.6 DSC Thermal Evaluation for Off-Normal Conditions

The NUHOMS®-24PTH system components are evaluated for the extreme ambient temperatures of -40°F (winter) and 117°F (summer). Should these extreme temperatures ever occur, they would be expected to last for a very short duration of time. Nevertheless, these ambient temperatures are conservatively assumed to occur for a significant duration to result in a steady-state temperature distribution in the NUHOMS®-24PTH system components.

P.4.6.6.1 Off-Normal Ambient Temperatures during Storage

The thermal performance of the NUHOMS®-24PTH DSC within the HSM-H and within HSM Model 102 under the extreme minimum ambient temperatures of -40°F with no insolation and extreme maximum ambient temperature of 117°F with maximum insolation are evaluated for HLZCs 1, 2, 3, 4 and 5.

P.4.6.6.2 Boundary Conditions, Off-Normal Storage

Off-normal conditions of storage analyses of the NUHOMS®-24PTH DSC within the HSM-H and within HSM Model 102 includes (refer to Table P.4-34 for HSM Model 102 cases):

- Maximum off-normal ambient temperature of 117°F with insolation, and
- Minimum off-normal ambient temperature of -40° F without insolation.

The HSM-H thermal model described in Section P.4.4.4 above provides the surface temperatures that are applied to the DSC shell, basket and payload model.

P.4.6.6.3 Off-Normal Ambient Temperatures during Transfer

The thermal performance of the NUHOMS®-24PTH DSC during transfer under the minimum ambient temperature of 0°F with no insolation and 117°F with maximum insolation, and HLZCs 1

(bounds configurations 2 and 3), 4 and 5 are examined. Note: A solar shield is used for transfer operations when ambient temperatures exceed 100°F up to 117°F.

P.4.6.6.4 Boundary Conditions, Off-Normal Transfer

In accordance with Section P.4.5, an analysis of a 24PTH DSC in the OS197FC cask and in the Standardized TC is performed for the following ambient conditions:

- Maximum normal ambient temperature of 117°F with solar shield in place in OS197FC cask,
- Maximum normal ambient temperature of 117°F with solar shield in place in Standardized cask.

These analyses determine maximum DSC shell surface temperatures. The maximum calculated DSC shell temperatures are applied to the exterior surface of the DSC shell in the DSC/basket/payload finite element model.

For Standardized TC, the DSC shell temperatures were calculated for 24 kW in Section 8.1.3. The results are summarized in Table P.4-39.

P.4.6.6.5 24PTH DSC Thermal Model Results for Off-Normal Conditions of Storage and Transfer

According to the NUHOMS® CoC 1004, Technical Specification 1.2.4, "TC/DSC Transfer Operations at High Ambient Temperatures" for transfer operations, when ambient temperatures exceed 100°F, a solar shield shall be used to provide protection against direct solar radiation.

Fuel Cladding Temperatures

The maximum fuel cladding temperatures during off-normal conditions of storage and transfer are evaluated for all HLZCs and compared with the corresponding fuel cladding temperature limits.

The results are reported in Table P.4-20 for HLZCs 1 (bounds HLZCs 2 and 3), 4 and 5.

DSC Basket Materials Component Temperatures

The maximum temperatures of the basket assembly for off-normal conditions of storage and transfer for HLZC 1 (bounds HLZCs 2 and 3), 4 and 5 are listed in Table P.4-21, Table P.4-22, and Table P.4-23, respectively.

P.4.6.6.6 Off-Normal 24PTH DSC Maximum Internal Pressure during Storage/Transfer

The maximum average helium backfill gas temperature for off-normal conditions of storage and transfer occurs when the 24PTH-L DSC with aluminum inserts, and a heat load of 31.2 kW (HLZC 4) is in OS197FC TC with an ambient temperature of 117°F and sunshade. The average helium temperature is 513°F (973°R). Per NUREG 1536 [4.7], the percentage of fuel rods ruptured for off-normal cases is 10%.

A summary of the maximum off-normal operating pressures for the various 24PTH DSC configurations are presented in Table P.4-24.

P.4.6.6.7 Maximum Thermal Stresses

The maximum thermal stresses during off-normal conditions of storage and transfer for the NUHOMS®-24PTH DSC are calculated in Section P.3.

P.4.6.6.8 Evaluation of 24PTH DSC Performance for Off-Normal Conditions

The NUHOMS®-24PTH DSC shell and basket are evaluated for calculated temperatures and pressures in Section P.3. The maximum fuel cladding temperatures are well below the allowable fuel temperature limit of 752°F (400°C) for transfer and 1058°F (570°C) for storage conditions. The maximum DSC internal pressures remain below 20.0 psig during off-normal conditions of storage and transfer used in Section P.3. The pressures and temperatures associated with off-normal conditions in the NUHOMS®-24PTH DSC design meet all applicable off-normal thermal requirements.

P.4.6.7 DSC Thermal Evaluation for Accident Conditions

The NUHOMS®-24PTH-S and 24PTH-L DSC is evaluated for accident conditions of storage and transfer over a range of design basis off-normal ambient temperatures. A transient analyses of the NUHOMS® system components is performed at these ambient temperatures.

Since the NUHOMS® HSMs are located outdoors, there is a remote possibility that the ventilation air inlet and outlet openings could become blocked by debris from such unlikely events as floods and tornadoes. The NUHOMS® HSM system design features such as the perimeter security fence and redundant protected location of the air inlet and outlet openings reduces the probability of occurrence of such an accident. A complete blockage of all air inlets and outlet vents simultaneously is not a credible event. However, to bound the blockage of all inlets or outlets for this generic analysis, a complete blockage of all inlets and outlet vents accident is conservatively postulated to occur and is analyzed in Section P.4.6.7.1.

The controlling transfer accident considered involves a drop of TC under maximum off-normal ambient temperature and insolation, the loss of the sun shield and the loss of liquid neutron shield and loss of air circulation in the TC as described in Section P.4.6.7.2.

The HSM-H and DSC contain no flammable material and the concrete and steel used for their fabrication can withstand any credible fire accident condition. Fire parameters are dependent on the amount and type of diesel and/or gasoline and/or other flammable liquids within the transporter and the fire accident conditions shall be addressed within site-specific applications. Licensees are required to verify that loadings resulting from potential fires and explosions are acceptable in accordance with 10CFR72.212(b)(2). The hypothetical fire evaluation for the NUHOMS®-24PTH system is presented in Section P.4.6.7.3.

P.4.6.7.1 Blocked Vent Accident Evaluation

For the postulated blocked vent accident condition, the HSM-H ventilation inlet and outlet openings are assumed to be completely blocked for a 40-hour period concurrent with the extreme off-normal ambient condition of 117°F with insolation.

For conservatism, a transient thermal analysis is performed using the 3-D model developed in Section P.4.5, for HLZCs 1 and 5. HLZCs 2, 3 and 4 are bounded by the temperature results for HLZC 1. When the inlet and outlet vents are blocked, the air surrounding the DSC in the HSM-H cavity is contained (trapped) in the HSM-H cavity. The temperature difference between the hot DSC surface and the surrounding HSM-H (cooler) heat shield and concrete surfaces results in closed cavity convection. This closed cavity convection is accounted for by calculating an effective conductivity of air as described in Section P.4.9.

Summaries of the calculated fuel cladding and DSC component temperatures are listed in Table P.4-25 through Table P.4-28.

P.4.6.7.2 Transfer Accident Evaluation

The postulated transfer accident event consists of 24PTH DSC transfer in the OS197FC TC in a 117°F ambient environment with loss of the solar shield and the loss of liquid neutron shielding. All five HLZCs were evaluated. HLZC 1 bounded the results of HLZCs 2 and 3. The results for HLZCs 1, 4 and 5 are shown in Table P.4-25 through Table P.4-28.

P.4.6.7.3 Hypothetical Fire Accident Evaluation

For the postulated worst-case fire accident, a 300 gallon diesel fire is simulated for a NUHOMS®-24PTH DSC with a decay heat load of 40.8 kW during transfer in the TC. This accident event bounds other fire scenarios associated with loading operations and storage within the HSM-H due to the large thermal mass of the HSM-H and its vent configuration which provides protection for the DSC and its payload.

Steady state, off-normal conditions are assumed prior to the fire, which consist of a 117°F ambient temperature without a solar shield in place on the TC but with water filled neutron shield. The fire has a temperature of 1,475°F, and an emittance of 0.9 and a duration of 15 minutes based on the 300-gallon diesel fuel source and complete engulfment of the TC for the duration of the fire. This is conservative because it allows the maximum amount of heat input into the NUHOMS® system components. Subsequent to the fire, the TC is subjected to 117°F ambient conditions with maximum insolation. Note that these hypothetical fire parameters and assumptions are very conservative.

It is assumed that liquid neutron shield (water) is present throughout the 15-minute fire transient even though it is expected to be lost and replaced with air very early in the fire transient. This assumption maximizes the heat input from the fire to the canister because of the high conductivity of water compared to air. To maximize the canister temperature during the post-fire transient, it is assumed that water in neutron shield cavity is lost at the beginning of post-fire transient and replaced by air as the heat flow is now from canister to the ambient.

The gaps included in the thermal model of the 24PTH DSC basket are summarized in Figure P.4-50. These gaps are not removed for calculating the cladding temperatures during accident conditions. The canister shell temperatures change by a small amount during the accident fire transient. This change is small during fire transient due to the large thermal mass of the transfer cask. This shows that heat input from the fire to the canister is not significant. Since the canister shell temperature is almost unchanged, the cladding temperatures during 15-minute fire transient also are almost unchanged. Therefore, the assumption of not removing the gaps during fire transient has negligible impact on the cladding temperatures.

The calculated temperature response of selected components in the TC and DSC during the first 2400 minutes of the fire accident is shown in Figure P.4-35. A summary of the calculated maximum fire transient temperatures for components is listed in Table P.4-13. The calculated maximum fire transient DSC surface temperature is 668°F, which is less than the transfer accident case maximum DSC temperature of 685°F as calculated in Section P.4.6.7.2. Therefore, the NUHOMS®-24PTH DSC temperatures and pressures calculated for the transfer accident case bound the hypothetical fire accident case.

P.4.6.7.4 Fuel Cladding and Basket Materials

The maximum fuel cladding temperatures for the blocked vent transients are reported at 38.5 hour transient for HLZC 1 and 4, and at 40 hours for HLZC 5 as shown in Table P.4-25. The transfer accident case results are reported at steady-state conditions for HLZCs 1 and 5. The maximum temperatures of the basket components are listed in Table P.4-26 through Table P.4-28.

P.4.6.7.5 Maximum Internal Pressures

The following conditions are considered in evaluating the maximum accident pressure for the 24PTH DSC:

1) The blocked vent case (24PTH-S and 24PTH-L, or -S-LC DSC in HSM-H or HSM Model 102) with maximum off-normal ambient temperature, and 10% fuel pin rupture. Note: 100% rupture is not assumed because a blocked vent cannot occur concurrently with a drop load,

2) The OS197FC transfer cask accident case with maximum off-normal ambient temperature, loss of sun shield, liquid neutron shield, and circulation if used, and 100% fuel pin rupture,

2) The Standard cask (solid neutron shield) accident case with maximum off-normal ambient temperature, loss of sun shield, and 100% fuel pin rupture.

The maximum accident case pressure occurs during 24PTH-L DSC (40.8 kW) transfer in the OS197FC cask under maximum off-normal ambient conditions, concurrent with loss of the solar shield, loss of liquid neutron shield, and loss of air circulation (if used). For this condition the average helium gas temperature is 653°F (1113°R) based on the results from Section P.4.6.7.2. In accordance with NUREG 1536, 100% of the fuel pins are assumed to rupture during this event. During the blocked vent case, the average helium gas temperature is 618°F (24PTH-S-LC DSC in HSM Model 102). However, since no DSC drop event can occur in conjunction with a blocked vent event, the maximum fraction of fuel pins that can be ruptured is limited to 10%.

A summary of the maximum accident operating pressures for the various 24PTH DSC configurations are presented in Table P.4-29.

P.4.6.7.6 Evaluation of the 24PTH DSC Performance During Accident Conditions

The NUHOMS®-24PTH DSC shell and basket are evaluated for the accident conditions pressures and temperatures as described in Section P.3.

The maximum fuel cladding temperature of 914°F is below the short-term limit of 1058°F (570°C). The accident pressure in the NUHOMS®-24PTH-S or -L DSC of 97.2 psig remains below the accident design pressure of 120 psig. The accident pressure in the 24PTH-S-LC DSC of 80.4 psig is also below the accident design pressure of 90 psig. It is concluded that the NUHOMS®-24PTH system maintains confinement during the postulated accident condition.

P.4.7 Thermal Evaluation for Loading/Unloading Conditions

All fuel transfer operations occur when the NUHOMS®-24PTH DSC and TC are in the spent fuel pool. The fuel is always submerged in free-flowing pool water permitting heat dissipation. After fuel loading is complete, the TC cask and DSC are removed from the pool and the DSC is drained, dried, sealed and backfilled with helium.

The unloading operation considered is the reflood of the 24PTH DSC with water.

P.4.7.1 Maximum Fuel Cladding Temperatures During Vacuum Drying

The loading condition evaluated for the NUHOMS®-24PTH DSC is the heatup of the DSC before its cavity is backfilled with helium. This typically occurs during the performance of the vacuum drying operation of the DSC cavity with the TC in the vertical configuration inside the fuel handling building, and the annulus between the TC and the DSC is full of water.

Analyses were performed for the vacuum drying condition in order to ensure that the fuel cladding and 24PTH DSC structural component temperatures remain below the maximum allowable material limits. In addition, a transient analysis was performed to ensure that the requirements defined by ISG-11 [4.19] for short-term operations (including vacuum during and helium backfilling operating conditions) are satisfied.

During vacuum drying operation, water in the DSC cavity is forced out of the cavity (blowdown operation) before the start of vacuum drying. Two alternate options for the gas medium used for the water blowdown operation are evaluated in the thermal analysis performed as described here.

In the first option, air is used as the gas medium to remove water and subsequent vacuum drying occurs with air environment in the DSC cavity. In the second option, helium is used as the medium to remove water and subsequent vacuum drying occurs with helium environment in the DSC cavity.

The vacuum drying of the DSC is assumed not to reduce the pressure sufficiently to reduce the thermal conductivity of the water vapor, air or helium in the DSC cavity [4.17], [4.18], and [4.35]. Therefore, whether air or helium are used for blowdown operation, correspondingly, air or helium are also assumed during vacuum drying operations. Radiation in the gaps within the basket and rail components is conservatively neglected.

A transient thermal analysis is performed using the three-dimensional model developed in Section P.4.6, with decay heat loads for HLZCs 1, 4, and 5 and an initial DSC shell surface temperature of 215°F. The initial temperature of the DSC, basket and fuel is assumed to be 215°F, based on the saturation boiling temperature of the fill water. Table P.4-30 provides the maximum calculated temperatures for the fuel cladding and Table P.4-31 through Table P.4-33 provide the maximum calculated basket component temperatures for all three configurations. Figure P.4-42 provides the maximum fuel cladding temperatures during the vacuum drying transient with air. The maximum cladding temperatures of 663°F, 668°F, and 645°F reached at 19 hours, 25 hours, and 28 hours during vacuum drying of 24PTH-S DSC with 40.8 kW, 31.2 kW, and 24 kW heat load, respectively, are below the limit of 752°F [4.19].

P.4.7.2 Evaluation of Thermal Cycling of Fuel Cladding During Vacuum Drying, Helium Backfilling and Transfer Operations

ISG-11 [4.19] also states that thermal cycling is to be minimized and imposes a limit of 65°C (117°F) on thermal cycling (reduction in fuel clad temperature from previous peak temperature). The basis for the limit is that as the cladding temperature is reduced more than 65°C the concentration of hydrogen available for hydride reorientation becomes significant.

The thermal analysis of the 24PTH DSC during blowdown operation assumes helium is used instead of air to drain the water from the 24PTH DSC cavity and subsequent vacuum drying occurs with a helium environment. This option eliminates a fuel cladding temperature drop that would take place during helium backfilling of the 24PTH DSC subsequent to vacuum drying in an air environment and it eliminates the need for a time limit on the vacuum drying operation, since the thermal conductivity of helium does not change with pressure during vacuum drying operations.

When air is used to blowdown and drain the water from the 24PTH DSC cavity, the cask is in the same configuration as described in Section P.4.7.1 and the annulus between the cask and DSC is filled with water. After vacuum drying operations, the DSC is backfilled with helium. This case results in the lowest steady state fuel cladding temperature during the DSC drying/backfilling operations.

The maximum fuel cladding temperature limit for vacuum drying in an air environment (before helium backfilling) is defined as the steady state maximum fuel cladding temperature achieved during helium backfilling operation plus 100°F (to provide an additional margin to the maximum ΔT= 117°F allowed):

$$T_{\text{fuel max allowed for vac dr}} = T_{\text{fuel max helium backfilling steaty-state}} + 100°F$$

For 24PTH DSC with HLZC # 1 the limit is:

$$T_{\text{fuel max allowed for vac dr}} = T_{\text{fuel max helium backfilling steaty-state}} + 100°F = 533°F + 100°F = 663°F$$

Thus, the maximum temperature difference for the fuel cladding during vacuum drying in air and subsequent helium backfilling operations is 100°F (See Table P.4-30). This temperature difference meets the thermal cycling criteria specified by ISG-11 [4.19].

Since there is no change in the maximum fuel cladding temperatures during vacuum drying in a helium environment and helium backfill operations, the thermal cycling limit of $\Delta T_{ISG\ limit}$ = 65°C (117°F) listed in ISG-11 [4.19] is satisfied for the 24PTH DSC for vacuum drying in helium and subsequent helium backfilling operations.

The conservative time limit for vacuum drying in an air environment for the 24PTH DSC is 19 hours for 40.8 kW/DSC (HLZC #1), 25 hours for 31.2 kW/DSC (HLZC #4), and 28 hours for 24.0 kW/DSC (HLZC #5).

As shown in Table P.4-30 the maximum fuel cladding temperature limit of $T_{ISG\ limit}$ = 400°C (752°F) and the 65°C (117°F) ΔT_{limit} listed in ISG-11 [4.19] are satisfied for the 24PTH DSC.

P.4.7.3 Reflooding Evaluation

For unloading operations, the DSC is filled with the spent fuel pool water through its siphon port. During this filling operation, the DSC vent port is maintained open with effluents routed to the plant's off-gas monitoring system. The NUHOMS®-24PTH DSC operating procedures recommend that the DSC cavity atmosphere be sampled prior to introducing any reflood water in the DSC cavity.

Initially, the pool water is added to the DSC cavity containing hot fuel and basket components, some of the water will flash to steam causing internal cavity pressure to rise. This steam pressure is released through the vent port. The procedures specify that the flow rate of the reflood water be controlled such that the internal pressure in the DSC cavity does not exceed 20 psig. This is assured by monitoring the maximum internal pressure in the DSC cavity during the reflood event. The reflood for the DSC is considered as a Service Level D event and the design pressure of the DSC is 120 psig for 24PTH-S or –L DSCs and 90 psig for 24PTH-S-LC DSC. Therefore, there is sufficient margin in the DSC internal pressure during the reflooding event to assure that the DSC will not be over pressurized.

The maximum fuel cladding temperature during reflooding event is significantly less than the vacuum drying condition owing to the presence of water/steam in the DSC cavity. The analysis results presented in Table P.4-30 show that the maximum cladding temperature during vacuum drying is 668°F. Hence, the peak cladding temperature during the reflooding operation will be less than 668°F.

To evaluate the effects of the thermal loads on the fuel cladding during reflooding operations, a conservative assumption of high maximum fuel rod temperature of 750°F and a low quench water temperature of 50°F are used.

The material properties, corresponding to a temperature of 750°F, are used in the evaluation:

Modulus of Elasticity, E (psi) = 11.1 x10^6 [from Figure 4 of 4.10]
Coefficient of thermal expansion, α, (in/in/°F) = 3.73 x 10-6 [4.11]
Poison's Ratio, ν, = 0.38 [4.12]
Yield Stress (irradiated), Sy, = 50,500 psi [4.13 [4.10]

The fuel cladding is evaluated as a hollow cylinder with an outer surface temperature of T (50°F), and the inner surface temperature of T+ΔT (750°F) using [4.13] equations. The maximum thermal stress in the fuel cladding due to the temperature gradient during reflooding is calculated as follows:

The maximum circumferential stress at the outer surface is given by:

$$\sigma_t = \frac{\Delta T * \alpha \cdot E}{2(1-\nu)\log_e(c/b)} * \left(1 - \frac{2 * b^2}{(c^2 - b^2)} * \log_e c/b\right)$$

The maximum circumferential stress at the inner surface is given by:

$$\sigma_t = \frac{\Delta T * \alpha \cdot E}{2(1-\nu)\log_e(c/b)} * (1 - \frac{2 * c^2}{(c^2 - b^2)} * \log_e c/b)$$

The maximum stresses are calculated as 22,420 psi (outer surface) and 24,325 psi (inner surface). Based on the results of the thermal stress analysis, these stresses in the cladding during reflood is much less than the yield stress of 50,500 psi [4.10]. Therefore, cladding integrity is maintained during reflood operations.

Therefore, no cladding damage is expected due to the reflood event. This is also substantiated by the operating experience gained with the loading and unloading of transportation packages like IF-300 [4.8] which show that fuel cladding integrity is maintained during these operations and fuel handling and retrieval is not impacted.

P.4.8 Determination of Effective Thermal Properties of the Fuel, Basket and Air Within the HSM-H Closed Cavity

This section presents the methodology and determines the effective thermal conductivity, specific heat and density for the fuels to be stored within NUHOMS®-24PTH DSC with helium backfill and vacuum for use in the analysis of the thermal performance of the NUHOMS®-24PTH DSC.

This section also determines the effective thermal conductivity, density and specific heat load of the 24PTH DSC basket for use in the transient thermal analysis in Section P.4.4 and P.4.5. Also included here is the calculation of effective thermal conductivity of air in the HSM-H cavity during blocked vent conditions which includes the effect of closed cavity convection.

P.4.8.1 Determination of Bounding Effective Fuel Thermal Conductivity

P.4.8.1.1 Fuel Assemblies Evaluated

The fuel assemblies that are considered for storage in the NUHOMS® 24PTH DSC, including the design data for each fuel assemblies, are listed in Section P.2. This section includes calculation of the bounding properties among fuels to store in 24PTH-S or -L DSC with maximum total decay heat per DSC up to 40.8 kW. The bounding properties of B&W 15x15 fuel assemblies were calculated for thermal analysis of 24PTH-S-LC DSC with maximum total decay heat of 24 kW per DSC.

P.4.8.1.2 Summary of Thermal Properties of Materials

The thermal conductivity and specific heat values of Zircaloy, UO_2 pellets, and Helium are presented in Section P.4.2. The emissivity of Zircaloy is also presented in Section P.4.2.

P.4.8.1.3 Calculation of Fuel Axial Effective Thermal Conductivity

The axial fuel conductivity is assumed to be limited to the cladding conductivity weighted by its fractional area as required in NUREG 1536 [4.7].

$$K_{axl} = (K_{zirc})(A_{zirc}/A_{eff}) \qquad (1)$$

K_{zirc} = Conductivity of Zircaloy 4
A_{eff} = (8.90") x (8.90") = 79.21 in^2
A_{zirc} = Cross section area of Zircaloy cladding in the fuel assembly

Equation (1) is used to calculate axial effective conductivity for the fuel assembly types listed in Section P.2. The results are plotted in Figure P.4-44.

P.4.8.1.4 Calculation of Fuel Transverse Effective Thermal Conductivity

The transverse fuel effective conductivity is determined by creating a two-dimensional finite element model of the fuel assembly centered within a fuel compartment. The outer surfaces, representing the fuel compartment tube walls, are held at a constant temperature and heat generating boundary condition is applied to the fuel pellets within the model. A maximum fuel assembly temperature is

then determined. The isotropic effective thermal conductivity of a heat generating square, such as the fuel assembly, can be calculated as described in [4.22].

$$K_{eff} = 0.29468 \times \frac{Q'''}{a^2 (T_c - T_o)} \qquad (2)$$

where:

Q''' = heat load per unit volume of fuel assembly (Btu/hr-in^3),
a = half width of fuel compartment opening = 8.9 / 2 = 4.45",
Tc = maximum temperature of fuel assembly (°F),
To = compartment wall temperature (°F).

with

$$Q''' = \frac{Q}{4a^2 L_a} \qquad (3)$$

where:

Q= decay heat load per assembly,
L_a = active fuel length

In determining the temperature dependent effective fuel conductivities, an average temperature, equal to $(T_c + T_o)/2$, is used for the fuel temperature.

2-D finite element models of each fuel assembly representing a quarter of the fuel assembly were modeled within ANSYS [4.6]. Plane 55 elements were used to model components such as the fuel pellets, fuel cladding, and the helium back fill gas. The gap between the fuel cladding and the fuel pellets is also included in the model.

Heat generated in the fuel pellets dissipates by conduction and radiation to the fuel compartment walls. Convection is not considered in the model. Radiation between the fuel rods, guide tubes, and basket walls was simulated using the radiation super-element processor (/AUX12). LINK32 elements were used for modeling of radiating surfaces in creating the radiation super-element and were unselected prior to the solution of the model. The compartment walls are not modeled as a solid entity. Only the LINK32 elements aligned with the outermost nodes of the model (not on symmetry lines) are given the emissivity of the compartment walls.

Emissivity of stainless steel (0.46) was applied to the LINK elements on fuel compartment tube walls. To eliminate the radiation heat transfer across the symmetry lines, the link elements on symmetry lines were given a very low emissivity (0.001).

The B&W 15x15 fuel assembly finite element model is shown in Figure P.4-43 as a typical for all the fuel types considered.

Since a quarter of fuel assembly is modeled in each case, the reaction solution after solving the 2D model is equal to the heat generated per unit length of the active fuel divided by four.

$$Q_{react} = \frac{Q}{4L_a} \qquad (4)$$

Substitution of equations (3) and (4) in equation (2) gives:

$$K_{eff} = 0.29468 \times \frac{Q_{react}}{(T_c - T_o)} \qquad (5)$$

Equation (5) is used to calculate the transverse effective fuel conductivity for each fuel assembly model.

The heat generating boundary conditions for each assembly is calculated as shown in equation 6.

$$dhl = \frac{Q/N}{n\left(\frac{\pi}{4} d_p^{\,2}\right) L_a} \qquad (6)$$

dhl = Heat generating boundary condition, Btu/min-in-°F
Q = Total decay heat load, Btu/min
N = Number of assemblies, 24
n = Number of fuel rods
d_p = Pellet outer diameter, in
L_a = Active fuel length, in

The models were run with a series of isothermal boundary conditions applied to the nodes representing the fuel compartment walls. The symmetry lines going through the center of the fuel assembly are kept at the adiabatic boundary conditions.

P.4.8.1.5 Results

Figure P.4-44 shows the calculated axial effective conductivities for fuel to store in 24PTH-S DSC and –L DSC. As Figure P.4-44 shows, WE 14x14 has the minimum (bounding) axial conductivity. Backfill gas property does not have any effect on the axial effective fuel conductivity. Therefore, identical axial effective fuel conductivity values can be used for helium and vacuum conditions.

Figure P.4-45 shows the calculated axial effective conductivities for the B&W 15x15 fuel to be stored in 24PTH-S-LC DSC. As Figure P.4-45 shows, BW 15x15 Mk-11 has the minimum (bounding) axial conductivity among BW 15x15 fuels. Backfill gas property does not have any effect on the axial effective fuel conductivity. Therefore, identical axial effective fuel conductivity values can be used for helium and vacuum conditions.

The calculated bounding axial effective conductivities for fuels to store in 24PTH-S DSC, -L DSC, and –S-LC DSC are listed in Section P.4.2.

The calculated transverse conductivities for fuels to store in 24PTH-S and –L DSC are presented in Figure P.4-46 and Figure P.4-47for helium and vacuum conditions, respectively. As shown herein, WE 14x14 assembly has the (bounding) minimum transverse conductivity for helium and vacuum conditions. The bounding transverse effective conductivity values for fuels to store in 24PTH-S DSC and -L DSC are listed in Section P.4.2.

The calculated transverse conductivities for B&W 15x15 fuels to store in 24PTH-S-LC DSC are presented in Figure P.4-48 and Figure P.4-49 for helium and vacuum conditions, respectively. The bounding transverse effective conductivity values for fuels to store in 24PTH-S-LC DSC are listed in Section P.4.2.

P.4.8.2 Calculation of Fuel Effective Specific Heat and Density

This section presents the calculation of the fuel effective specific heat and density used in the transient thermal analyses.

Volume average density and weight average specific heat are calculated to determine the effective density and specific heat for the fuel assembly.

The equations to determine the fuel effective density ρ_{eff} and specific heat $C_{p\,eff}$ are shown below.

$$\rho_{eff} = \frac{\sum \rho_i V_i}{V_{assembly}} = \frac{\rho_{UO2}\ V_{UO2} + \rho_{Zr4}\ V_{Zr4}}{4a^2 L_a}$$

$$C_{P,eff} = \frac{\sum \rho_i V_i C_{Pi}}{\sum \rho_i V_i} = \frac{\rho_{UO2}\ V_{UO2}\ C_{P,UO2} + \rho_{Zr4}\ V_{Zr4}\ C_{P,Zr4}}{\rho_{UO2}\ V_{UO2} + \rho_{Zr4}\ V_{Zr4}}$$

where:

ρ_i, $C_{p,i}$, V_i = density, specific heat, and volume of component,
L_a = active fuel length, and
a = half of compartment width.

The properties of Zircaloy-4 and UO_2 are provided in Section P.4.2.

The calculated minimum (bounding) values of fuel effective specific heat and fuel effective density for fuel to store in 24PTH-S DSC, -L DSC and -S-LC DSC are summarized in Section P.4.2.

P.4.8.3 24PTH DSC Basket Effective Thermal Properties

The 24PTH DSC basket effective density, thermal conductivity and specific heat are calculated for use in the transient analyses of the 24PTH DSC in the OS197FC transfer cask and in the HSM-H. The calculation of these thermal effective properties is based on the DSC component weights.

The 24PTH DSC effective density $\rho_{eff\ DSC\ basket}$, and specific heat $c_{p\ eff\ DSC\ basket}$ are calculated as volumetric and weight average values, respectively.

The effective transverse thermal conductivity is determined by theoretical solution for conduction in an infinite cylinder with uniform heat generation [4.41]:

$$k_{eff-basket} = \frac{Q}{4\pi \cdot L \cdot (T_c - T_s)}$$

where
- Q is total heat load, W
- L is cylinder (DSC cavity) length, m,
- T_C is temperature at the cylinder center, ℃
- T_S is temperature at the cylinder surface. ℃

The effective transverse thermal conductivities of the 24PTH DSC basket $k_{eff\text{-}basket}$ are calculated for 40.8, 31.2, and 24 kW total heat loads per DSC, using the 24PTH DSC ANSYS models.

The heat generation is applied to the fuel assemblies uniformly without a peaking factor. The temperatures from 100°F to 800°F are applied uniformly to the DSC shell.

An average, $(T_s+T_c)/2$, is used as the reference temperature, for which $k_{eff\text{-}basket}$ is reported.

The criterion for determining the bounding 24PTH DSC basket effective density $\rho_{eff\ DSC\ basket}$, and specific heat $c_{p\ eff\ DSC\ basket}$ is based on the lowest value of $c_{p\ eff\ DSC\ basket}$ and $\rho_{eff\ DSC\ basket}$.

The DSC basket axial effective thermal conductivity is conservatively calculated based on axial fuel effective thermal conductivity:

$$k_{basket\ axial} = k_{fuel\ axial} \cdot A_{fuel\ cells} / A_{\ DSC\ internals}\ .$$

where
- $k_{basket\ axial}$ is DSC axial effective thermal conductivity,
- $k_{fuel\ axial}$ is fuel axial effective thermal conductivity,
- $A_{fuel\ cells}$ is total fuel cells cross-section area,
- $A_{\ DSC\ internals}$ is cross-section area within DSC shell.

The bounding radial and axial thermal conductivity values for 24PTH-S and 24PTH-L, and -S-LC DSCs are shown in Section P.4.2.

P.4.8.4 Effective Air Conductivity in the HSM-H Closed Cavity

During blockage of the inlet and outlet vents, the air within the HSM-H is trapped. The convection heat transfer under these circumstances reduces to free convection in closed cavities. To simplify

the model, an effective conductivity is calculated that includes the conduction and convection heat transfer through the air within the closed cavity of the HSM-H.

Reference [4.17] introduces the following correlation that is used to calculate the conduction and convection heat transfer in closed cavities for eccentric horizontal cylinders.

$$Nu = [Nu_{COND}, Nu_I]_{max} \qquad (1)$$

With

q' = heat transfer by conduction and convection from the inner cylinder to the outer one per unit axial length of cylinder

$$Nu_{COND} = \frac{\ln(D_o / D_i)}{\cosh^{-1}[(D_o^2 + D_i^2 - 4E^2)/2D_oD_i]}$$

$$Nu_I = 0.603\,\overline{C}_I \frac{(\ln D_o / D_i)\, Ra^{1/4}}{[(L/D_i)^{3/5} + (L/D_o)^{3/5}]^{5/4}}$$

where,

$$Ra = \frac{g\beta(T_i - T_o)L^3}{\nu^2} \times \Pr \qquad \text{with} \qquad L = (D_o - D_i)/2 \qquad \text{and}$$

$$\overline{C}_I = \tfrac{1}{3} \frac{0.503}{[1 + (0.492/\Pr)^{9/16}]^{1/9}}$$

The geometry and dimensions to use in the correlations are shown in the following figure.

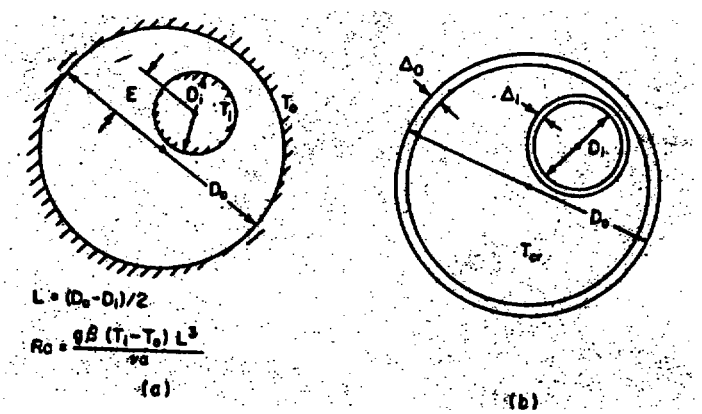

Sketch of concentric and eccentric cylinder and sphere problems [4.22]

The Nu in correlation (1) is defined as

$$Nu = \frac{q' \ln(D_o / D_i)}{2\pi(T_i - T_o)k}$$

The above equation shows that the air effective conductivity is equal to the product of the Nusselt number and the air conductivity for the closed cavity between cylinders.

$k_{eff} = Nu\ k_w$

k_{eff} = *effective conductivity for conduction and convection from inner to outer cylinder*
k = conductivity of air

All air properties are evaluated at an average temperature, as given by:

$$T_{avg} = (T_o + T_i)/2$$

In order to use the above correlations for the HSM-H cavity, a hydraulic diameter is calculated for the cross section of the HSM-H cavity surrounded by the side and top shields. The hydraulic diameter of the HSM-H cavity is given by:

$$D_{h,HSM} = \frac{4A}{P} = \frac{4\times(82.375\times168)}{2\times(82.375+168)} = 115"$$

The air effective conductivity defined in the above correlations depends on the inner cylinder and outer cylinder temperatures (T_i and T_o) and the associated radial gradient. A study of the effect of T_i and T_o on the effective conductivity of air in the closed cavity of the HSM-H is performed. In the study, the inner temperature (T_i) varies from 425°F to 825°F, which represents the DSC shell temperature during blockage of the vents. The outer temperature (T_o) varies from 150°F to 350°F, which represents the HSM-H thermal shield and/or the concrete temperatures. The gradient between T_i and T_o varies from 275°F to 475°F.

The minimum temperature gradient observed in the model occurs between the middle of the side heat shield and the DSC side. The minimum gradient after 40 hour blockage of the vents is:

574 (DSC side) – 451 (side heat shield) = 123°F

The maximum temperature gradient occurs between the uncovered top corner of the HSM-H and top of the DSC shell. The maximum gradient after 40 hour blockage of the vents is:

581 (DSC side) – 214 (side heat shield) = 367°F

The temperature gradients covered in the study are higher than the gradients observed after solving the model. Nonetheless, using the calculated value of 0.05 Btu/hr-in-°F for effective air conductivity is deemed acceptable since the concrete temperature is the limiting factor in the blocked vent thermal analysis. Using a higher temperature gradient, which results in a higher air effective conductivity value, increases the heat transfer from the DSC shell to the concrete walls and causes a higher concrete temperature during blockage of the vents. To study the maximum temperature gradients during blockage of the vents, the single HSM-H model is modified for the transient run with -40°F ambient conditions.

The calculated effective conductivity of air with the HSM-H cavity for all of the blocked vent cases is 0.05 Btu/hr-in-°F.

P.4.9 Determination of Convection Heat Transfer Coefficients for the HSM-H Surfaces and Components

P.4.9.1 Convection Coefficient for the HSM-H Side Heat Shield

For the side heat shield, the fin width, W, is much larger than the distance between the parallel fin plates, S, the convection coefficient is the same as for parallel –plate channels. Reference [4.17] specifies the following correlations for parallel-plate channels, when W/S≥5.

$$Nu \approx \frac{Ra}{24} \qquad \text{for Ra} \le 10$$

$$Nu = 0.62\, Ra^{1/4} \qquad \text{for } 10 < \text{Ra} < 1000$$

$$Nu = \left[\left(\frac{Ra}{24}\right)^{m} + \left(0.62\, Ra^{1/4}\right)^{m}\right]^{1/m} \qquad \text{with m=-1.9 for Ra} < 10^5$$

The Rayleigh number for the above correlations is defined in the following figure

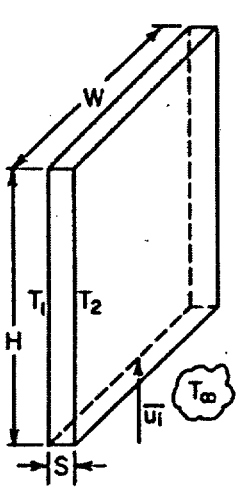

Specified wall temperatures

$$Nu = \frac{qS}{2HW\,(\bar{T}_w - T_\infty)\,k}$$

$$Ra = \frac{g\beta(\bar{T}_w - T_\infty)\,S^3}{\nu\alpha}\,\frac{S}{H}$$

$$Re = \bar{u}_i\, S/\nu$$

$$\bar{T}_w = \frac{1}{2}\,(T_1 + T_2)$$

$$T^* = \frac{T_2 - T_\infty}{T_1 - T_\infty};\ T_1 \ge T_2;\ 0 \le T^* \le 1$$

Geometry and nomenclature for natural-convection heat transfer from a wide ($W \gg S$), rectangular cooling slot with temperature-specified conditions on the walls.

Since the average plate temperature is first unknown, the model is solved iteratively. The final results for the convection coefficients on side heat shields for various decay heat load and ambient temperature range from 0.0035 Btu/hr-in^2-°F to 0.0045 Btu/hr-in^2-°F.

The fins are modeled as flat plates to reduce the number of SHELL57 elements in the creation of an ANSYS radiation super-element in Section P.4.4.4. To compensate for the reduced area, an effective convection coefficient is calculated for the fins.

The value of h_{fin} used in the model is 0.031 Btu/hr-in^2-°F which bounds all ambient conditions and decay heat loads.

The distance between the base plate of the HSM-H side heat shield and the HSM-H side wall is 2". The intersections of the HSM-H base plate and the HSM-H side walls create a narrow channels behind the side heat shield. The convection coefficient for these narrow channels are calculated using the same methodology described above.

The value of $h_{channel}$ used in the model is 0.003 Btu/hr-in^2-°F which bounds all ambient conditions and decay heat loads.

Convection Coefficients for a Horizontal Cylinders (DSC):

The following equations from Reference [4.17] are used to calculate the free convection coefficients.

$$Nu = \left[(Nu_l)^m + (Nu_t)^m\right]^{1/m} \qquad with \quad m = 3.3 \quad for \quad 10^{-10} < Ra < 10^{10}$$

$$h_c = \frac{Nu\ k}{D}$$

with:

D = diameter of the horizontal cylinder,
k = air conductivity.

$$Ra = Gr\ \mathrm{Pr} \quad , \quad Gr = \frac{g\beta(T_w - T_\infty)D^3}{\nu^2}$$

$$Nu_l = \frac{2f}{\ln(1 + 2f / Nu^T)}$$ (Nusselt number for fully laminar heat transfer)

$Nu_t = \overline{C}_t\ Ra^{1/3}$ (Nusselt number for fully turbulent heat transfer)

$\overline{C}_t = 0.103$ -for horizontal cylinders [4.14].

Convection Coefficients for the HSM-H Vertical Flat Surfaces (End Wall, Side Wall, Vertical Surface of the DSC Plugs, and Side Heat Shield without Fins):

$$Nu = \left[(Nu_l)^m + (Nu_t)^m\right]^{1/m} \qquad with \quad m = 6 \quad for \quad 1 < Ra < 10^{12}$$

$$h_c = \frac{Nu\ k}{L}$$

with:

L = height of the vertical surface

k = air conductivity

$$Nu_l = \frac{2.8}{\ln(1+2.8/Nu^T)}$$ (Nusselt number for fully laminar heat transfer)

$Nu^T = \overline{C}_l \; Ra^{1/4}$, $\overline{C}_l = 0.515$ for gases [4.30],

$Nu_t = C_t^V \; Ra^{1/3}$ (Nusselt number for fully turbulent heat transfer)

$$C_t^V = \frac{0.13\,\mathrm{Pr}^{0.22}}{(1+0.61\,\mathrm{Pr}^{0.81})^{0.42}}$$

Convection Coefficients for the HSM-H Horizontal Surfaces Facing Upwards (Basemat):

$Nu = \left[(Nu_l)^m + (Nu_t)^m\right]^{1/m}$ *with* $m = 10$ *for* $Ra > 1$

$$h_c = \frac{Nu\,k}{L}$$

with:

L = A/P
A = Surface area of heated surface
P = perimeter of the heated surface
k = air conductivity

$Ra = Gr\,\mathrm{Pr}$, $Gr = \frac{g\beta(T_w - T_\infty)L^3}{\nu^2}$

$$Nu_l = \frac{1.4}{\ln(1+1.4/Nu^T)}$$ (Nusselt number for fully laminar heat transfer)

$Nu^T = 0.835\,\overline{C}_l \; Ra^{1/4}$, and $\overline{C}_l = 0.515$ for gases [4.17]

$Nu_t = C_t^H \; Ra^{1/3}$ (Nusselt number for fully turbulent heat transfer)

$C_t^H \approx 0.14$ for Pr < 100 [4.17]

Convection Coefficients for the HSM-H Horizontal Surfaces Facing Downwards (Ceiling):

$Nu = Nu_l$

$$h_c = \frac{Nu\,k}{L}$$

with:

L = A/P
A = surface area of heated surface
P = perimeter of the heated surface
k = air conductivity

$$Ra = Gr\ \mathrm{Pr} \quad ; \quad Gr = \frac{g\,\beta (T_w - T_\infty) L^3}{\nu^2}$$

$$Nu_l = \frac{0.527\,Ra^{1/5}}{[1+(1.9/\mathrm{Pr})^{9/10})^{2/9}}$$

Convection Coefficients for the HSM-H Inclined Surfaces, Positive Angled (Web and Upper side of Supporting Beam Flange):

Reference [4.17] gives the following correlations for free convection over inclined flat plates. The angle of inclined surface is measured from vertical line. The positive or negative sign of the angle is defined in figure below.

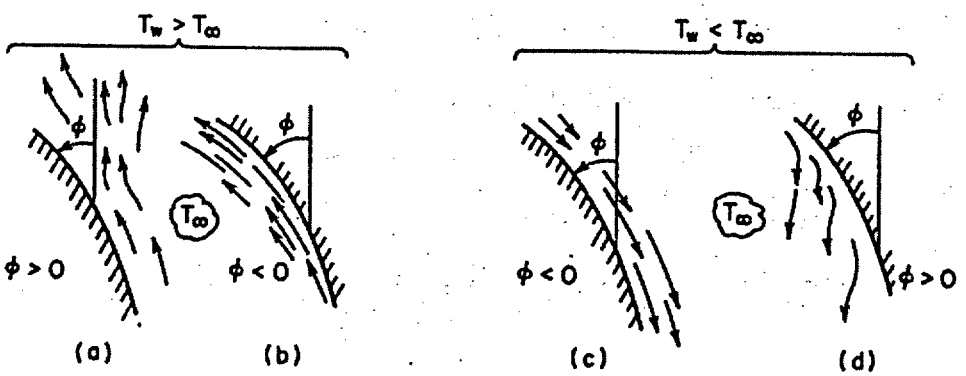

Definition of surface angle ϕ for a heated wall (a and b), and a cooled wall (c and d). If the flow is turbulent, a and d depict detached flow, b and c attached flow.

Definition of Surface Angle ϕ for a Heated Wall

$$Nu = \left[(Nu_l)^m + (Nu_t)^m\right]^{1/m} \qquad with \quad m = 6 \quad for \quad 1 < Ra < 10^{12}$$

$$h_c = \frac{Nu\ k}{L}$$

with:

L = length of the inclined plate
k = air conductivity

$$Ra = Gr\ \mathrm{Pr} \quad ; \quad Gr = \frac{g\,\beta (T_w - T_\infty) L^3}{\nu^2}\cos\phi$$

$$Nu_l = \frac{2.8}{\ln(1+2.8/Nu^T)} \qquad \text{(Nusselt number for fully laminar heat transfer)}$$

$$Nu^T = \overline{C}_l\ Ra^{1/4} \qquad , \ \overline{C}_l = 0.515 \quad \text{for gases}$$

$$Nu_t = C_t\ Ra^{1/3} \qquad \text{(Nusselt number for fully turbulent heat transfer)}$$

$$C_t = C_t^V \cos^{1/3}\phi \quad \text{for} \quad -90^\circ \le \phi \le \tan^{-1}\left(\frac{C_t^V}{C_t^H}\right)^3$$

$$C_t = C_t^H \sin^{1/3}\phi \quad \text{for} \quad \tan^{-1}\left(\frac{C_t^V}{C_t^H}\right)^3 \le \phi \le 90^\circ$$

with:

$$C_t^V \approx \frac{0.13\,\mathrm{Pr}^{0.22}}{(1+0.61\,\mathrm{Pr}^{0.81})^{0.42}}$$

$$C_t^H \approx 0.14 \qquad \textit{for} \qquad \mathrm{Pr} < 100$$

Convection Coefficients for the HSM-H for Inclined Surfaces, Negative Angled (Lower Side of Supporting Beam Flange):

$$Nu = \left[(Nu_l)^m + (Nu_t)^m\right]^{1/m} \qquad \textit{with} \quad m = 6 \quad \textit{for} \quad 1 < Ra < 10^{12}$$

$$h_c = \frac{Nu\,k}{L}$$

with:

L = length of the inclined plate
k = air conductivity

$$Ra = Gr\,\mathrm{Pr} \quad , \quad Gr = \frac{g\,\beta\,(T_w - T_\infty)\,L^3}{\nu^2} \times \cos\phi$$

$$Nu_{l,V} = \frac{2.8}{\ln(1+2.8/Nu^T)}$$

$$Nu^T = \overline{C}_l\,Ra^{1/4} \quad , \; \overline{C}_l = 0.515 \quad \text{for gases}$$

$$Nu_{l,H} = \frac{0.527\,Ra^{1/5}}{[1+(1.9/\mathrm{Pr})^{9/10})^{2/9}}$$

$Nu_l = \max[Nu_{l,V}, Nu_{l,H}]$ (Nusselt number for fully laminar heat transfer)

$Nu_t = C_t\,Ra^{1/3}$ (Nusselt number for fully turbulent heat transfer)

$$C_t = C_t^V \cos^{1/3}\phi \quad \text{for} \quad -90^\circ \le \phi \le \tan^{-1}\left(\frac{C_t^V}{C_t^H}\right)^3$$

$$C_t = C_t^H \sin^{1/3}\phi \quad \text{for} \quad \tan^{-1}\left(\frac{C_t^V}{C_t^H}\right)^3 \le \phi \le 90^\circ$$

with $C_t^V \approx \dfrac{0.13\,\mathrm{Pr}^{0.22}}{(1+0.61\,\mathrm{Pr}^{0.81})^{0.42}}$

$$C_t^H \approx 0.14 \qquad \textit{for} \qquad \mathrm{Pr} < 100$$

The above correlations are incorporated in ANSYS model described in Section P.4.4.4.

P.4.9.2 Convection Coefficient for the HSM-H Top Heat Shield

The top shield is a louver design that consists of several inclined plates. Because of the relative large opening between these inclined plates and their collective short length, the interference of the thermal boundary layers is assumed to be minimal such that the convection coefficient can be calculated separately for each plate. The total convection from each inclined plate is given by:

$$q_{conv} = (h_{up} + h_{down}) A_p (T_p - T_\infty)$$

with h_{up} = convection coefficient on upper surface of louver plates (positive angled)
h_{down} = convection coefficient on lower surface of louver plates (negative angled)
$Ap = l \times h = 24 \times 2 = 48 \text{ in}^2$ plate surface area
$T_\infty = T_g = 178^\circ F$ air temperature (See Section P.4.4.3)

h_{up} and h_{down} are calculated using the correlations described above in Section P.4.9.1 for inclined plates.

The louver is modeled as a flat plat to reduce the number of SHELL57 elements as required in creation of an ANSYS radiation super-element. To compensate for the reduced area, an effective convection coefficient is calculated for the louver, as follows:

$$h_{louver,eff} = (h_{up} + h_{down}) \cdot \frac{A_{louver}}{A_{model}}$$

$$A_{louver} = n_{louver} \times n_{segments} \times A_p$$

$$A_{model} = 15'2" \times 6'2" = 14196 \text{ in}^2$$

P.4.9.3 Combination of Heat Transfer Coefficients for the HSM-H Roof and Front Wall

The HSM-H roof and the front wall dissipate heat to the ambient via free convection and radiation. The total heat transfer coefficient, H_t, is used to combine the convection and radiation heat transfer together, as follows:

$$H_t = h_r + h_c$$

where:

h_r = radiation heat transfer coefficient
h_c = free convection heat transfer coefficient,
horizontal surface facing upwards for roof and
vertical flat surface for front wall described above in Section P.4.9.1

The radiation heat transfer coefficient, h_r, is given by the equation:

$$h_r = \varepsilon F_{12} \left[\frac{\sigma(T_1^4 - T_2^4)}{T_1 - T_2} \right] Btu/hr - ft^2 - {}^o F$$

where,

ε = surface emissivity,
F_{12} = view factor from surface 1 to ambient,
σ = 0.1714×10^{-8} Btu/hr-ft^2-R^4,
T_1 = surface temperature, (R),
T_2 = ambient temperature, (R).

The above correlations for heat transfer coefficients are incorporated in ANSYS model of Section P.4.4.4.

P.4.10 Confirmatory Thermal-Hydraulic Analysis Of The HSM-H

A confirmatory thermal-hydraulic analysis [4.46] of the NUHOMS® HSM-H under bounding normal and off-normal conditions of storage was conducted using the Fluent™ code [4.44] with the Icepak™ module [4.45]. The Fluent™ code is a general purpose CFD (i.e., computational fluid dynamics) code that is recognized internationally as one of the premier codes in its class. The general modeling capabilities of the code as they relate to this application include:

- Meshing flexibility using structured and unstructured mesh generation with hexahedra, non-hexahedra, and tetrahedral mesh types
- Capability to model low speed, buoyancy driven flow regimes
- Steady-state and transient flows
- Inviscid, laminar, and turbulent flows
- Heat transfer including forced, natural, and mixed convection, conjugate heat transfer, as well as several radiation models
- Custom materials property database

The Icepak™ module is a fully interactive, object-based graphical interface that serves as pre- and post-processor to the Fluent™ code. While the Icepak™ module is specifically designed for the analysis of electronic enclosures, its operational features are fully capable of handling the geometry for this application. The verification and validation of the codes was performed for the computation of the convection process within an enclosure.

This confirmatory analysis uses a CFD methodology to directly calculate the prototypical flow regime from the inlet vents of the HSM-H, through the inlet structure, around the DSC and heat shields, and through the exit vents and back to the ambient. The analysis is conducted for steady-state conditions of 105°F ambient air (i.e., equivalent to a peak ambient temperature of 117°F) and with a decay heat loading within the DSC of 40.8 kW. With some simplifications, The Fluent™/Icepak™ model of the HSM-H uses the same geometry, material properties, and heat load distribution assumptions as the ANSYS analytical model described in Section P.4.4.4.

Figure P.4-51 and Figure P.4-52 illustrate the elevation and isometric wire frame views of the thermal-hydraulic model developed for this evaluation. The +x axis of the model's coordinate system extends across the width of the HSM-H from left to right when facing the front of the HSM-H. The +y axis is aligned with the elevation of the HSM-H with the 0 dimension at the top of the basemat and the maximum dimension at the top of the HSM's roof. The +z axis extends from the back of the HSM-H to the front face of the HSM-H. As seen from the solid shaded depiction in Figure P.4-53, the model accurately captures the geometry of the inlet and flow structure along the sides of the model.

The modeling of the DSC within the HSM-H (see Figure P.4-54) uses 3 cylindrical blocks: a 7.45-inch long solid block representing the bottom closure plug, a 8.95-inch long solid block representing the top closure plug, and a 169.6-inch long hollow block representing the 0.5-inch thick shell of the

DSC over the length of the fuel basket. The decay heat loading is simulated as a uniform heat flux applied over the 169.6-inch length of the DSC shell between the closure plugs. For conservatism, the minimum DSC length is assumed for the analysis which is the same as the ANSYS model in Section P.4.4.4.

While the fins on the side heat shields are ignored for simplicity and conservatism, the top heat shield is modeled as individual plates to accurately capture the geometry and the flow regime through the louvers.

The ability of the Fluent™ program to create unstructured computational meshes was used to concentrate the mesh density in those areas requiring greater fluid flow and/or thermal resolution and decrease the mesh density in those areas (i.e., within the concrete walls, etc.) that do not experience large gradients. The resultant unstructured mesh used for this evaluation is illustrated in Figure P.4-55. The total size of the mesh used in the modeling of the HSM-H exceeds 1,629,250 elements.

Table P.4-40 presents a comparison of the peak component temperatures obtained using the ANSYS analytical model vs. those obtained using the confirmatory analysis methodology. As seen from the table, general good agreement is seen between the methodologies, with the CFD based confirmatory methodology predicting lower peak surface temperatures on the DSC by approximately 20°F and essentially the same peak concrete within the base unit. The confirmatory methodology does predict a higher peak roof concrete temperature than the ANSYS analytical model by approximately 25°F, a hotter louvered (i.e., top) heat shield temperature by approximately 15°F, and a hotter side heat shield temperature by approximately 40°F.

The lower predicted DSC temperatures are due to differences in the vertical profile of the air temperature within the HSM-H and differences in the computed convection coefficients. The ANSYS analytical model assumes a linear increase in the air temperature, whereas the computed temperature profile from the CFD analysis places the greatest increase in the air temperature near the top shield and module roof due to the cooling of these structures by the airflow as it passes. This conclusion is supported by the differences in the temperature profiles for the concrete walls and heat shield with vertical height, as predicted by the different methodologies.

The higher side heat shield temperature is directly related to the simplification by the confirmatory analysis in ignoring the approximately 10-fold increase in convective surface area represented by the fins provide on the side shields. The higher peak temperature in the louvered heat shield is due to differences in the airflow distribution across the length and width of the heat shield and to differences in the vertical temperature profile. In keeping with its assumption of uniform flow and temperature profiles, the ANSYS analytical model analysis predicts a nearly flat temperature profile across the shield (i.e., 185.8 to 187.6°F). In contrast, the confirmatory analysis predicts a 12°F variation across the surface of the heat shield, with an average temperature of 197°F.

The difference in the peak temperature of the roof concrete is partly due to differences in the computed view factors between the DSC and the underside of the roof through the louvered heat shield and partially due to differences in the flow distribution within the HSM. The ANSYS analytical model assumption of a fully mixed air temperature within each fluid zones does not factor in the 'plume' of hot air rising from the centerline of the DSC.

In conclusion, while some temperature differences exist between the ANSYS analytical model and the CFD based confirmatory analysis, the differences are understandable and related to the different methodologies employed by the analyses. Further, each analysis predicts that the peak temperatures of the various components are within their respective allowable temperature limits. These results demonstrate that the CFD based confirmatory analysis confirms the overall temperature levels and safety basis of the ANSYS analytical model.

P.4.11 References

4.1 Report, "Topical Report on Actinide-Only Burnup Credit for PWR Spent Nuclear Fuel Packages," Office of Civilian Radioactive Waste Management, DOE/RW-0472, Revision 2, September 1998.

4.2 ASME Boiler and Pressure Vessel Code, Section II, Part D, Properties, 1998, including 2000 addenda.

4.3 Roshenow, W. M., J. P. Hartnett, and Y. I. Cho, *Handbook of Heat Transfer*, 3rd Edition, 1998.

4.4 Bolz, R. E., G. L. Tuve, *CRC Handbook of Tables for Applied Engineering Science*, 2nd Edition, 1973. Transfer, McGraw Hill, 1989.

4.5 Bucholz, J. A., *Scoping Design Analysis for Optimized Shipping Casks Containing 1-, 2-, 3-, 5-, 7-, or 10-Year old PWR Spent Fuel*, Oak Ridge National Laboratory, January, 1983, ORNL/CSD/TM-149.

4.6 ANSYS, Inc., ANSYS Engineering Analysis System User's Manual for ANSYS, Houston, PA.

4.7 NUREG-1536, *Standard Review Plan for Dry Cask Storage Systems,* January 1997.

4.8 Consolidated Safety Analysis Report for IF-300 Shipping Cask, CoC 9001.

4.9 J.P. Holman, Heat Transfer, McGraw Hill, 1989.

4.10 Chun, Ramsey; Witte, Monika; Schwartz, Martin, "Dynamic Impact Effects on Spent Fuel Assemblies," Lawrence Livermore National Laboratory, Report UCID-21246, October, 1987.

4.11 NUREG/CR-0497, "MATPRO-Version 11: "A Handbook of Materials Properties for Use in the Analysis of Light Water Reactor, Fuel Rod Behavior," EG&G, Inc. February, 1979.

4.12 Glasstone, S., Seasonske, A., "Nuclear Reactor Engineering," Third Edition, 1981.

4.13 Young, W.C., "Roark's Formulas for Stress and Strain," Sixth Edition, McGraw Hill.

4.14 Kreith, "The CRC Handbook of Thermal Engineering", 2000.

4.15 Aluminum. Volume 1, Properties, Physical Metallurgy and Phase Diagrams, edited by Kent R. Van Horn, American Society for Metals, Metals Park, Ohio, 1967.

4.16 ASHRAE Handbook, 1981 Fundamentals, 4th Printing, 1983.

4.17 Rohsenow, Hartnett, "Handbook of Heat Transfer Fundamentals, " 2nd Edition, 1985.

4.18 Roth, A., "Vacuum Technology," 2nd Edition, 1982.

4.19 Interim Staff Guidance No. 11, Revision 2, "Cladding Considerations for the Transportation and Storage of Spent Fuel," July 30, 2002.

4.20 TN Response to RAI No. 2 and Submittal of Revision 4 of Application for Amendment No. 5 to the NUHOMS® Certificate of Compliance No. 1004 (TAC No. L23343), January 24, 2003 (Docket 72-1004).

4.21 J. M. Creer, et al, "The TN-24 PWR Spent Fuel Storage Cask: Testing and Analyses," PNL Report, Report No. PNL-6054, 1987.

4.22 SAND90–2806, Sanders, T. L., et al., "A Method for Determining the Spent Fuel Contribution to Transport Cask Containment Requirements," TTC-1019, UC-820, November 1992.

4.23 Oak Ridge National Laboratory, RSIC Computer Code Collection, "SCALE, A Modular Code System for Performing Standardized Computer Analysis for Licensing Evaluation for Workstations and Personal Computers", NUREG/CR-0200, Rev. 6, ORNL/NUREG/CSD-2/V3/R6.

4.24 Report, Azzazy, M., Emissivity Measurements of 304 Stainless Steel, Prepared for Southern California Edison, September 6, 2000, Transnuclear File No. NUH32PT.0100-01

4.25 Duke Energy's letter, Transnuclear, Inc., File No. NUH24PTH-0100-01.

4.26 Frank Kreith, Principles of Heat Transfer, Third Edition, Harper and Row Publishers.

4.27 Incropera and DeWitt, Handbook of Heat And Mass Transfer Fundamentals, 5th edition, Wiley Publishers, 2002, Table A.6 pp 924.

4.28 Bentz, "A Computer Model to Predict the Surface Temperature and Time-of-wetness of Concrete Pavements and Bridge Decks", Report # NISTIR 6551, National Institute of Standards and Technology, 2000.

4.29 Zoldners, "Thermal Properties of Concrete under Sustained Elevated Temperatures", ACI Publications, Paper SP 25-1, American Concrete Institute, Detroit, MI, 1970, Cavanaugh, Guide to Thermal Properties of Concrete and Masonry Systems, Reported by ACI Committee 122, Report #ACI 122R-02, American Concrete Institute, Detroit, MI, 2002.

4.30 Siegel, Howell, "Thermal Radiation Heat Transfer", 4th Edition, 2002.

4.31 ANSYS Computer Code and User's Manuals, Rev. 6.0, See Test Report E-19197, Rev. 0 and E-20184, Rev. 0 for validation of computer code.

4.32 NRC, Code of Federal Regulations, Part 71, "Packaging and Transportation of Radioactive Material", 2003.

4.33 I.E. Idelchik, Handbook of Hydraulic Resistance, 3rd Edition, 1994.

4.34 Rohsenow, Hartnett, and Ganic, Handbook of Heat Transfer Fundamentals, 2nd edition, McGraw-Hill Publishers, 1995

4.35 David R. Lide, *CRC Handbook of Chemistry and Physics*, 83rd edition, 2002-2003, CRC Press.

4.36 SINDA/FLUINT™, Systems Improved Numerical Differencing Analyzer and Fluid Integrator, *Version 4.5, Cullimore & Ring Technologies, Inc., Littleton, CO, 2002*

4.37 Thermal Desktop™, *Version 4.5, Cullimore & Ring Technologies, Inc., Littleton, CO, 2002.*

4.38 Section M.4 of Appendix M, Revision 6 of Application for Amendment No. 5 to the NUHOMS® Certificate of Compliance No. 1004, (TAC NO. L23343).

4.39 "ASHRAE Handbook, Fundamentals" – SI Edition, 1997

4.40 White, F. M., Fluid Mechanics, 2nd Edition, McGraw-Hill, 1986.

4.41 Incropera, F. P., D. P. DeWitt, *Fundamentals of Heat and Mass Transfer*, 3rd Edition, Wiley, 1990.

4.42 Cavanaugh et al., *Guide to Thermal Properties of Concrete and Masonry Systems,* Reported by ACI Committee 122, Report # ACI 122R-02, American Concrete Institute, Detroit, MI, 2002.

4.43 Transnuclear, Inc., TN-68 Dry Storage Cask Final Safety Analysis Report, Revision 0, Hawthorne, NY, 2000 (Docket 72-1027).

4.44 FLUENT™, Version 5.6, Fluent Inc., Lebanon, NH, 2003.

4.45 ICEPAK™, Version 4.08, Fluent Inc., Lebanon, NH, 2003.

4.46 TN Calculation, NUH32PT.0414, Rev. 0, "Validation of FLUENT™/ICEPAK™ for Convective Flow in Enclosures."

4.47 Perry, Chilton, et al, "Chemical Engineer's Handbook," 5th Edition, 1973.

Table P.4-1
Bulk Air Temperatures at Specified HSM-H Regions for the Various Cases[2]

HSM-H Region[1]	Bulk Air Temperatures, (°F)							
	-40°F Case 8	117°F Case 7	-40°F Case 6	117°F Case 5	-40°F Case 4	0°F Case 3	100°F Case 2	117°F Case 1
T0	-37	108	-37	109	-36	4	105	110
T1	-35	112	-34	113	-33	8	110	115
T2	-30	119	-28	122	-25	16	120	125
T3	-25	126	-22	130	-18	24	130	135
T4	-20	133	-16	138	-11	32	140	145
T5	-15	139	-10	146	-4	40	149	155
T6	-10	145	-4	155	4	48	159	165
T7	-5	153	2	163	11	56	169	175
T8	0	160	8	171	18	64	179	185
Ts	-22	130	-19	135	-14	29	135	141

(1) HSM-H Region T1 through T8 are as shown in Figure P.4-2.

(2) Cases are as listed in Section P.4.4.3.

Table P.4-2
HSM-H Components Normal and Off-Normal Maximum Temperatures, 40.8 kW Heat Load

Component	Maximum Temperature (°F)			
	Ambient 117°F Case 1	Ambient 100°F Case 2	Ambient 0°F Case 3	Ambient -40°F Case 4
DSC Shell	448	445	367	333
Concrete	202	197	76	25
Top Heat Shield	188	182	65	18
Side Shield	181	175	60	14
DSC Support Rail	280	276	177	135

Table P.4-3
HSM-H Components Normal and Off-Normal Maximum Temperatures, 31.2 kW Heat Load

Component	Maximum Temperature (°F)		
	Ambient 117°F Case 5[1]	Ambient 117°F Case 5A[2]	Ambient -40°F Case 6
DSC Shell	391	401	270
Concrete	183	201	9
Top Heat Shield	173	176	8
Side Heat Shield	164	221	1
DSC Support Rail	248	254	99

Notes:
(1) The results are with fins on side heat shields.
(2) The results are without fins on side heat shields.

Table P.4-4
HSM-H Components Normal and Off-Normal Maximum Temperatures, 24 kW Heat Load

Component	Maximum Temperature (°F)	
	Ambient 117°F Case 7	Ambient -40°F Case 8
DSC Shell	344	216
Concrete	168	-2
Top Heat Shield	162	0
Side Heat Shield	152	-9
DSC Support Rail	221	71

Table P.4-5
HSM-H Components Maximum Temperatures (°F), 40.8 kW Decay Heat Load, 117°F Ambient, Blocked Vent Accident (Case 9)

Component	38.5 hr Blockage
DSC Shell	578
Concrete[1]	405[1]
Top Heat Shield	313
Side Heat Shield	446
DSC Support Rail	530

1. The calculated temperature is above the 350°F limit given in [4.7]. Testing will be performed to document that concrete compressive strength will be greater than that assumed in the structural analyses.

Table P.4-6
Single HSM-H Components Maximum Temperatures, 40.8 kW Heat Load, -40°F Ambient, Blocked Vent Accident (Case 10)

Component	38.5 hr Blockage
DSC Shell	486
Concrete	234
Top Heat Shield	119
Side Heat Shield	291
DSC Support Rail	434

Table P.4-7
Summary of OS197FC Cases

Description	Applicable Conditions			
	Ambient Temperature (°F)	Insolation		Decay Heat, kW
		Max.[1]	Zero	
Off-Normal Hot	117		x [3]	40.8 [6]
Normal Cold	0		x	40.8 [6]
Off-Normal Hot	117		x [3]	31.2 [7]
Normal Cold	0		x	31.2 [7]
Normal Hot	100	x		31.2 [7]
Vertical Load Transient [4]	100		x	40.8 [6]
Loss of Neutron Shield Transient [5]	100	x		40.8 [6]
Vertical Load Transient [4]	100		x	31.2 [7]
Loss of Neutron Shield Transient [5]	100	x		31.2 [7]
Loss of Air Circulation Transient [8]	100	x		40.8 [6]
Loss of Air Circulation Transient [8]	100	x		31.2 [7]
Normal Hot [9]	100	x		31.2 [6]
Fire Accident [10]	117/1475/117	x		40.8 [6]
Horizontal Load Transient [4]	100	x		40.8 [6]
Off-Normal Hot [9]	117		x [3]	31.2 [6]
Off-Normal Hot	117		x [3]	40.8 [2]
Off-Normal Hot [11]	117		x [3]	31.2 [2]

(1) Insolation in accordance with 10 CFR §71.71(c)(1).

(2) Decay heat load applied as surface heat flux to DSC shell and a 450 cfm air circulation with external fan is assumed.

(3) Sunshade assumed.

(4) Assumes initial steady-state conditions with 215°F water in the cask DSC annulus. At time = 0, the water is drained, and bolting of TC top cover is initiated, and the system begins to heat up. Transient concludes with a steady-state analysis with no insolation.

(5) Assumes initial steady-state conditions. At time = 0, the water in the neutron shield is drained, and the air circulation with external fan (if used) is assumed to be lost. Transient concludes with a steady-state analysis for horizontal operation, maximum insolation, a drained neutron shield, and no air circulation with external fan (if used).

(6) Decay heat load applied as volumetric heat source to solid cylindrical representation of the fuel basket. The fuel basket thermal properties assume the presence of aluminum inserts in R45 transition rails..

(7) Decay heat load applied as volumetric heat source to solid cylindrical representation of the fuel basket. The fuel basket thermal properties assume no aluminum inserts in R45 transition rails.

(8) Assumes initial steady-state conditions. At time = 0, external air circulation is assumed lost. Transient concludes with a steady-state analysis for horizontal operation, maximum insolation.

(9) Steady-state analysis for horizontal operation, maximum insolation.

(10) 15 minute fire transient. 10 CFR 71.73 criteria used for fire properties. Sunshade assumed prior to fire, but lost during for fire and post-fire analysis.

(11) The fuel basket thermal properties assume no aluminum inserts.

Table P.4-8
Cask DSC Gap Hydraulic Characteristics as Function of Circumferential Position

Angle [1]	DSC 'X' loc, Inches	DSC 'Y' loc, Inches	Cask 'X' loc, Inches	Cask 'Y' loc, Inches	Gap Width, Inches	Angle Segment	Flow Area, Sq. Inches	Hydraulic Dia., Inches
0°	0.0000	33.3003	0.0000	34.0000	0.6997	0 to 15	6.120	1.288
15°	-8.6214	32.1753	-8.7998	32.8415	0.6897	15 to 30	5.948	1.254
30°	-16.6699	28.8731	-17.0000	29.4449	0.6602	30 to 45	5.615	1.188
45°	-23.6079	23.6079	-24.0416	24.0416	0.6134	45 to 60	5.144	1.094
60°	-28.9665	16.7238	-29.4449	17.0000	0.5524	60 to 75	4.565	0.976
75°	-32.3766	8.6753	-32.8415	8.7998	0.4813	75 to 90	3.919	0.844
90°	-33.5950	0.0000	-34.0000	0.0000	0.4050	90 to 105	3.248	0.705
105°	-32.5240	-8.7148	-32.8415	-8.7998	0.3287	105 to 120	2.598	0.568
120°	-29.2217	-16.8712	-29.4449	-17.0000	0.2577	120 to 135	2.015	0.443
135°	-23.9026	-23.9026	-24.0416	-24.0416	0.1966	135 to 150	1.538	0.340
150°	-16.9251	-29.3151	-17.0000	-29.4449	0.1498	150 to 165	1.020	0.226
165°	-8.7687	-32.7252	-8.7998	-32.8415	0.1203	165 to 180	0.845	0.188
180°	0.0000	-33.8897	0.0000	-34.0000	0.1103	N/A	N/A	N/A

Notes:
(1) 0° is at top of horizontal cask, 180° is at bottom of horizontal cask.
(2) DSC and cask 'X' and 'Y' positions measured with X= 0 and Y= 0 at the cask centerline.

Table P.4-9
OS197FC TC Components and DSC Shell Temperatures with 40.8 kW Decay Heat Load under Normal and Off-Normal Conditions

Component	Temperature (°F) [1]			
	100°F Ambient with Insolation [2]	117°F Ambient with Sunshade [3]	0°F Ambient without Insolation [4]	Max. Allowable
Max. DSC Shell	445	444	444	800
TC Inner Liner	294	297	271	800
TC Gamma Shield	289	292	266	620
TC Structural Shell	237	242	201	800
TC Neutron Shield, Max. / Ave.	233 / 206	238 / 204	196 / 106	- / 287
TC Top/Bottom Lids, Bulk Average NS-3	166	164	96	250
TC Outer Skin	222	278	181	800

Notes

(1) Assumes 24PTH-S DSC with aluminum inserts in R45 transition rails. Analyses are transient, and at t=0, the annulus is drained and cask top cover bolted on, the TC is rotated to horizontal position and moved outdoors.

(2) 11.5 hours after TC DSC annulus is drained and TC top cover bolting initiated.

(3) 11.5 hours after TC DSC annulus is drained and TC top cover bolting initiated.

(4) 12.75 hours after TC DSC annulus is drained and TC top cover bolting initiated.

Table P.4-10
OS197FC TC Components and DSC Shell Temperatures with 31.2 kW Decay Heat Load, without Aluminum Inserts under Normal and Off-Normal Conditions

Component	Temperature (°F) [1]			
	100°F Ambient with Insolation [2]	117°F Ambient with Sunshade [3]	0°F Ambient without Insolation [4]	Max. Allowable
Max. DSC Shell	475	474	454	800
TC Inner Liner	310	317	265	800
TC Gamma Shield	306	313	259	620
TC Structural Shell	258	267	200	800
TC Neutron Shield, Max. / Ave.	255 / 225	263 / 223	108 / 82	- / 287
TC Top/Bottom Lids, Bulk Average NS-3	170	168	82	250
TC Outer Skin	243	252	181	800

Notes

(1) Analyses are transient, and at t=0, the annulus is drained and cask top cover bolted on, the TC is rotated to horizontal position and moved outdoors.

(2) 27.3 hours after TC DSC annulus is drained and TC top cover bolting initiated.

(3) 28.3 hours after TC DSC annulus is drained and TC top cover bolting initiated.

(4) 30 hours after TC DSC annulus is drained and TC top cover bolting initiated.

Table P.4-11
OS197FC TC Components and DSC Shell Temperatures with 31.2 kW Decay Heat Load, with Aluminum Inserts under Normal and Off-Normal Conditions

Component	Temperature (°F)		
	100°F Ambient with Insolation	117°F Ambient with Sunshade	Max. Allowable
Max. DSC Shell	551	548	800
TC Inner Liner	380	384	800
TC Gamma Shield	375	379	620
TC Structural Shell	322	329	800
TC Neutron Shield, Max. / Ave.	317 / 275	324 / 273	- / 287
TC Top/Bottom Lids, Bulk Average NS-3	200	198	250
TC Outer Skin	300	307	800

Table P.4-12
Steady-State Temperatures for a Loss of Neutron Shield

Component	Temperature (°F) [1]		
	40.8 kW [2]	31.2 kW [3]	Max. Allowable
Max. DSC Shell	685	610	800
TC Inner Liner	530	465	800
TC Gamma Shield	525	461	620
TC Structural Shell	488	428	800
TC Neutron Shield, Max. / Ave.	N/A	N/A	N/A
TC Top/Bottom Lids, Bulk Average NS-3	254	230	250
TC Outer Skin	325	292	800

1) Assumes simultaneous loss of air circulation with fan (if used) and loss of water from neutron shield, with 100°F ambient with insolation
2) 24PTH-S DSC with aluminum inserts in R45 transition rails.
3) 24PTH-S DSC without aluminum inserts in R45 transition rails.

Table P.4-13
Fire Accident Temperatures with 40.8 kW Decay Heat Load

Component	Temperature (°F) [1]		
	End of Fire [2]	Post-Fire Steady-State [3]	Max. Allowable, Short Term / Long Term
Max. DSC Shell	454	668	1000 / 800
TC Inner Liner	354	508	1000 / 800
TC Gamma Shield	349	502	620/620
TC Structural Shell	341	462	1000 / 800
TC Neutron Shield, Max. / Ave.	N/A	N/A	- / 287
TC Top/Bottom Lids, Bulk Average NS-3	627	219	1300 / 250
TC Top Forging	918	368	1000 / 800
TC Bottom Forging	1076	292	1000 / 800
TC Outer Skin	896	279	1000/800

1) Assumes initial conditions with 24PTH-S DSC with aluminum inserts in R45 transition rails, 40.8 kW, 117°F ambient with sunshade, and 450 cfm air circulation.
2) Component temperatures at end of 15-minute fire transient
3) Assumes loss of air circulation and also loss of water in the neutron shield, 117°F ambient with insolation

Table P.4-14
Fuel Cladding Normal Condition Maximum Temperatures

Operating Condition	HLZC 1[4] (°F)	HLZC 4 (°F)	HLZC 5 (°F)	Limit (°F)
DSC in HSM, 0°F ambient	646	<646[1]	< 551[2] / 551[3]	752[6]
DSC in HSM, 100°F ambient	708	<708[1]	< 624[2] / 624[3]	
DSC in TC, 0°F ambient	<711 @ 12.8 hrs	<732 @ 30 hrs	630	
DSC in TC, 100°F ambient	711 @ 11.5 hrs	732 @ 27.3 hrs	714	
DSC in TC, 100°F ambient[5]	N/A	733	N/A	

1) Temperature is bounded by temperature for HLZC 1.
2) Temperature for storage in HSM-H is bounded by temperature for storage in HSM model 102.
3) Temperature for storage in HSM model 102.
4) Temperatures for HLZC 1 bounds the temperatures for HLZC 2 and 3.
5) Temperatures with aluminum inserts in R45 transition rails.
6) ISG-11, Revision 2 [4.20]

Table P.4-15
DSC Basket Assembly Maximum Normal Operating Component Temperatures; HLZC 1 (40.8 kW)

Operating Condition	T_{alum} (°F)	T_{poison} (°F)	T_{tube} (°F)	$T_{DSC\ shell}$ (°F)
DSC in HSM-H, 0°F ambient	565	566	568	367
DSC in HSM-H, 100°F ambient	637	638	640	445
DSC transfer in OS197FC, 0°F ambient	<641[1]	<642[1]	<643[1]	444[2]
DSC transfer in OS197FC, 100°F ambient	641[2]	642[2]	643[2]	445

1) Temperatures are bounded by temperatures for 100°F ambient case.
2) Temperatures are provided using bounding storage in HSM-H case with 117°F ambient. See Table P.4-21.

Table P.4-16
DSC Basket Assembly Maximum Normal Operating Component Temperatures; HLZC 4 (31.2 kW)

Operating Condition	T_{alum} (°F)	T_{poison} (°F)	T_{tube} (°F)	$T_{DSC\ shell}$ (°F)
DSC in HSM-H, 0°F ambient[1]	<565	<566	<568	<367
DSC in HSM-H, 100°F ambient[1]	<637	<638	<640	<445
DSC in OS197FC cask, 0°F ambient[3]	<680[2]	<681[2]	<682[2]	454
DSC in OS197FC cask, 100°F ambient[3]	680	681	682	475
DSC in OS197FC cask, 100°F ambient[4] (with inserts)	678	679	680	548

1) Temperatures are bounded by temperatures for HLZC 1 (Table P.4-16).
2) Temperatures are bounded by temperatures for 100°F ambient case.
3) Assumes 24PTH-S DSC without aluminum inserts in R45 transition rails.
4) Assumes 24PTH-S DSC with aluminum inserts in R45 transition rails.

Table P.4-17
DSC Basket Assembly Maximum Normal Operating Component Temperatures; HLZC 5 (24 kW)

Operating Condition	T_{alum} (°F)	T_{poison} (°F)	T_{tube} (°F)	$T_{DSC\ shell}$ (°F)
DSC in HSM Model 102[1], 0°F Ambient	494	495	496	277
DSC in HSM Model 102[1], 100° Ambient	575	576	577	374
DSC horizontal in Standardized cask, 0°F Ambient	618	619	620	387
DSC horizontal in Standardized cask, 100°F Ambient	673	673	674	448

1) Based on the conclusion documented in Table P.4-23, temperature bounds temperature for storage in HSM-H conditions.

Table P.4-18
24PTH DSC Initial Helium Fill Gas Molar Quantities

DSC Type	HLZC	Helium Fill, g-moles
24PTH-S DSC	1, 3, 4	131.2
	2	137.1
24PTH-L DSC	1, 3, 4	135.4
24PTH-S-LC DSC	5	153.5

Table P.4-19
24PTH DSC Maximum Normal Operating Condition Pressures

DSC Type / HLZC #	DSC Cavity Volume (in^3)	DSC Cavity Helium Fill Gas (g-moles)	Fuel Rod Helium Filled Gas (g-moles)	CC Gas (g-moles)	Fission Products Gases (g-moles)	Total Gas (g-moles)	DSC Cavity Pressure (psig)	DSC Design Pressure (psig)	Bounding case
24PTH-S DSC / HLZC 4	255,000	131.2	1.3	0.0	3.4	136.0	6.5	15	31.2 kW transfer in OS197FC, inserts, 100°F amb
24PTH-L DSC HLZC 4	263,000	135.4	1.3	0.5	3.4	140.6	6.6	15	31.2 kW transfer in OS197FC, inserts, 100°F amb
24PTH-S-LC DSC / HLZC 5	292,000	153.5	1.3	0.5	3.4	158.8	7.1	15	24 kW transfer in Standard cask, 100°F amb

Table P.4-20
Fuel Cladding Off-Normal Condition Maximum Temperatures

Operating Condition	HLZC 1[5] (°F)	HLZC 4 (°F)	HLZC 5 (°F)	Limit (°F)
DSC in HSM, -40°F ambient	620	580	< 521[1] / 521[2]	1058
DSC in HSM, 117°F ambient	711	674	< 643[1] / 643[2]	
DSC in TC, 117°F ambient [3][4]	<711 @ 11.5 hrs	<732 @ 27.3 hrs	718	752
DSC in OS197FC, 117°F ambient [3][6] (31.2 kW HLZC 4 with inserts)	N/A	733	N/A	752
DSC in OS197FC, 117°F ambient [3][7]	681	638	N/A	752

1) Temperature for storage in HSM-H is bounded by temperature for storage in HSM model 102.
2) Temperature for storage in HSM model 102.
3) Sunshade is used for ambient temperatures >100°F and ≤117°F.
4) Temperatures are bounded by transfer in OS197FC without sunshade, 100°F ambient.
5) Temperatures for HLZC 1 bound the temperatures for HLZC 2 and 3.
6) Assumes 24PTH-S DSC with aluminum inserts in R45 transition rails.
7) Assumes 24PTH-S DSC without aluminum inserts in R45 transition rails and use of 475 cfm air circulation with external fan per Table P.4-41 for HLZC 1 and Table P.4-42 for HLZC 4.

Table P.4-21
DSC Basket Assembly Maximum Off-Normal Operating Component Temperatures, HLZC 1[4] (40.8 kW)

Operating Condition	T_{alum} (°F)	T_{poison} (°F)	T_{tube} (°F)	$T_{DSC\ shell}$ (°F)
DSC in HSM-H, -40°F Ambient	534	535	537	333
DSC in HSM-H, 117° F Ambient	641	642	643	448
DSC in OS197FC with sunshade, 117°F ambient[2]	<641[1]	<642[1]	<643[1]	444
DSC in OS197FC with sunshade, 117°F ambient[3]	604	605	607	480

1) Temperature is provided using bounding storage in HSM-H case with 117°F ambient.
2) Assumes 24PTH-S DSC with aluminum inserts in R45 transition rails.
3) Assumes 24PTH-S DSC without aluminum inserts in R45 transition rails and use of 475 cfm air circulation with external fan per Table P.4-41.
4) HLZC 1 bounds the temperatures for HLZC 2 and 3.

Table P.4-22
DSC Basket Assembly Maximum Off-Normal Operating Component Temperatures, HLZC 4 (31.2 kW)

Operating Condition	T_{alum} (°F)	T_{poison} (°F)	T_{tube} (°F)	$T_{DSC\ shell}$ (°F)
DSC in HSM-H, -40°F Ambient	510	510	512	270
DSC in HSM-H, 117°F Ambient	617	618	619	391
DSC in OS197FC with sunshade, 117°F Ambient[2]	<680[1]	<681[1]	<682[1]	474
DSC in OS197FC with sunshade, 117°F Ambient[3]	682	683	684	548
DSC in OS197FC with sunshade, 117°F Ambient[4]	575	576	577	415

1) Temperature are bounded by temperatures for transfer 100°F ambient without sunshade case reported in Table P.4-16.
2) Assumes 24PTH-S DSC without aluminum inserts in R45 transition rails.
3) Assumes 24PTH-S DSC with aluminum inserts in R45 transition rails.
4) Assumes 24PTH-S DSC without aluminum inserts in R45 transition rails and use of 475 cfm air circulation with external fan per Table P.4-42.

Table P.4-23
DSC Basket Assembly Maximum Off-Normal Operating Component Temperatures, HLZC 5 (24 kW)

Operating Condition	T_{alum} (°F)	T_{poison} (°F)	T_{tube} (°F)	$T_{DSC\ shell}$ (°F)
DSC in HSM Model 102[1], -40°F Ambient	461	462	463	237
DSC in HSM Model 102[1], 117°F Ambient	596	596	598	399
DSC in Standardized cask with sunshade, 117°F Ambient	677	678	679	470

1) Temperature bounds temperature for storage in HSM-H conditions based on DSC shell temperature comparison to the results shown in Table P.4-4.

Table P.4-24
24PTH DSC Maximum Off-Normal Operating Condition Pressures

DSC Type / HLZC #	DSC Cavity Volume (in^3)	DSC Cavity Helium Fill Gas (g-moles)	Fuel Rod Helium-Fill Gas (g-moles)	CC Gas (g-moles)	Fission Products Gases (g-moles)	Total Gas (g-moles)	DSC Cavity Pressure (psig)	DSC Design Pressure (psig)	Bounding case
24PTH-S DSC / HLZC 4	255,000	131.2	13.1	0.0	34.3	178.7	13.1	20	31.2 kW transfer in OS197FC, inserts, 117°F amb
24PTH-L DSC / HLZC 4	263,000	135.4	13.1	5.4	34.3	188.2	13.7	20	31.2 kW transfer in OS197FC, inserts, 117°F amb
24PTH-S-LC DSC / HLZC 5	292,000	153.5	13.1	5.4	34.3	206.3	13.6	20	24 kW transfer in Standard cask, 117°F amb

Table P.4-25
Fuel Cladding Accident Condition Maximum Temperatures

Heat Load Zoning	HLZC 1[2] (°F)	HLZC 4 (°F)	HLZC 5 (°F)	Limit (°F)
DSC in HSM, Blocked Vent, 117°F	833[1]	<833[2]	< 809[3] /809[4]	1058[5]
DSC in TC, loss of sun shade, neutron shield water and air circulation with fan,if used, 117°F	914	843	747	

1) Temperature at 38.5 hour of blocked vent.
2) Temperatures for HLZC 1 bound the temperatures for HLZC 2, 3, and 4.
3) Temperature for storage in HSM-H is bounded by temperature for storage in HSM Model 102.
4) Temperature for storage in HSM Model 102 at 40 hours of blocked vent.
5) ISG-11, Revision 2 [4.20]

Table P.4-26
DSC Basket Assembly Accident Maximum Component Temperatures; HLZC 1 (40.8 kW)

Operating Condition	T_{alum} (°F)	T_{poison} (°F)	T_{tube} (°F)	$T_{DSC\ shell}$ (°F)
DSC in HSM-H, Blocked Vent[1], 117°F	778	779	780	578
DSC horizontal in OS197FC loss of sun shade, neutron shield water and air circulation with fan, if used, 117°F Ambient	860	861	862	685

1) Temperature at 38.5 hour of blocked vent.

Table P.4-27
DSC Basket Assembly Accident Maximum Component Temperatures; HLZC 4 (31.2 kW)

Operating Condition	T_{alum} (°F)	T_{poison} (°F)	T_{tube} (°F)	$T_{DSC\ shell}$ (°F)
DSC in HSM-H, Blocked Vent, 117°F Ambient	(1)	(1)	(1)	(1)
DSC horizontal in OS197FC loss of sun shade water and air circulation with fan, if used,, neutron shield, 117°F	801	801	802	610

(1) Temperature is bounded by temperature for HLZC 1 reported in Table P.4-26.

Table P.4-28
DSC Basket Assembly Accident Maximum Component Temperatures; HLZC 5 (24 kW)

Operating Condition	T_{alum} (°F)	T_{poison} (°F)	T_{tube} (°F)	$T_{DSC\ shell}$ (°F)
DSC in HSM Model 102[1], 40 hours of Blocked Vent, 117°F Ambient	774	775	776	613
DSC horizontal in Standardized cask loss of sun shade, 117°F Ambient	708	708	709	487

(1) Temperature bounds temperature for storage in HSM-H conditions.

Table P.4-29
24PTH DSC Maximum Accident Condition Pressures

DSC Type / HLZC #	DSC Cavity Volume (in^3)	DSC Cavity Helium Fill Gas (g-moles)	Fuel Rod Helium-Fill Gas (g-moles)	CC Gas (g-moles)	Fission Products Gases (g-moles)	Total Gas (g-moles)	DSC Cavity Pressure (psig)	DSC Design Pressure (psig)	Bounding Case
24PTH-S DSC/HLZC 1	255,000	131.2	131.4	0.0	342.8	605.4	90.6	120	40.8 kW transfer accident in OS197FC, 117°F amb
24PTH-L DSC/HLZC 1	263,000	135.4	131.4	53.8	342.8	663.3	97.2	120	40.8 kW transfer accident in OS197FC, 117°F amb
24PTH-S-LC DSC/ HLZC 5	292,000	153.5	131.4	53.8	342.8	681.4	80.4	90	24 kW transfer accident in Standard cask, 117°F amb

Table P.4-30
Vacuum Drying Fuel Cladding Maximum Temperatures (°F)

Operating Condition	HLZC 1	HLZC 2	HLZC 3	HLZC 4	HLZC 5	Limit (°F)
Vacuum Drying in air environment, transient	663[1]	(2)	(2)	668[3]	645[4]	752[5]
Vacuum Drying in helium environment (or helium backfilling), steady-state	563	(2)	(2)	568	545	

(1) Temperature at 19 hour of vacuum drying,
(2) Temperature is bounded by temperature for HLZC 1.
(3) Temperature at 25 hours of vacuum drying,
(4) Temperature at 28 hours of vacuum drying.
(5) ISG-11, Revision 2 [4.20]

Table P.4-31
DSC Basket Assembly Maximum Component Temperatures during Vacuum Drying, HLZC 1 (40.8 kW)

Operating Condition	T_{alum} (°F)	T_{poison} (°F)	T_{tube} (°F)	$T_{DSC\ shell}$ (°F)
Vacuum Drying in air environment, transient[1]	572	575	580	215
Vacuum Drying in helium environment, steady-state	468	469	471	215

(1) Temperature conservatively shown for 21 hours of vacuum drying even though the time limit is 19 hours as shown in Table P.4-30.

Table P.4-32
DSC Basket Assembly Maximum Component Temperatures during Vacuum Drying, HLZC 4 (31.2 kW)

Operating Condition	T_{alum} (°F)	T_{poison} (°F)	T_{tube} (°F)	$T_{DSC\ shell}$ (°F)
Vacuum Drying in air environment, transient[1]	616	618	622	215
Vacuum Drying in helium environment, steady-state	496	497	498	215

(1) Temperature shown for 25 hours of vacuum drying.

Table P.4-33
DSC Basket Assembly Maximum Component Temperatures during Vacuum Drying, HLZC 5 (24 kW)

Operating Condition	T_{alum} (°F)	T_{poison} (°F)	T_{tube} (°F)	$T_{DSC\ shell}$ (°F)
Vacuum Drying in air environment, transient[1]	567	570	573	215
Vacuum Drying in helium environment, steady-state	470	471	472	215

(1) Temperature shown for 28 hours of vacuum drying.

Table P.4-34
24PTH-S-LC DSC Shell Temperatures for Storage in HSM Model 102

Ambient Temperature (°F)	Top (°F)	Side (°F)	Bottom (°F)
-40	237	210	158
0	277	247	191
100	374	339	273
117	399	362	295
Blocked Vent	611	568	452

Table P.4-35
NUHOMS®-24PTH DSC Cavity Free Volumes

DSC Type	24PTH-S DSC		24PTH-L DSC	24PTH-S-LC DSC
Cavity Volume, (in^3)	583580	583580	604226	596243
Basket Volume, (in^3)	191256	191256	197743	159337
HLZC #	1, 4	2	1, 4	5
Number of Fuel Assemblies and CC	24 w/o CC	20 w/o CC	24 w/ CC	24 w/ CC
Fuel Volume, (in^3)	135845	113204	142432	142432
Free DSC Volume (in^3)	256479	279120	264050	294473
Free DSC Volume used in calculation (in^3)	255000	278000	263000	292000

Table P.4-36
Fuel Rod Helium Fill Gas Released per DSC

Operating Conditions	Percentage of rods ruptured	HLZC 1 for 24 FAs (g-moles)	HLZC 2 for 20 FAs (g-moles)
Normal	1	1.3	1.1
Off-Normal	10	13.1	10.9
Accident	100	131.4	109.5

Table P.4-37
Fission Gas Released per DSC

Operating Conditions	Percentage of Rods Ruptured	HLZC 1 for 24 FAs (g-moles)	HLZC 2 for 20 FAs (g-moles)
Normal	1	3.4	2.9
Off-Normal	10	34.3	28.6
Accident	100	342.8	285.7

Table P.4-38
CC Gas Released per DSC

Operating Conditions	Percentage of Rods ruptured	CC Gas Released (g-moles)
Normal	1	0.5
Off-Normal	10	5.4
Accident	100	53.8

Table P.4-39
24PTH-S-LC DSC Shell Maximum Temperatures during Transfer in Standardized TC with 24 kW Heat Load

Operating Condition	Top, °F
DSC horizontal in Standardized TC, 0°F amb	387
DSC horizontal in Standardized TC, 100°F amb	448
DSC horizontal in Standardized TC, 117°F amb	470
DSC horizontal in Standardized TC loss of sun shade, 117°F amb	487

Table P.4-40
Comparison Of Peak Component Temperatures For 117°F Ambient With 40.8 kW Decay Heat Load

Component	ANSYS Analytical Model (°F)	CFD Based Confirmatory Calculation (°F)
DSC Shell	448	428
Base Unit Concrete	202	199
Roof Concrete	186	211
Top Heat Shield	188	203
Side Heat Shield	181	220

Table P.4-41
Maximum Normal and Off-Normal OS197 TC Component Temperatures with 40.8 kW Decay Heat Load (with Air Circulation)

Component	Temperature (°F) [1]	
	117°F Ambient with Sunshade	Max. Allowable
Max. DSC Shell	480	800
TC Inner Liner	344	800
TC Gamma Shield	340	620
TC Structural Shell	294	800
TC Neutron Shield, Max. / Ave.	289 / 210	- / 287
TC Top/Bottom Lids Bulk Average NS-3	186	250
Air, Inlet / Exit	100 / 265	n/a
TC Outer Skin	278	800

(1) Assumes 24PTH-S DSC with aluminum inserts in R45 transition rails and 450 cfm of airflow at ambient temperature supplied at the ram access and exiting at the cask lid.

Table P.4-42
Maximum Normal and Off-Normal OS197 TC Component Temperatures with 31.2 kW Decay Heat Load (with Air Circulation)

Component	Temperature (°F)[1]	
	117°F Ambient with Sunshade	Max. Allowable
Max. DSC Shell	415	800
TC Inner Liner	300	800
TC Gamma Shield	296	620
TC Structural Shell	258	800
TC Neutron Shield, Max. / Ave.	254 / 191	- / 287
TC Top/Bottom Lids Bulk Average NS-3	172	250
TC Outer Skin	246	800

(1) Assumes 24PTH-S DSC without aluminum inserts in R45 transition rails and 450 cfm of airflow at ambient temperature supplied at the ram access and exiting at the cask lid.

Table P.4-43
HSM-H Concrete and DSC Shell temperatures with and without Side Heat Shield Fins

Case	Heat Load (kW)	Maximum DSC Shell Temperature (°F)	Maximum Concrete Temperature (°F)	Reference
with fins	31.2	391	183	Figure P.4-8
without fins	31.2	401	201	Figure P.4-10
with fins	40.8	448	202	Figure P.4-11

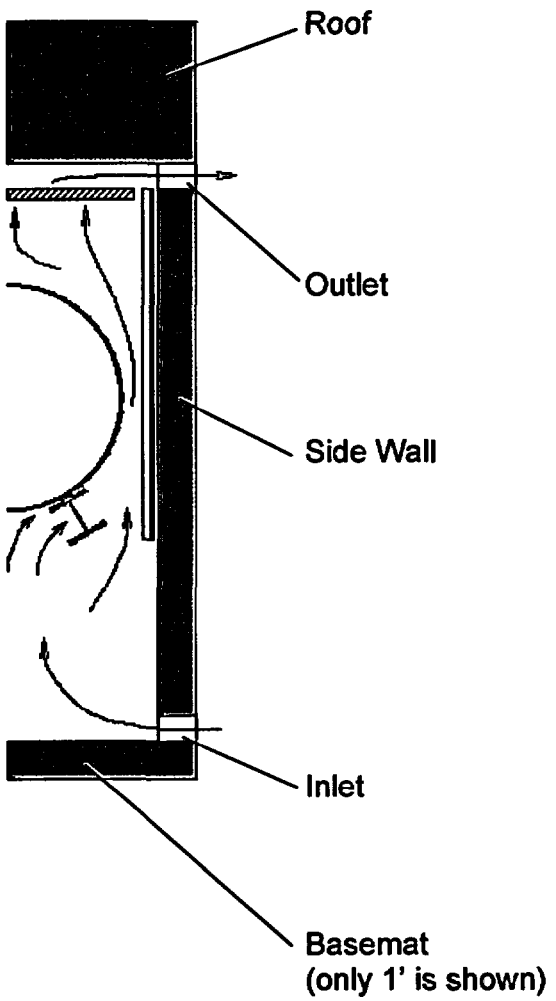

Figure P.4-1 HSM-H Air Flow Diagram

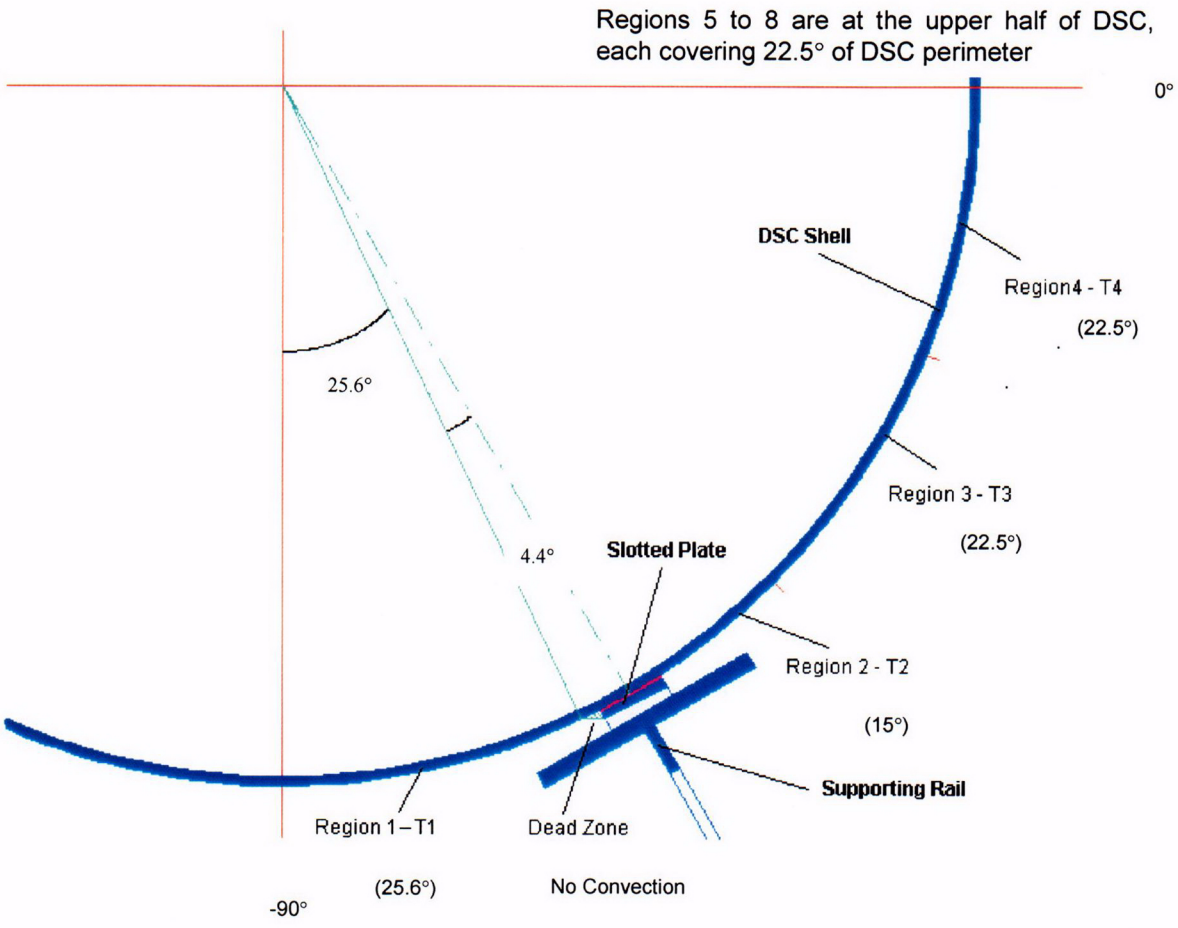

Figure P.4-2 Convection Regions around 24PTH DSC in the HSM-H

C01

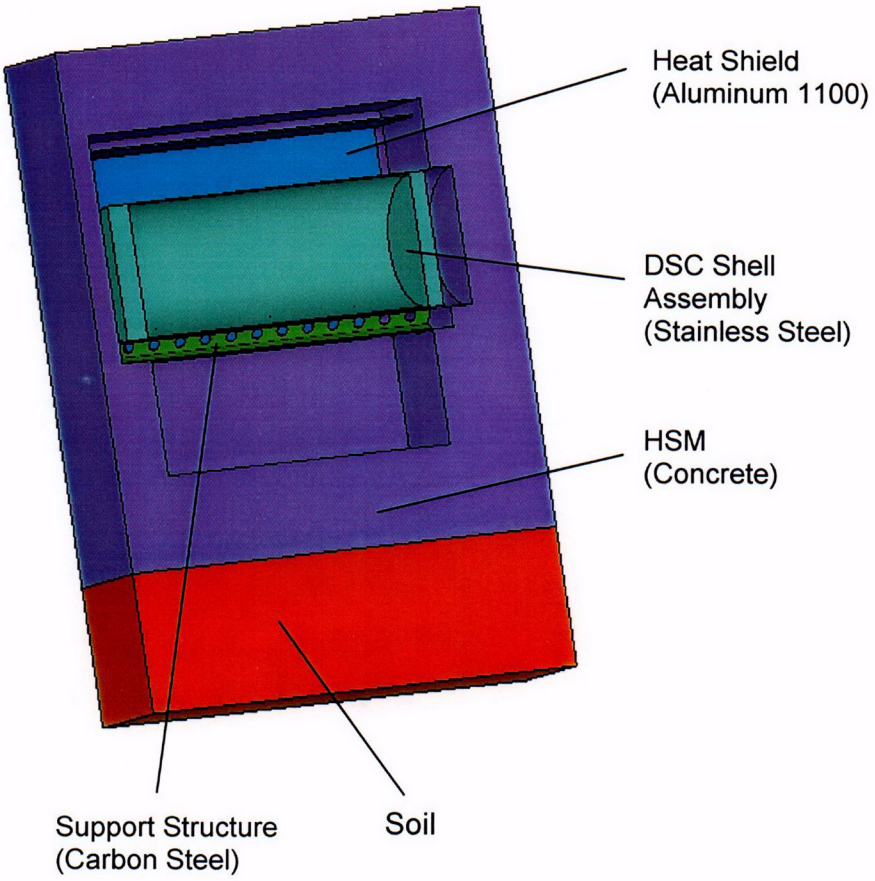

Figure P.4-3 24PTH DSC Shell Assembly in HSM-H Finite Element Model

C02

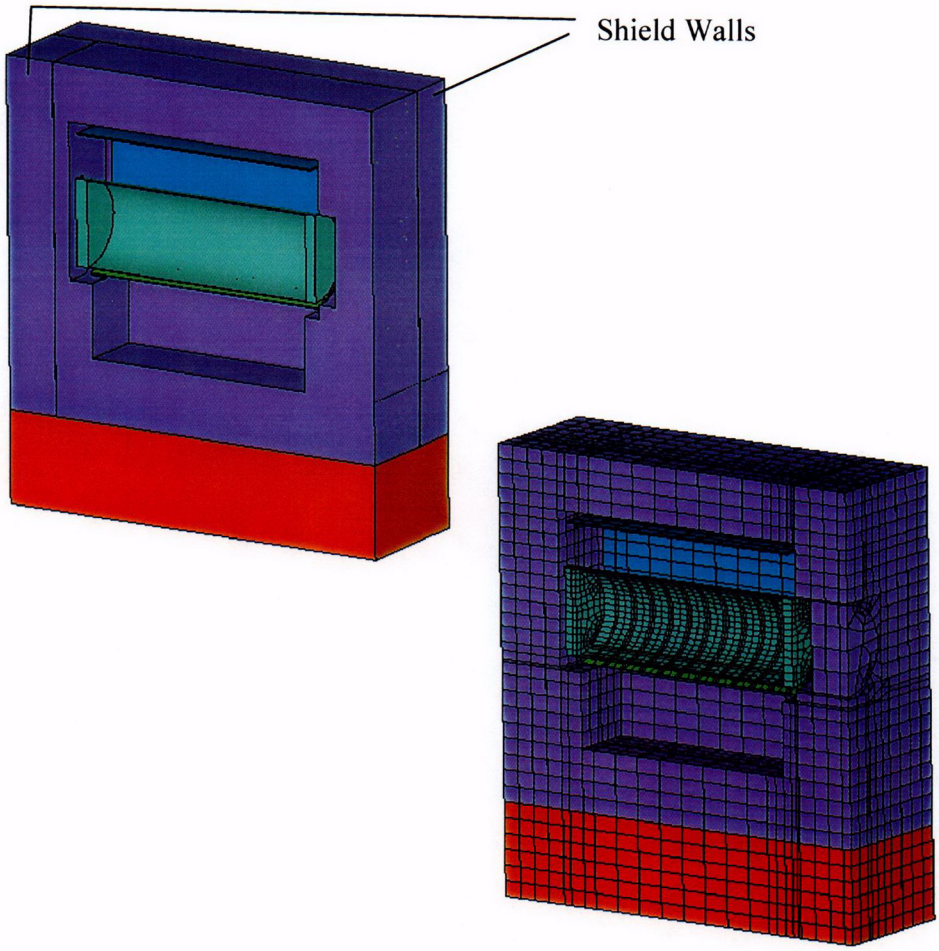

Figure P.4-4 Single HSM-H with 24PTH DSC Shell Assembly Finite Element Model

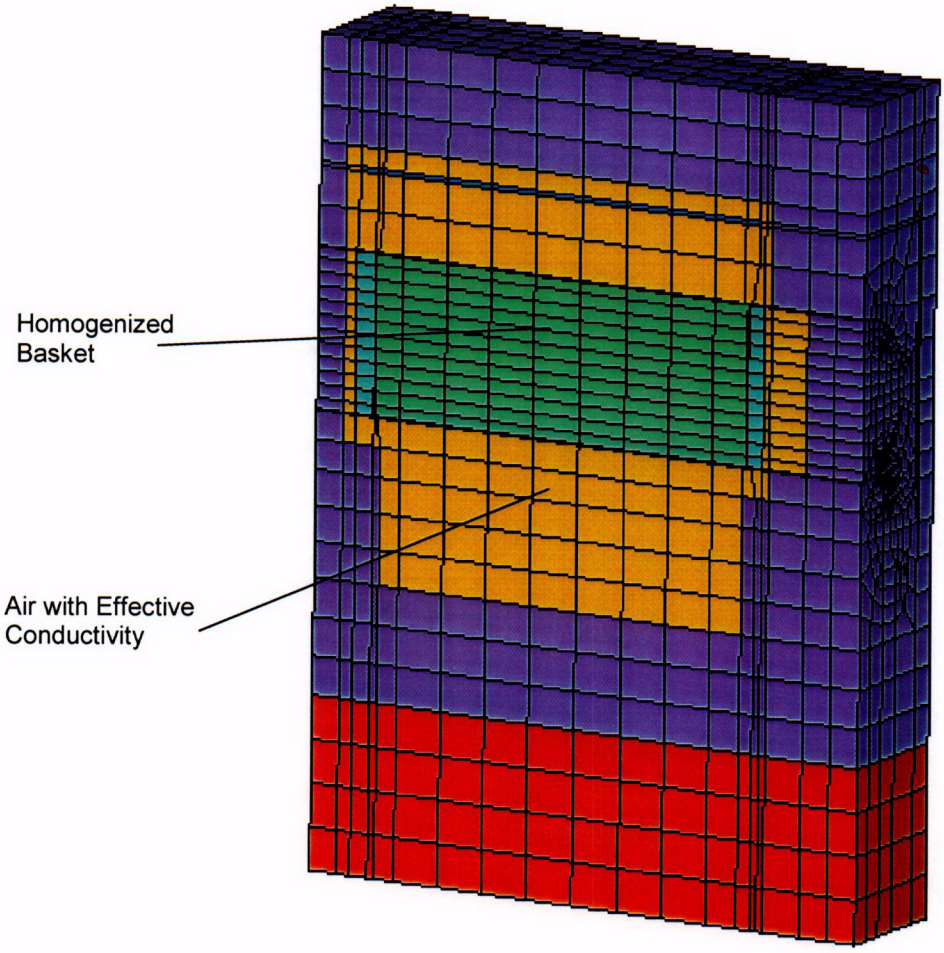

Figure P.4-5 HSM-H with 24PTH DSC Finite Element Model for Blocked Vent Analysis

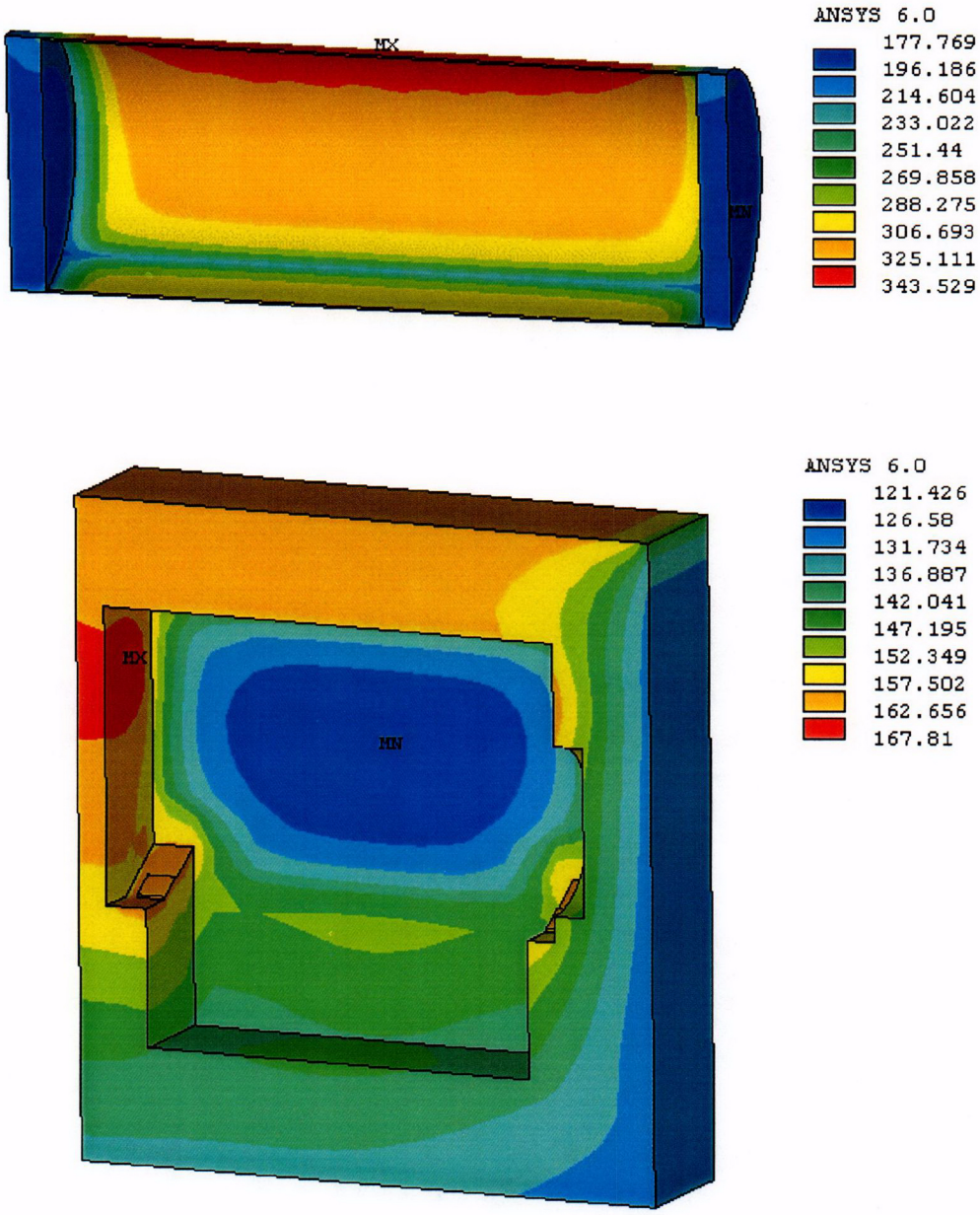

Figure P.4-6 Temperature Distribution in HSM-H and 24PTH-S-LC DSC Shell Assembly, 24 kW Heat Load, 117°F Ambient

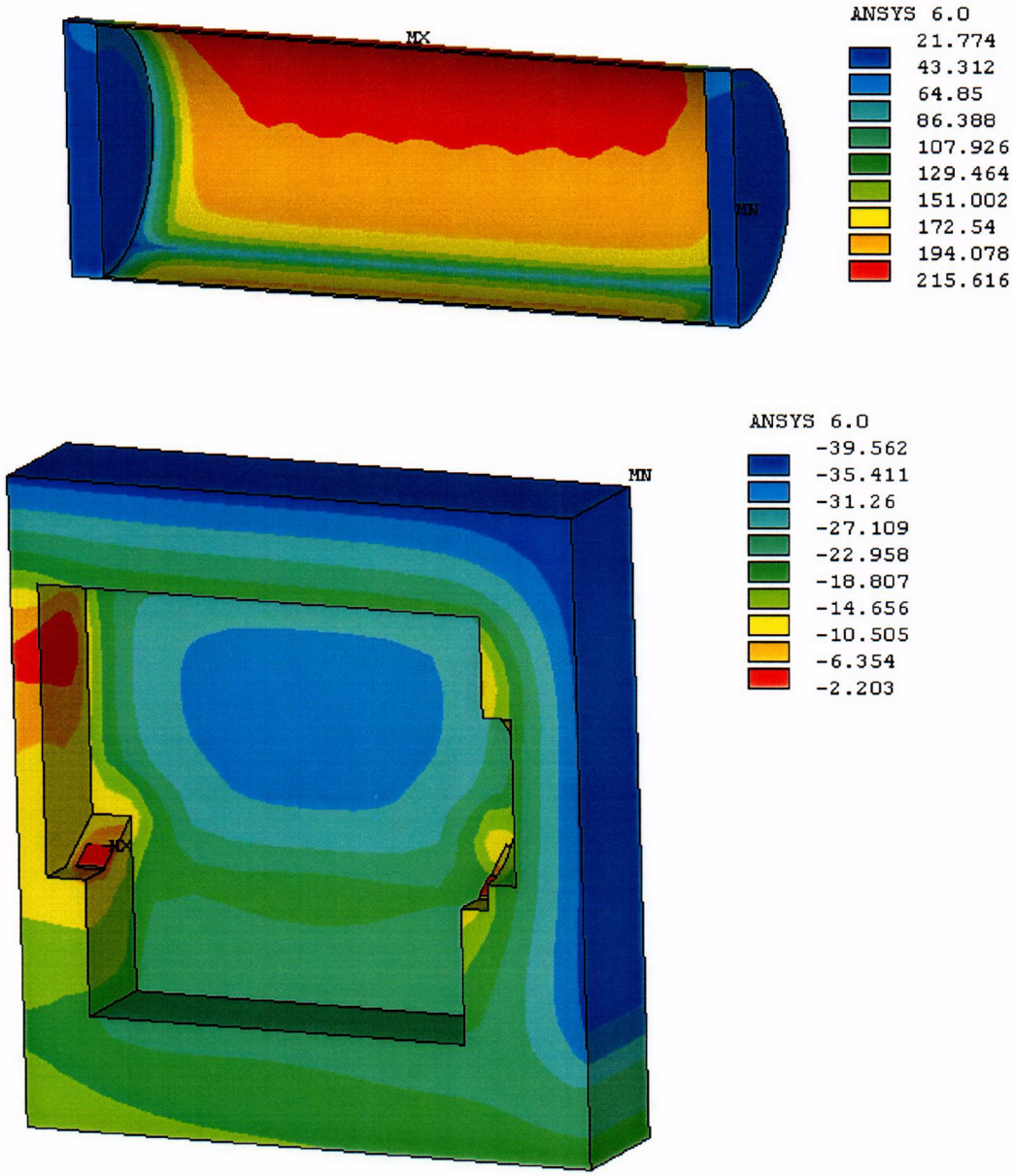

Figure P.4-7 Temperature Distribution in HSM-H and 24PTH-S-LC DSC Shell Assembly, 24 kW Heat Load, -40°F Ambient

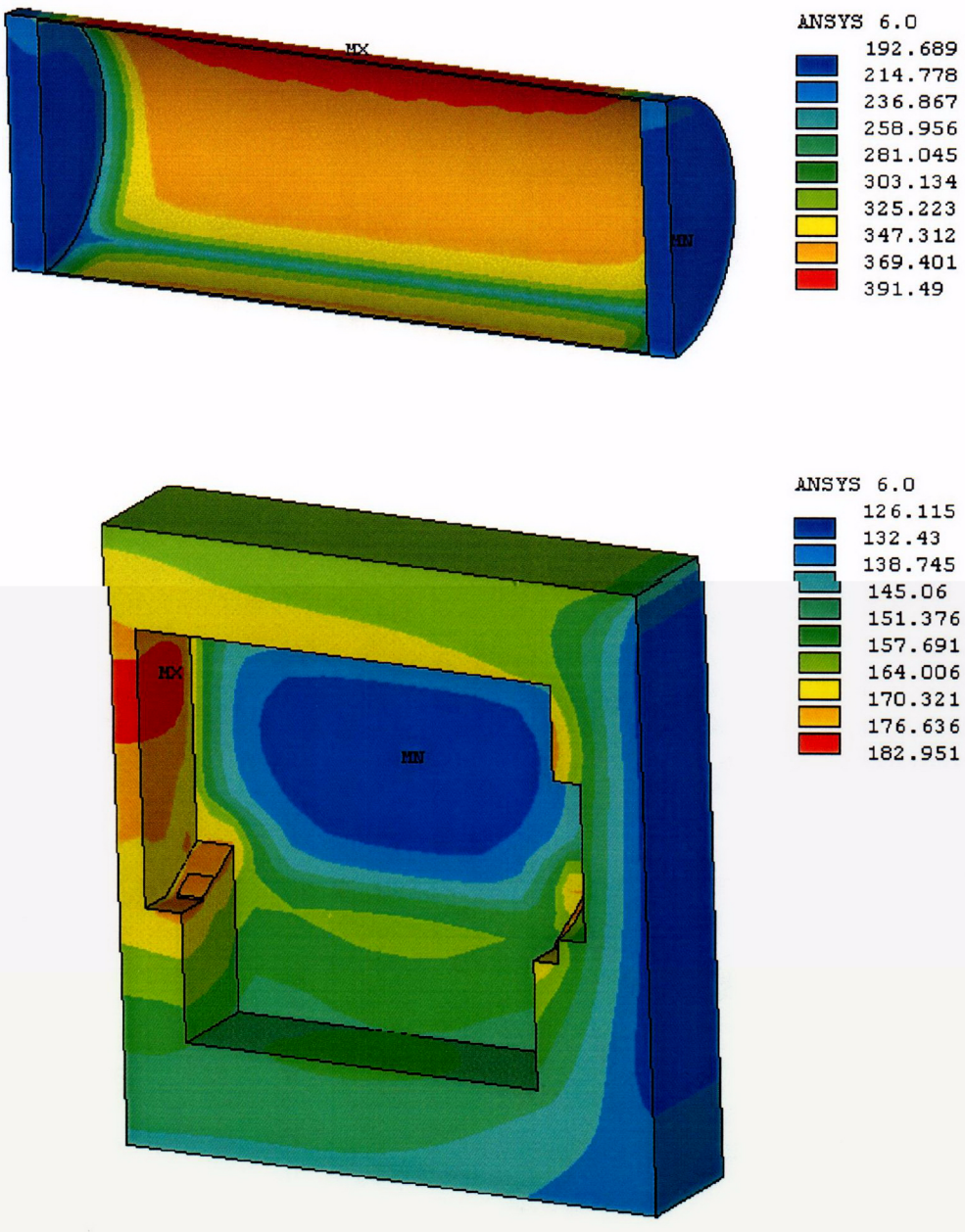

Figure P.4-8 Temperature Distribution in HSM-H and 24PTH-S or -L DSC Shell Assembly, 31.2 kW Heat Load, 117°F Ambient

C07

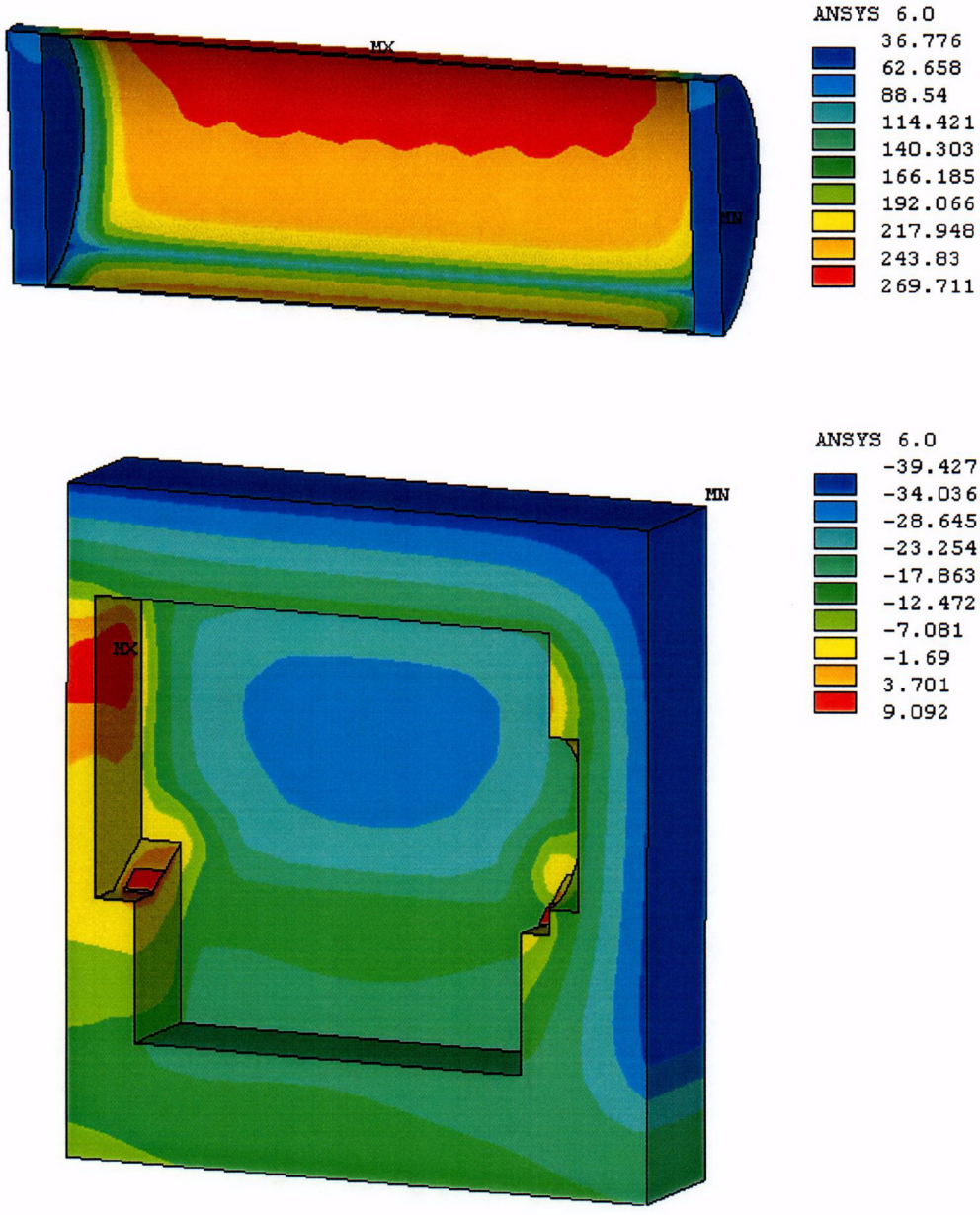

Figure P.4-9 Temperature Distribution in HSM-H and 24PTH-S or -L DSC Shell Assembly, 31.2 kW Heat Load, -40°F Ambient

C08

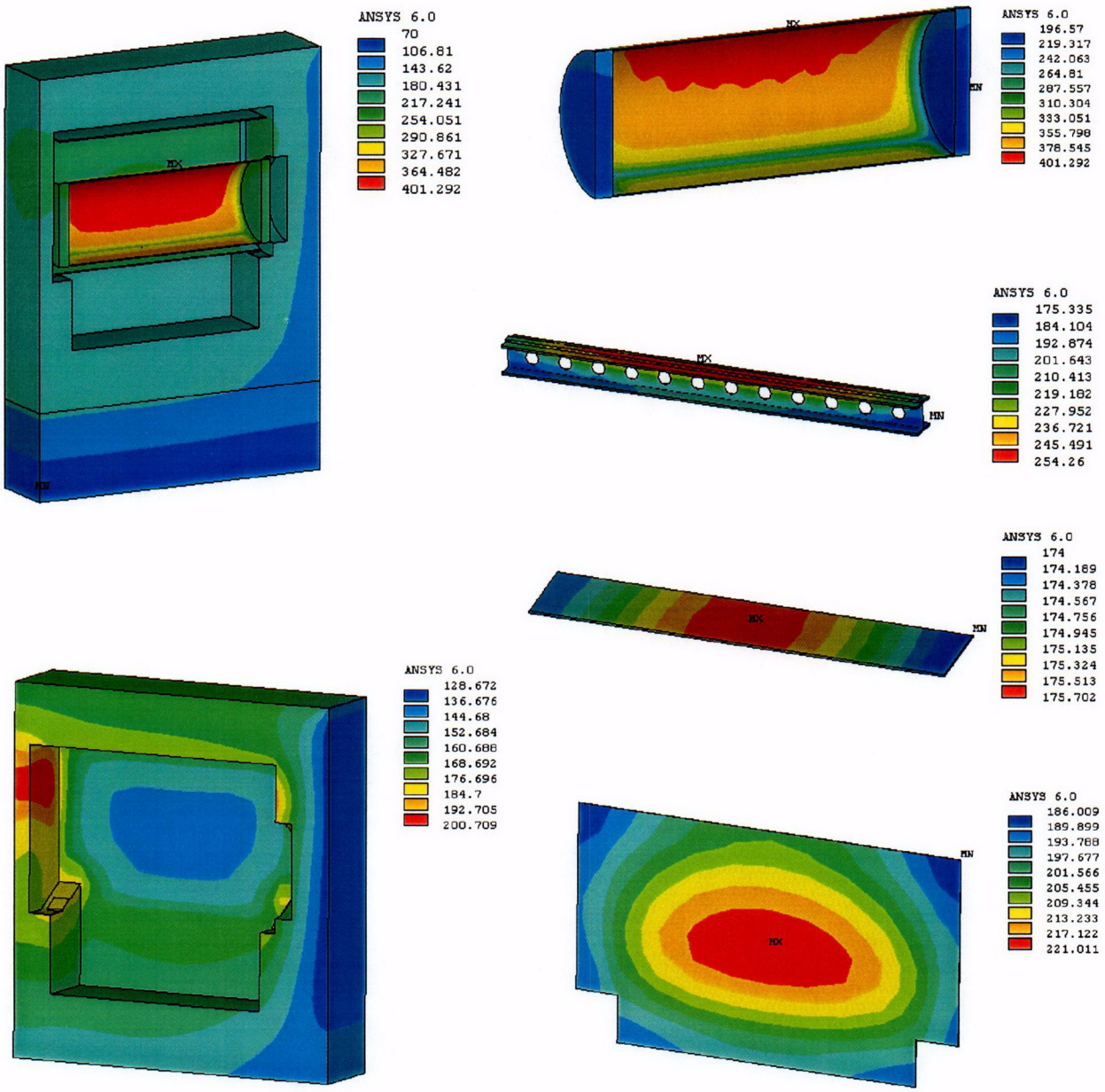

Figure P.4-10 Temperature Distribution in HSM-H, Heat Shield, Support Rail, and 24PTH-S or –L DSC Shell Assembly, 31.2 kW Heat Load, without Fins on the Side Heat Shield, 117°F Ambient

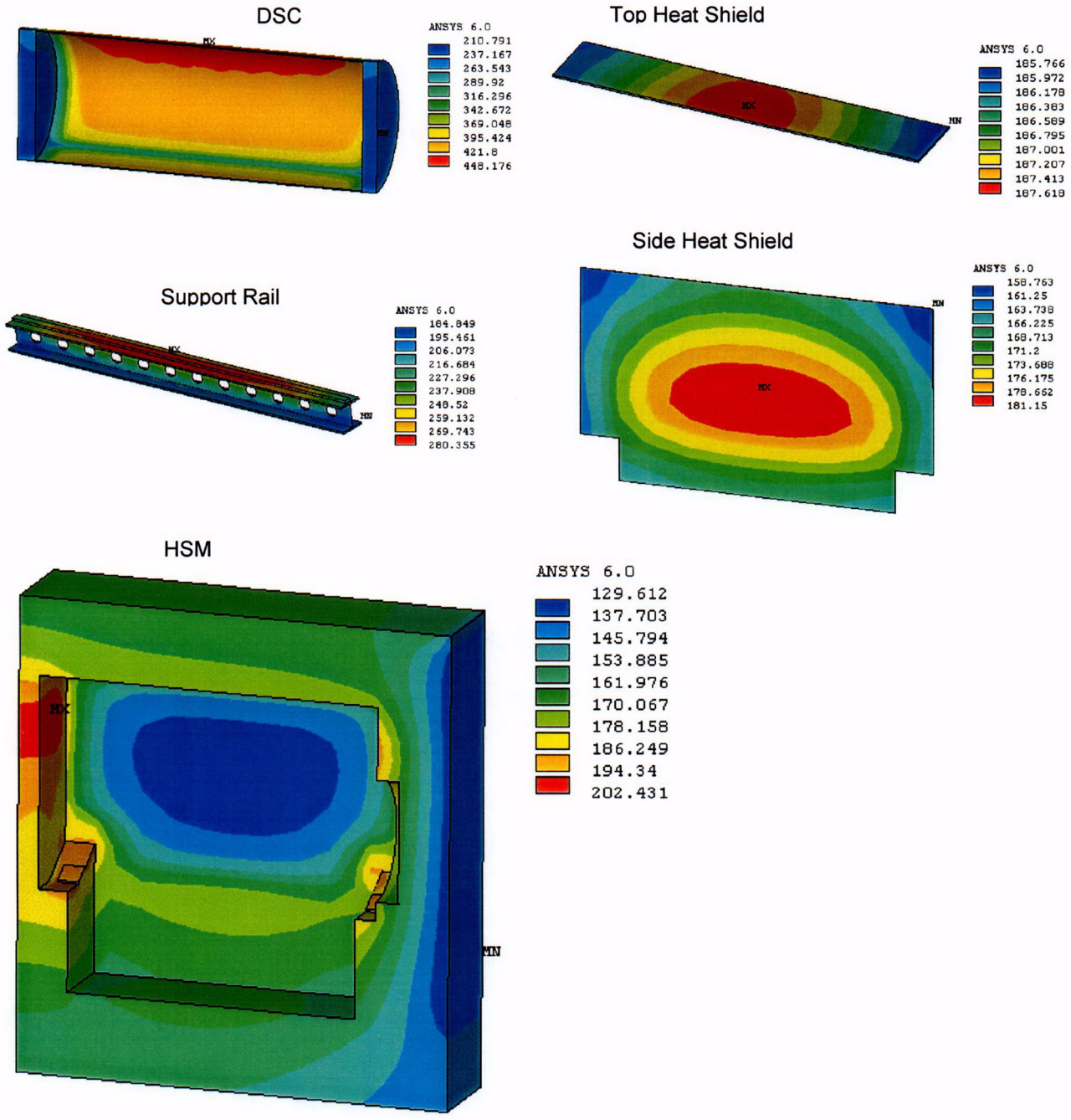

Figure P.4-11 Temperature Distribution in HSM-H, Heat Shield, Support Rail, and 24PTH-S or –L DSC Shell Assembly, 40.8 kW Heat Load, 117°F Ambient

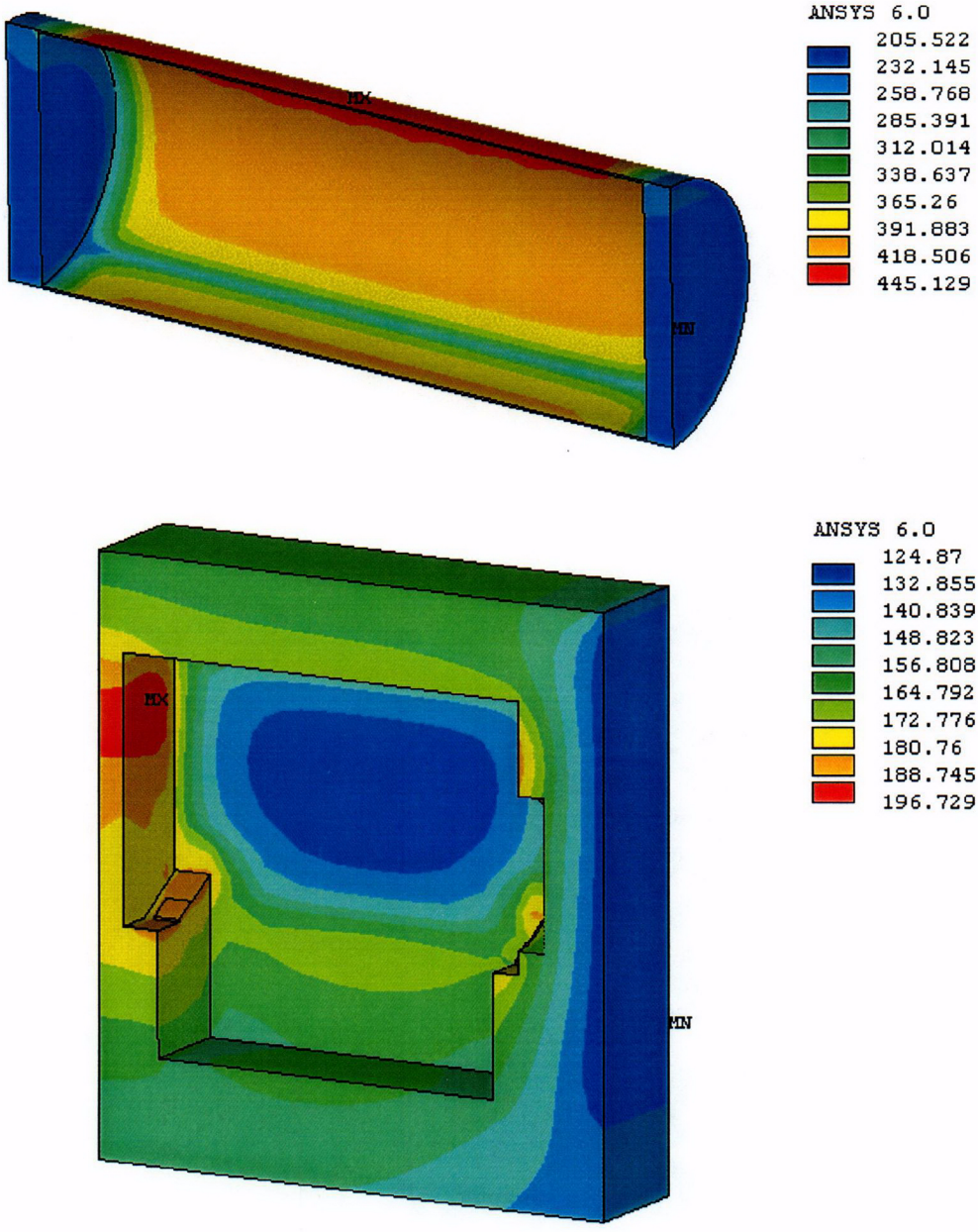

Figure P.4-12 Temperature Distribution in HSM-H, Heat Shield, Support Rail, and 24PTH-S or –L DSC Shell Assembly, 40.8 kW Heat Load, 100°F Ambient

C11

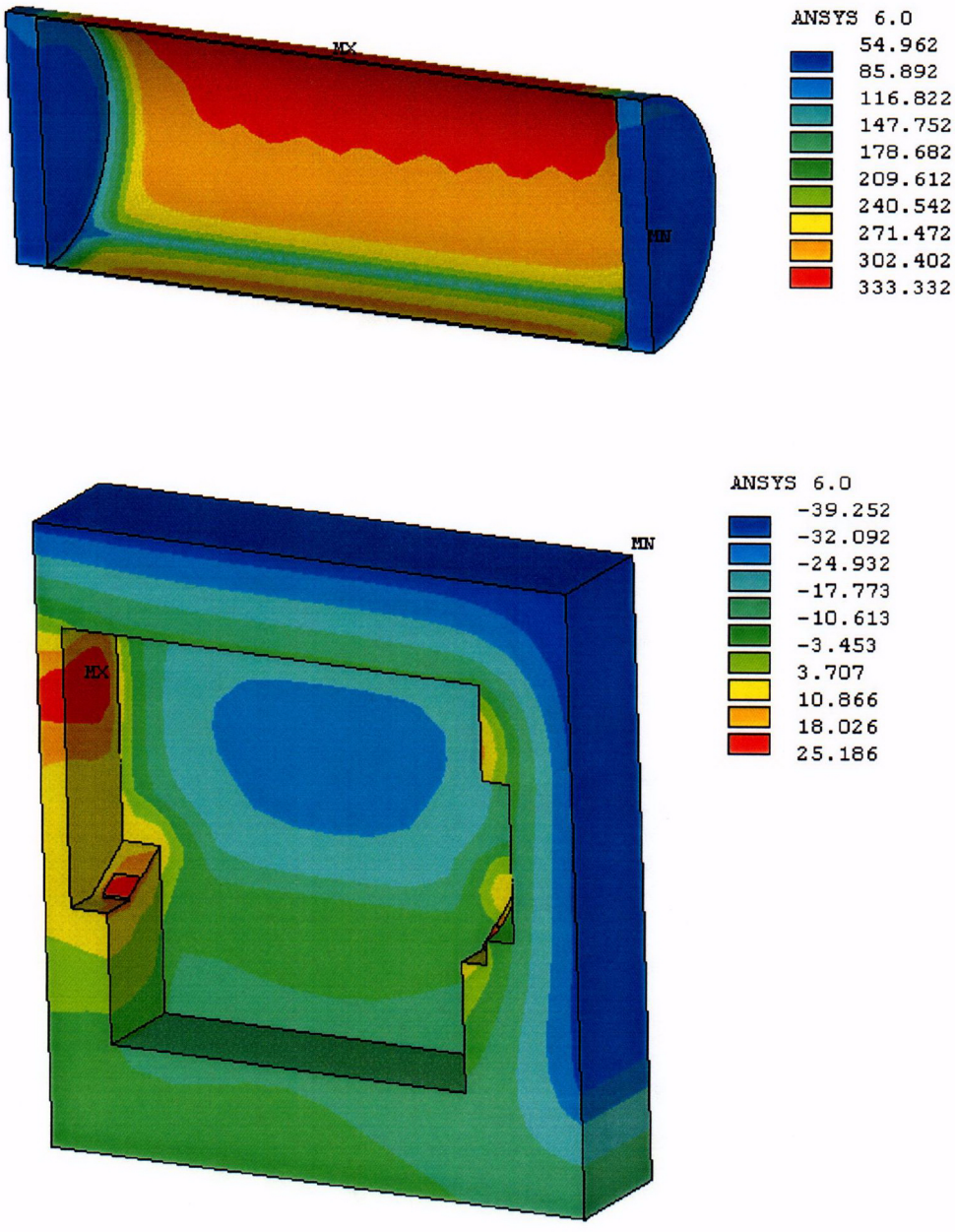

Figure P.4-13 Temperature Distribution in HSM-H and 24PTH DSC Shell Assembly, 40.8 kW Heat Load, -40°F Ambient

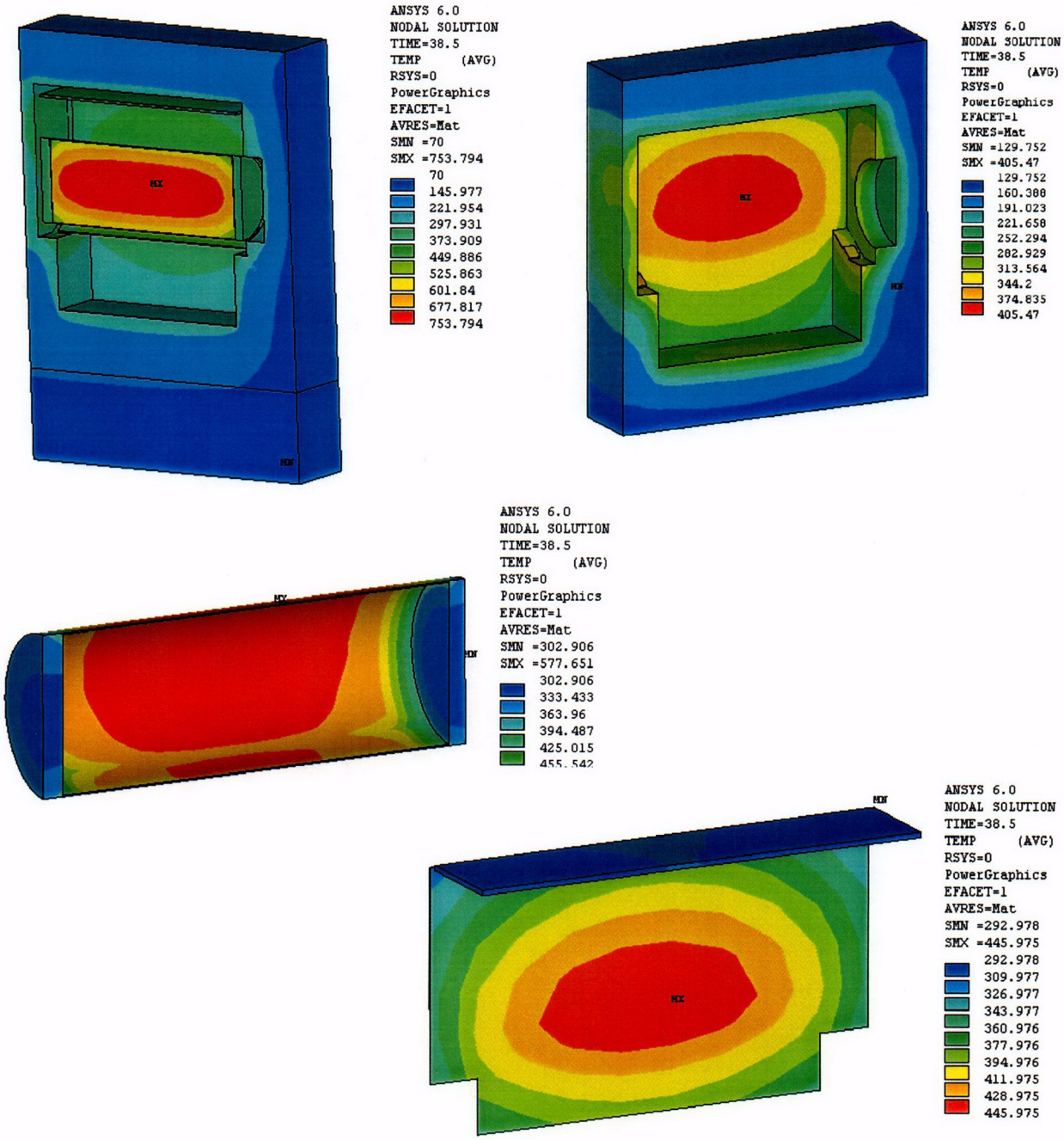

Figure P.4-14 Temperature Distribution in HSM-H and 24PTH DSC Shell Assembly, 40.8 kW heat load, at 38.5 (typical) hours of Blocked vent, 117°F ambient

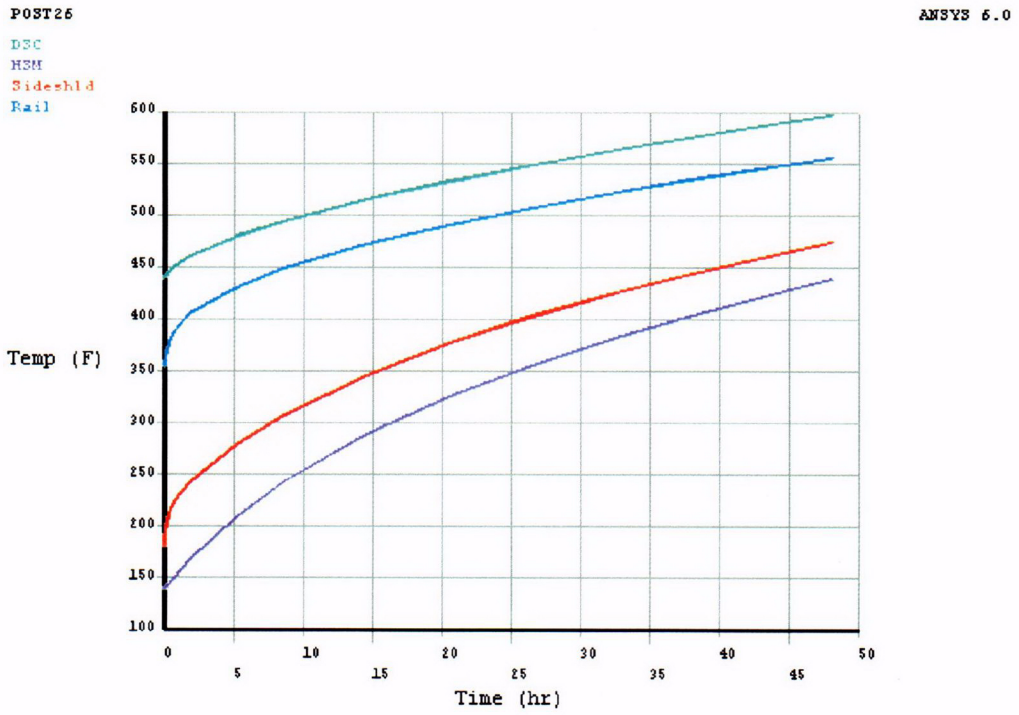

Figure P.4-15 Temperature-Time Histories of HSM-H Model Components during Blocked Vents Accident Case, 40.8 kW, 117°F Ambient

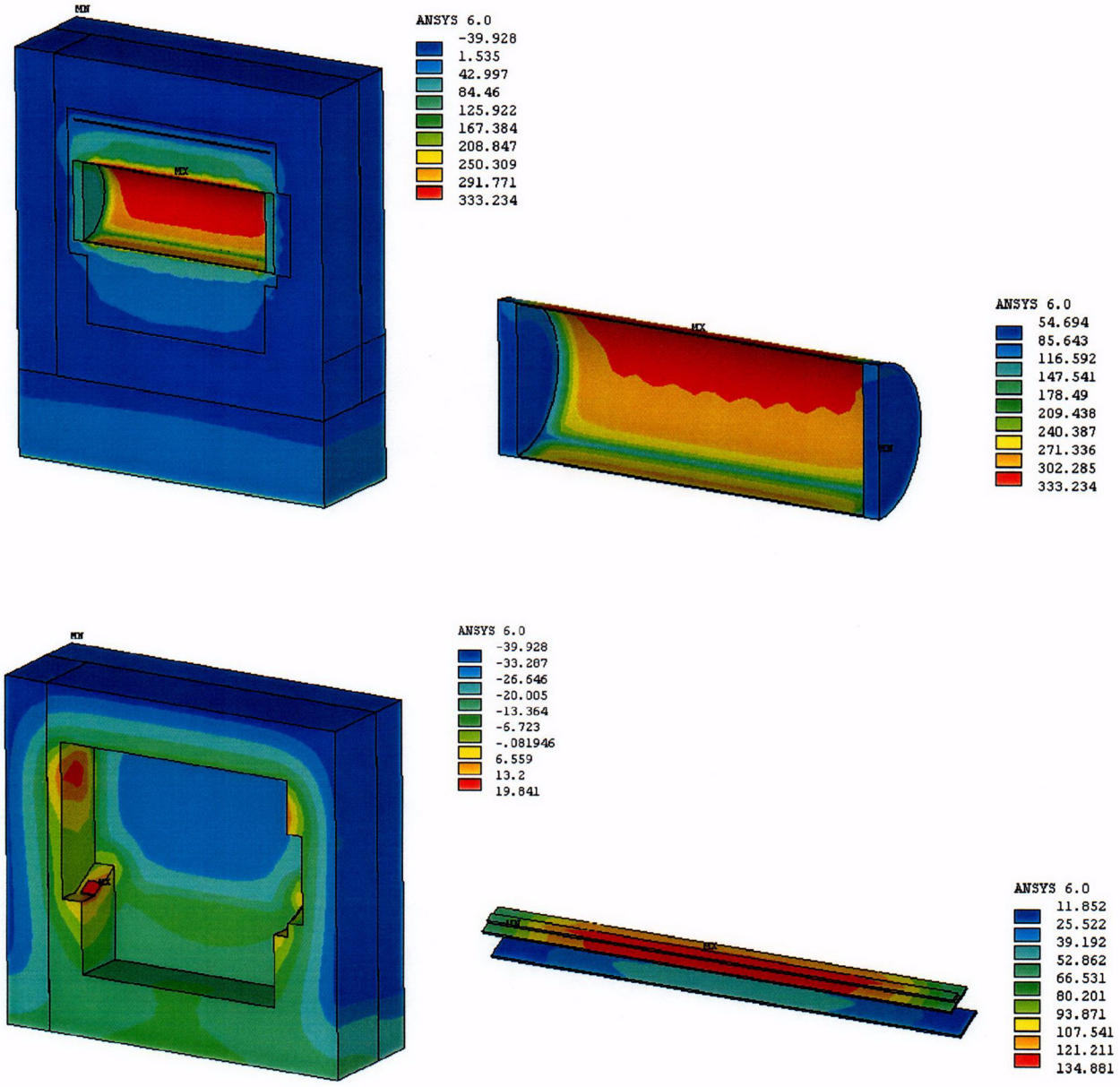

Figure P.4-16 Temperature Distribution in a Single HSM-H and 24PTH DSC Shell Assembly, 40.8 kW Heat Load, -40°F Ambient, Maximum Temperature Gradients through Concrete Walls